Response to Anonymous Reviewer 1

The manuscript topic fits well within the journal scope is providing new insights on biomass burning aerosol layers. Nevertheless, it needs major revisions before being ready for publication.

REPLY: Thanks for your helpful comments. Corrections have been made considering your suggestions as well as other reviewers'. Please find our point-by-point response and first revised version in the supplement. Remark: The figure numbers and the page numbers in the referee comments and in our replies correspond to the original manuscript.

Major comments:

1. A substantiated and consolidated verification of the measurement quality and the potential role of systematic errors affecting the measurements is a preliminary paramount step when such high PLDR values are measured. This is particularly true for stratospheric aerosols as calibration of aerosol depolarization measurements of stratospheric particles is quite difficult and cannot rely on molecular calibration approach.

REPLY: Thank you for this comment. Indeed, the calibration of the depolarization measurements is very crucial for any aerosol study. For the calibration of the depolarization measurements used in this study we followed the "*Δ±45 depolarization calibration*" method proposed by Freudenthaler et al. (2009). Specifically, for the PLDR measurements used here, the systematic errors are 0.015 at 355nm, 0.006 at 532nm and 0.007 at 1064nm as presented in Haarig et al. (2018). A detailed discussion on the parameters affecting the depolarization measurements of the BERTHA lidar system is presented in Haarig et al. (2017) (APPENDIX A).

To highlight this comment, we added the following paragraph to the manuscript (**page 7, line 14**):

“To ensure the high quality of depolarization measurements, the Δ±45 depolarization calibration method proposed by Freudenthaler et al. (2009) was followed, while the effect of different parameters on the depolarization measurements of the BERTHA lidar system has been carefully assessed and is presented in detail in Haarig et al. (2017).”

References *(that are not included in the initial version of the manuscript)*:

Freudenthaler, V., Esselborn, M., Wiegner, M., Heese, B., Tesche, M., Ansmann, A., Müller, D., Althausen, D., Wirth, M., Fix, A., Ehret, G., Knippertz, P., Toledano, C., Gasteiger, J., Garhammer, M., Seefeldner, M.: Depolarization ratio profiling at several wavelengths in pure Saharan dust during SAMUM 2006, Tellus B: Chemical and Physical Meteorology, 61:1, 165-179, DOI: 10.1111/j.1600-0889.2008.00396.x, 2009.

Haarig, M., Ansmann, A., Althausen, D., Klepel, A., Groß, S., Freudenthaler, V., Toledano, C., Mamouri, R.-E., Farrell, D. A., Prescod, D. A., Marinou, E., Burton, S. P., Gasteiger, J., Engelmann, R., and Baars, H.: Triple-wavelength depolarization-ratio profiling of Saharan dust over Barbados during SALTRACE in 2013 and 2014, Atmos. Chem. Phys., 17, 10767–10794, https://doi.org/10.5194/acp-17-10767-2017, 2017.

2.The fact that such high PLDR values were reproduced using T-matrix simulations, assuming near-spherical shapes, for biomass burning is not itself a verification of the fact that observed particles were indeed transported stratospheric smoke plumes. More information on possible particle composition, and its possible organic origin, should be inferred from other optical measurements (multi-wavelength particle extinction and backscatter measurements).

REPLY: Thank you very much for this comment. Indeed, the origin/composition of the particles cannot be deduced only from the measurements presented in the manuscript (multi-wavelength PLDR and LR measurements). Detailed discussion on the transport of the smoke plumes that are presented in our analysis is included in several previous studies referring to the Canadian wildfires of August 2017. For example, Khaykin et al. (2018) present CALIPSO data that are used to follow the evolution of the plume since two days after the PyroCb eruption on 14 August 2017 (Peterson et al., 2017) to 30 August 2017 (see Fig. 3a in supplement S2 from Khaykin et al., 2018). The ground-based lidar observations at Leipzig on 23 August 2017 presented in the manuscript, observe the smoke plume, which was located above Germany during 21 – 24 August 2017 (Khaykin et al., 2018). In Ansmann et al. (2018), HYSPLIT backward and forward trajectories were used to depict the route of the smoke plume from North America to central Europe and identify the smoke source regions. Results were found to be in good agreement with CALIPSO observations and UV aerosol index maps from OMPS presented in Khaykin et al. (2018). In Hu et al. (2019) MODIS maps, UV aerosol index from OMPS as the CO product from AIRS were used to determine whether the observed aerosol plumes over northern France were indeed smoke transported from Canada. Indeed, the strong spatio-temporal correlation between UV aerosol index and CO revealed the smoke presence. Apart from the high PLDR values measured from the ground-based lidar system in Leipzig, lidar ratio (LR) values are also available at 3 wavelengths and used in our simulations: 40 ± 16sr, 66 ± 12sr, 92 ± 27sr at 355, 532 and 1064nm. Although LR of smoke presents a large variability due to different particle characteristics between fresh and aged smoke particles, these LR values are in good agreement with past measurements for smoke LR at 355 and 532nm (i.e. Fiebig et al., 2002; Muller et al., 2005; Ortiz-Amezua et al., 2017).

References *(that are not included in the initial version of the manuscript)*:

Fiebig, M., Petzold, A., Wandinger, U., Wendisch, M., Kiemle, C., Stifter, A., Ebert, M., Rother, T., and Leiterer, U.: Optical closure for an aerosol column: Method, accuracy, and inferable properties applied to a biomass-burning aerosol and its radiative forcing, J. Geophys. Res., 107, 8130, https://doi.org/10.1029/2000JD000192, 2002.

Ortiz-Amezcua, P., Guerrero-Rascado, J. L., Granados-Muñoz, M. J., Benavent-Oltra, J. A., Böckmann, C., Samaras, S., Stachlewska, I. S., Janicka, L., Baars, H., Bohlmann, S., and AladosArboledas, L.: Microphysical characterization of long-range transported biomass burning particles from North America at three EARLINET stations, Atmos. Chem. Phys., 17, 5931–5946, https://doi.org/10.5194/acp-17-5931-2017, 2017.

3. Because of 2) the proposed approach is rater weak. It is not possible to generalize statements just from a single case study. Moreover, it seems a sort of ill-posed problem and the minimum in Eq. 8 might be relative, i.e. what happens if instead a mono-modal distribution a bimodal is chosen? or a gamma instead of normal distribution? Probably Eq. 8 will provide independently a solution.

REPLY: As discussed in Hansen and Travis (1974), the sensitivity of the optical properties of the particles to different types of size distributions (e.g. standard gamma, log normal, bimodal and a power-law) is limited. Maybe the reviewer is also interested in the answer provided for a similar comment (Comment 11) made by anonymous Reviewer 3.

In the revised version of the manuscript, we have included the following (**page 4, line 20**):

"The fixed width of the size distribution σ_g is again a simplification we used in order to reduce the retrieval complexity, considering that this parameter does not greatly affect the lidar-derived optical properties (e.g. Burton et al., 2016). Choosing a log-normal size distribution over any other plausible type of distribution is not expected to alter our results significantly (Hansen and Travis, 1974)."

Regarding the first part of the comment, we agree with the reviewer. For this reason, we updated the manuscript, including the retrievals for all available measurements of stratospheric smoke in the literature, using the proposed near-spherical model. Figure 1 below presents some examples of successful reproduction of the measurements for all the cases assuming near-spherical shapes, and Table 2 below presents the retrieved values for the mean axial ratio ε_s of the near-spherical shapes, the complex refractive index m and the effective radius $reff$ of the particles. All the retrievals (using near-spherical and Chebyshev particles) are available in the manuscript Supplement (for Hu et al., 2019 fitting of the measurements of 31 August 2017 are presented. For Ohneiser et al., 2020 fitting of the measurements of 8 January 2020 are presented).

Furthermore, we added the following section to the text (**page 8, line 23**):

"Although the available literature on the PLDR and LR values of stratospheric smoke is for now limited, we see that we can reproduce all reported of PLDR and LR using the near-spherical shape model (Table 1-9 and Fig. 1-9 in the Supplement). All cases listed in Table 2 are associated with Pyro-cumulonimbus activity. As already mentioned the case studies of Burton et al. (2015), Hu et al. (2019) and Haarig et al. (2018) refer to Canadian smoke, while the most recent case study presented by Ohneiser et al. (2020) refer to Australian wildfires of 2019-2020. Table 5 present the retrieved mean axial ratio, complex refractive index and geometric radius of the size distribution. For Hu et al. (2019), measurements on 24, 29 and 31 August were reported. For Ohneiser et al. (2020) measurements on 8, 9 and 10 January 2020 were reported."

Table. 1: Reported PLDR and LR values for UTLS smoke. For Hu et al. (2019) and Ohneiser et al. (2020), one of the available observations is included in the table.

	$PLDR_{355}$ (%)	$PLDR_{532}$ (%)	$PLDR_{1064}$ (%)	LR_{355} (sr)	LR_{532} (sr)	LR_{1064} (sr)
Burton et al. (2015)	20.3 ± 3.6	9.3 ± 1.5	1.8 ± 0.2	X	X	X
Hu et al. (2019)	24 ± 4	19 ± 3	5 ± 1	41 ± 7	54 ± 9	X
Ohneiser et al. (2020)	26 ± 5.2	15 ± 1.5	X	53 ± 15.9	76 ± 15.2	X

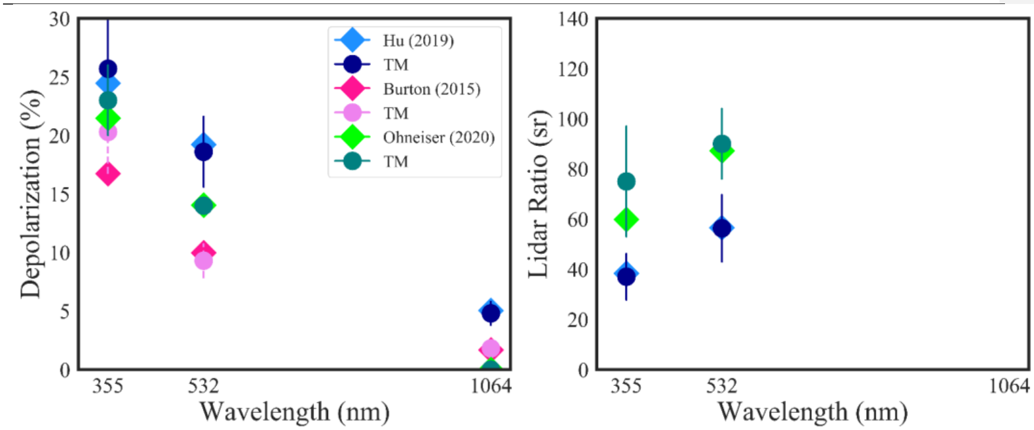

Figure 1. Example fittings of the PLDR and LR measurements presented in Hu et al. (2019), Burton et al. (2015) and Ohneiser at al. (2020), using the near-spherical model. First two cases refer to Canadian wildfires of 2017 and 2014, respectively. The third case refers to the Australian wildfires of last 2019 – 2020. All cases are associated with PyroCb activity. TM in the legend stands for the T-matrix simulations with near-spherical particles: blue circles denote to the simulations reproducing the observations of Hu (2019), pink circles denote the simulations reproducing the observations of Burton (2015), and green

circles denote to the simulations reproducing the observations of Ohneiser (2020). All of the retrievals are included in the manuscript Supplement.

Table 2. The simulations with the near-spherical shape model, used to reproduce the measurements presented in Table 1.

	r_g (μm)	ε_s	m_i	m_r
Burton et al. (2015)	0.3	1.15	0.005	1.45
Hu et al. (2019)	0.25	1.45	0.02	1.55
Ohneiser et al. (2020)	0.35	0.9	0.035	1.45

References *(that are not included in the initial version of the manuscript)*:

Hansen, J.E., Travis, L.D. Light scattering in planetary atmospheres. Space Sci Rev 16, 527–610 (1974). https://doi.org/10.1007/BF00168069

Ohneiser, K., Ansmann, A., Baars, H., Seifert, P., Barja, B., Jimenez, C., Radenz, M., Teisseire, A., Floutsi, A., Haarig, M., Foth, A., Chudnovsky, A., Engelmann, R., Zamorano, F., Bühl, J., and Wandinger, U.: Smoke of extreme Australian bushfires observed in the stratosphere over Punta Arenas, Chile, in January 2020: optical thickness, lidar ratios, and depolarization ratios at 355 and 532 nm, Atmos. Chem. Phys., 20, 8003–8015, https://doi.org/10.5194/acp-20-8003-2020, 2020.

4. As stated by Sassen and Khvorostyanov, smoke can directly act as ice nuclei before liquid clouds form (https://iopscience.iop.org/article/10.1088/1748-9326/3/2/025006). This fact can partially explain *the higher PLDR (considering a process in progress). This aspect, very likely is not mentioned in the manuscript and can be the reason of PLDR increase.*

REPLY: We agree with the reviewer that the PLDR values alone could indicate the formation of ice crystals inside the stratospheric smoke layer. However, the reported PLDR values of ~20% at 532nm are small compared to those usually observed (>40%) for cirrus clouds containing ice crystals (Chen at al., 2002; Noel et al., 2002; Voudouri et al., 2020). Furthermore, the available data from Leipzig include also the lidar ratio (LR) values of 66 ± 12 sr at 532nm. This is similar to the LR observed in the past for aged smoke particles (i.e. Fiebig et al., 2002; Veselovskii et al., 2015; Burton et al., 2012) but quite high for cirrus clouds which present values of the order of 25 sr (Gouveia et al., 2017). A recent study by Yu et al. (2019) also showed that the largest fraction of stratospheric smoke particles consisted of organic carbon (98% compared to 2% for black carbon). Particles of such high organic carbon content serve poorly as ice nuclei (Kanji et al., 2017; Phillips et al., 2013).

We would also like to refer the reviewer to Comment 5 from anonymous Reviewer 3, who raised a similar concern on ice formation.

To highlight this for the reader we included the following in the manuscript **(page 6, line 24):**

"Owning to the altitude of the smoke plume, one could attribute such PLDR values to the beginning of ice formation. Indeed, radiosonde temperature profiles from three stations located underneath the smoke plume (green stars in Fig.3b), reveal that the temperature above 11 km drops below -40C, at which point homogeneous ice formation can occur (Wallace and Hobbs, 2006). However, the PLDR values of cirrus clouds are usually no less than 40% (Chen at al., 2002; Noel et al., 2002; Voudouri et al., 2020). A recent study by Yu et al. (2019) also showed that the largest fraction of stratospheric smoke particles consisted of organic carbon (98% compared to 2% for black carbon). Particles of such high organic carbon content serve poorly as ice nuclei (Kanji et al., 2017; Phillips et al., 2013). Although the possibility of small ice crystals formed inside the smoke layers cannot be excluded, (largely due to the absence of in situ measurements) the aforementioned characteristics indicate that this plume consists of smoke particles rather than ice crystals.”

References *(that are not included in the initial version of the manuscript)*:

Burton, S. P., Ferrare, R. A., Hostetler, C. A., Hair, J. W., Rogers, R. R., Obland, M. D., Butler, C. F., Cook, A. L., Harper, D. B., and Froyd, K. D.: Aerosol classification using airborne High Spectral Resolution Lidar measurements – methodology and examples, Atmos. Meas. Tech., 5, 73–98, https://doi.org/10.5194/amt-5-73- 2012, 2012.

Chen WN, Chiang CW, Nee JB. Lidar ratio and depolarization ratio for cirrus clouds. *Appl Opt.* 2002;41(30):6470-6476. doi:10.1364/ao.41.006470

Fiebig, M., Petzold, A., Wandinger, U., Wendisch, M., Kiemle, C., Stifter, A., Ebert, M., Rother, T., and Leiterer, U.: Optical closure for an aerosol column: Method, accuracy, and inferable properties applied to a biomass-burning aerosol and its radiative forcing, J. Geophys. Res., 107, 8130, https://doi.org/10.1029/2000JD000192, 2002.

Gouveia, D. A., Barja, B., Barbosa, H. M. J., Seifert, P., Baars, H., Pauliquevis, T., and Artaxo, P.: Optical and geometrical properties of cirrus clouds in Amazonia derived from 1 year of ground-based lidar measurements, Atmos. Chem. Phys., 17, 3619–3636, https://doi.org/10.5194/acp-17-3619-2017, 2017.

Kanji, Z. A., Ladino, L. A., Wex, H., Boose, Y., Burkert-Kohn, M., Cziczo, D. J., and Krämer, M.: Chapter 1: Overview of ice nucleating particles, Meteor Monogr., Am. Meteorol. Soc., 58, 1.1-1.33, https://doi.org/10.1175/amsmonographs-d-16-0006.1, 2017.

Noel, V., Chepfer, H., Ledanois, G., Delaval, A., and Flamant, P.: Classification of Particle Effective Shape Ratios in Cirrus Clouds Based on the Lidar Depolarization Ratio, Appl. Optics, 41, 4245–4257, https://doi.org/10.1364/AO.41.004245, 2002.

Phillips, V. T. J., P. J.Demott, C.Andronache, K. A.Pratt, K. A.Prather, R.Subramanian, and C.Twohy, 2013: Improvements to an empirical parameterization of heterogeneous ice nucleation and its comparison with observations. J. Atmos. Sci., 70, 378–409, doi:https://doi.org/10.1175/JAS-D-12-080.1.

Veselovskii, I., Whiteman, D. N., Korenskiy, M., Suvorina, A., Kolgotin, A., Lyapustin, A., Wang, Y., Chin, M., Bian, H., Kucsera, T. L., Pérez-Ramírez, D., and Holben, B.: Characterization of forest fire smoke event near Washington, DC in summer 2013 with multi-wavelength lidar, Atmos. Chem. Phys., 15, 1647– 1660, https://doi.org/10.5194/acp-15-1647-2015, 2015.

Voudouri, K. A., Giannakaki, E., Komppula, M., and Balis, D.: Variability in cirrus cloud properties using a Polly^{XT} Raman lidar over high and tropical latitudes, Atmos. Chem. Phys., 20, 4427–4444, https://doi.org/10.5194/acp-20-4427-2020, 2020.

5) The simulations themselves are not original as in fact similar simulations were performed in the past by Bi et al. 2018, Mishchenko et al. 2016; Ishimoto et al., 2019, as the authors explicitly admit. What is different with respect to those manuscript?

REPLY: Bi et al. (2018) is an interesting modeling study on the properties of spheroid and super-ellipsoid particles for a large suite of refractive indices and size parameters. It is though a generic study, not focused on stratospheric smoke particles. Also, the simulations in Bi et al. (2018) refer only to PLDR and not to other intensive properties (e.g. LR) as we do in our study. On the other hand, Mishchenko et al. (2016) used four different models to reproduce the PLDR values observed by Burton et al., (2015).

Our results are comparable, but the study is only limited to PLDR since there were no available LR measurements at the time. Ishimoto et al. (2019) use fractal aggregates coated by water soluble materials. In this study both the PLDR and LR are examined, but the simulations refer only to monodisperse particles. The results are comparable to ours only for coated fractals, producing a shape that closely resembles the near-spherical shape (i.e. shapes of “Type-B, size 11, Vr = 20” shown in Fig. 4 of Ishimoto et al. 2019).

In our study we propose a simple model of compact near-spherical particles, that can reproduce both the PLDR and LR values measured by sophisticated lidar systems, part of the EARLINET, that are capable of providing quality-assured retrievals for stratospheric smoke particles. We further examine whether this model could be used on an operational level to extend the AERONET retrieval scheme. The introduction of the manuscript has been updated in order to present how our research is differentiated by previous research (**page 3, line 9**):

“In contrast to prior studies, for our investigation for the stratospheric smoke originating from the Canadian wildfires, we do not adopt morphologically complex shapes of bare or coated smoke aggregates, which are associated with excessive computations. Instead, we propose a much simpler model of compact near-spherical particles. Our starting point and main assumption is that the particle near-spherical-shape can be highly depolarizing, as shown in the work of Mishchenko and Hovenier (1995) and Bi et al. (2018). Our analysis shows that for the Canadian stratospheric smoke observed above Europe in August 2017, the PLDR and LR measurements along with their spectral dependence, can be successfully reproduced with the proposed model of compact near-spherical particles. The size and refractive index of the particles are estimated as well, and seem to agree well with past observations for aged smoke. We further examine the capability of this model to be used on an operational level and in particular as an extension to the AERONET operational aerosol retrieval (Dubovik et al., 2006), since it provides a much simpler and faster solution with respect to more complicated shapes for stratospheric smoke particles (e.g. Mishchenko et al.,2016; Ishimoto et al., 2019)."

6) The title (i found it funny) might be misinterpreted and considered inappropriate.

REPLY: Thank you for your comment.

We reply to specific comments in the attached manuscript below:

Page 1, line 15: *We added: "of axial ratio 0.7 to 1.5"*

Page 2, line 1: We rephrased to: "Smoke particles in the atmosphere can be identified with lidar measurements which provide valuable information on the optical properties of aerosol particles, such as the depolarization of the backscattered light in terms of the particle linear depolarization ratio (PLDR)."

Page 9, line 4: please see response to Comment 3.

Response to Anonymous Reviewer 2

The authors use an example of transported stratospheric smoke from the 2017 Canadian wildfire pyroCB to model the spectral dependence of depolarization and lidar ratio at 355, 532, and 1064 nm. Near-spherical, Chebyshev, and fractal shapes are used, but only the near-spherical shapes are able to match the results obtained from lidar measurements. The subject is quite relevant and the results could be very significant for scientific community. However, there are some issues with the manuscript which must be clarified before it is suitable for publication. Examples are provided below:

REPLY: Thank you very much for your helpful comments. Please find our point-by-point response below.

Remark: The figure numbers and the page numbers in the referee comments and in our replies correspond to the original manuscript

1. Firstly, the title implies that the near spherical shape may be the "new black" for smoke. However, the case study focuses on a stratospheric smoke case. It follows to ask if this is only the "new black" for smoke in the stratosphere only or should we assume this might apply to the troposphere also? From the example shown, my guess is no.

REPLY: Thank you for this question. To the best of our knowledge, up to now the majority of the cases reported for smoke particle linear depolarization ratio (PLDR) approximating 20% at 532nm, refer to smoke found in the stratosphere. The sole exception is the case study reported in Burton et al. (2015) for a smoke plume found at 8km height. All the cases were associated with PyroCb activity and all are indicative of high depolarization values in both troposphere and stratosphere, this is why we didn't separate in the title. We make sure we mention this throughout the revised manuscript and we further included the following to make this more obvious to the reader (**page 7, line 24**):

"To the best of our knowledge, up to now the majority of observations for such smoke PLDR values, refer to smoke particles found in the stratosphere (i.e. Ohneiser et al., 2020). The sole exception is the case study reported by Burton et al. (2015) (see also Table 2). "

2. Page 3, Line 10: Is the spectral dependence really non-typical? The authors do a good job of convincing us that the high depolarization values are non-typical for smoke, but spectral dependence seems the opposite. In fact, decreasing depolarization with increasing wavelength is closer to typical from the references cited by the authors.

REPLY: We agree with the reviewer that this statement should be reworded, primarily because there is still limited amount of information on such case studies for smoke. The only cases that up to now have reported observations at three lidar wavelengths are Haarig et al. (2018), Hu et al. (2019) and Burton et al. (2015). The first two refer to the same case of British Columbia fires of 2017, while the last one refers to the Pacific Northwest fires of 2014. There is a notable difference in PLDR values at 532nm reported from Haarig and Hu (~18%), compared to those reported from Burton (~9%), but still this may not be sufficient information to characterize the spectral dependence as non-typical.

The following has been re-worded in the manuscript in order to highlight this comment (**page 3, line 10**):

"In contrast to prior studies, for our investigation for the stratospheric smoke originating from the Canadian wildfires, we do not adopt morphologically complex shapes of bare or coated smoke aggregates, which are associated with excessive computations. Instead, we propose a much simpler model of compact near-spherical particles. Our starting point and main assumption is that the particle near-spherical-shape can be highly depolarizing, as shown in the work of Mishchenko and Hovenier (1995) and Bi et al. (2018).

Our analysis shows that for the Canadian stratospheric smoke observed above Europe in August 2017, the PLDR and LR measurements along with their spectral dependence, can be successfully reproduced with the proposed model of compact near-spherical particles."

3. Page 3, Line 12: Something is missing from this sentence or perhaps the wording is intended to be: The starting point and main assumption of our investigation is that the particle near-spherical-shape can be highly depolarizing as shown in the work of Mishchenko and Hovenier (1995); Mishchenko et al. (2016); Bi et al. (2018) and Ishimoto et al. (2019).

REPLY: Thank you, we have rephrased the following in the revised manuscript (**page 3, line 12**):

"Our starting point and main assumption is that the particle near-spherical-shape can be highly depolarizing, as shown in the work of Mishchenko and Hovenier (1995) and Bi et al. (2018). "

4. Figure 2: The images seem to be incorrectly placed, given the aspect ratios. Oblate sphere should be flattened and prolate stretched.

REPLY: Thank you for noticing this, the figure has been updated.

5. Page 6, Line 20 - 26 and Figure 6: The latitude limits in the text do not match those in the Figure and the red dashed lines do not match the section highlighted in Figure 4. But even more importantly, the corresponding browse images indicate a complex mixture of aerosol and ice from cirrus clouds which would explain the high depolarization ratios in these cases.

https://www.calipso.larc.nasa.gov/products/lidar/browse_images/show_detail.php?s=production&v=V4-10&browse_date=2017-08-15&orbit_time=17-55-33&page=3&granule_name=CAL_LID_L1-Standard-V4-10.2017-08-15T17-55-33ZD.hdf

https://wwwcalipso.larc.nasa.gov/products/lidar/browse_images/show_detail.php?s=production&v=V4-10&browse_date=2017-08-15&orbit_time=17-55-33&page=4&granule_name=CAL_LID_L1-Standard-V4-10.2017-08-15T17-55-33ZD.hdf

REPLY: Figure 6 has been corrected. Regarding the next part of the question, CALIOP measurements at the northeastern Canada on 15 August 2017 (https://www-calipso.larc.nasa.gov/products/lidar/browse_images/show_v4_detail.php?s=production&v=V4-10&browse_date=2017-08-15&orbit_time=17-55-33&page=3&granule_name=CAL_LID_L1-Standard-V4-10.2017-08-15T17-55-33ZD.hdf), show the stratospheric smoke layer at 11-14.5 km, where radiosonde measurements show temperatures below -40°C (Fig. 1 below). The radiosonde temperature profiles are from three stations close to the position of the smoke plume (Fig. 4b in manuscript): Churchill (Lat: 58.73, Lon: -94.08), Inukjuak (Lat: 58.45, Lon: -78.11) and Baker Lake (Lat: 64.31, Lon: -96.00). Moreover, the ground-based lidar measurements on 23 August 2017 at Leipzig, show the stratospheric smoke layer at 14-16 km, where radiosonde measurements from the closest station (Lindenberg) provide temperatures below -50°C. Indeed, at such low temperatures homogenous ice formation can occur (Wallace and Hobbs, 2006; Fig. 6.29).

However**,** the CALIOP PLDR values are below 20% both for the aforementioned overpass and for the closest overpass from Leipzig on 23 August 2017 (https://www-calipso.larc.nasa.gov/products/lidar/browse_images/show_v4_detail.php?s=production&v=V4-10&browse_date=2017-08-23&orbit_time=01-29-01&page=1&granule_name=CAL_LID_L1-Standard-V4-10.2017-08-23T01-29-01ZN.hdf(~90 km away and approximately 1 hour after the end of the ground based lidar measurements reported from Haarig et al., 2018), while the attenuated color ratio (i.e., the ratio of particle backscatter coefficient at 532nm to particle backscatter coefficient at 1064nm) is below 1. Further analysis of CALIOP data provides a mean (median) value of the backscatter related Angstrom exponent at 532/1064nm of 0.9 (0.9) with a standard deviation on 1.07. For PLDR, typical values for cirrus clouds are usually no less than 40% (Chen at al., 2002; Noel et al., 2002; Voudouri et al., 2020) and the color ratio is expected to be close to 1 due to the large size of ice crystals compared to the lidar wavelengths. For the Angstrom exponent values close to zero are expected, although, as indicated by the large standard deviation, CALIPSO data are highly noisy at these altitudes

Moreover, for the overflight close to Leipzig on 23 August 2017, the lidar ratio (LR) measured from the ground-based system is (66 ± 12) sr at 532nm. This is similar to the LR observed in the past for aged smoke particles (i.e. Fiebig et al., 2002; Veselovskii et al., 2015; Burton et al., 2012) but quite high for cirrus clouds (Gouveia et al., 2017).

Based on the above, although we cannot exclude the possibility of small ice crystals formed inside the stratospheric plume, we believe that the aforementioned characteristics indicate that this is not an ice cloud but rather a large smoke plume.

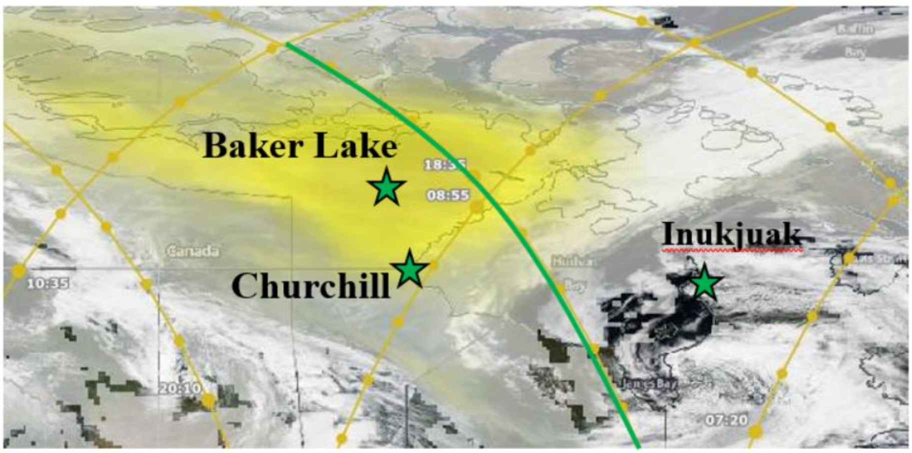

Figure 1. Corrected surface reflectance from MODIS on 15 August 2017, over-plotted with the PyroCb aerosol index product from Suomi NPP/OMPS (in yellow). Green stars indicate the position of the radiosonde stations used, while the green line marks the CALIPSO overflight during 18:22 – 18:35 UTC. The map is generated from the NASA Worldview Snapshots.

Figure 2. Same as Fig. 1 but for 23 August 2017. The CALIPSO overflight is approximately 90 km from Leipzig station, at 01:23 – 01:48 UTC, 1 hour after the end of the ground based lidar measurements.

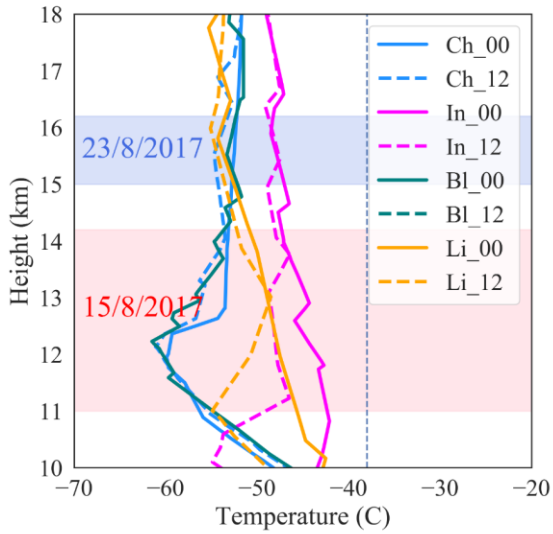

Figure 3. Radiosonde temperature (T) profiles from Churchill (Ch), Inukjuak (In), Baker Lake (Bl) and Lindenberg stations. Solid lines denote the measurements at 00:00 UTC, while dashed lines the measurements at 12:00 UTC. For the first three stations (Ch, In, Bl) measurements from 15 August 2017 are used, while for Li station from 23 August 2017. The pink box indicates the height of the smoke plume above northeastern Canada (11 -14 km) and the blue box the height of the plume after 8 days above Leipzig station (15 - 16 km).

To highlight this comment, we included the following paragraph in the revised manuscript: **(page 6, line 24)**:

"Owning to the altitude of the smoke plume, one could attribute such PLDR values to the beginning of ice formation. Indeed, radiosonde temperature profiles from three stations located underneath the smoke plume (green stars in Fig.3b), reveal that the temperature above 11 km drops below -40C, at which point homogeneous ice formation can occur (Wallace and Hobbs, 2006). However, the PLDR values of cirrus clouds are usually no less than 40% (Chen at al., 2002; Noel et al., 2002; Voudouri et al., 2020). Further analysis of CALIOP data provides a mean (median) value of the backscatter related Angstrom exponent (BAE) at 532/1064nm of 0.9 (0.9) with a standard deviation on 1.07. For the BAE values close to zero are expected for cirrus clouds, although, as indicated by the large standard deviation, CALIPSO data are highly noisy at these altitudes. A recent study by Yu et al. (2019) also showed that the largest fraction of stratospheric smoke particles consisted of organic carbon (98% compared to 2% for black carbon). Particles of such high organic carbon content serve poorly as ice nuclei (Kanji et al., 2017; Phillips et al., 2013). Although the possibility of small ice crystals formed inside the smoke layers cannot be excluded, (largely due to the absence of in situ measurements) the aforementioned characteristics indicate that this plume consists of smoke particles rather than ice crystals."

References *(that are not included in the initial version of the manuscript)*:

Burton, S. P., Ferrare, R. A., Hostetler, C. A., Hair, J. W., Rogers, R. R., Obland, M. D., Butler, C. F., Cook, A. L., Harper, D. B., and Froyd, K. D.: Aerosol classification using airborne High Spectral Resolution Lidar measurements – methodology and examples, Atmos. Meas. Tech., 5, 73–98, https://doi.org/10.5194/amt-5-73- 2012, 2012.

Chen WN, Chiang CW, Nee JB. Lidar ratio and depolarization ratio for cirrus clouds. *Appl Opt*. 2002;41(30):6470-6476. doi:10.1364/ao.41.006470

Fiebig, M., Petzold, A., Wandinger, U., Wendisch, M., Kiemle, C., Stifter, A., Ebert, M., Rother, T., and Leiterer, U.: Optical closure for an aerosol column: Method, accuracy, and inferable properties applied to a biomass-burning aerosol and its radiative forcing, J. Geophys. Res., 107, 8130, https://doi.org/10.1029/2000JD000192, 2002.

Gouveia, D. A., Barja, B., Barbosa, H. M. J., Seifert, P., Baars, H., Pauliquevis, T., and Artaxo, P.: Optical and geometrical properties of cirrus clouds in Amazonia derived from 1 year of ground-based lidar measurements, Atmos. Chem. Phys., 17, 3619–3636, https://doi.org/10.5194/acp-17-3619-2017, 2017.

Kanji, Z. A., Ladino, L. A., Wex, H., Boose, Y., Burkert-Kohn, M., Cziczo, D. J., and Krämer, M.: Chapter 1: Overview of ice nucleating particles, Meteor Monogr., Am. Meteorol. Soc., 58, 1.1-1.33, https://doi.org/10.1175/amsmonographs-d-16-0006.1, 2017.

Noel, V., Chepfer, H., Ledanois, G., Delaval, A., and Flamant, P.: Classification of Particle Effective Shape Ratios in Cirrus Clouds Based on the Lidar Depolarization Ratio, Appl. Optics, 41, 4245–4257, https://doi.org/10.1364/AO.41.004245, 2002.

Phillips, V. T. J., P. J.Demott, C.Andronache, K. A.Pratt, K. A.Prather, R.Subramanian, and C.Twohy, 2013: Improvements to an empirical parameterization of heterogeneous ice nucleation and its comparison with observations. J. Atmos. Sci., 70, 378–409, doi:https://doi.org/10.1175/JAS-D-12-080.1.

Veselovskii, I., Whiteman, D. N., Korenskiy, M., Suvorina, A., Kolgotin, A., Lyapustin, A., Wang, Y., Chin, M., Bian, H., Kucsera, T. L., Pérez-Ramírez, D., and Holben, B.: Characterization of forest fire smoke event near Washington, DC in summer 2013 with multi-wavelength lidar, Atmos. Chem. Phys., 15, 1647– 1660, https://doi.org/10.5194/acp-15-1647-2015, 2015.

Voudouri, K. A., Giannakaki, E., Komppula, M., and Balis, D.: Variability in cirrus cloud properties using a Polly^{XT} Raman lidar over high and tropical latitudes, Atmos. Chem. Phys., 20, 4427–4444, https://doi.org/10.5194/acp-20-4427-2020, 2020.

Wallace, J.M., Hobbs, P.V. Atmospheric Science: An Introductory Survey: Second Edition (2006), DOI: 10.1016/C2009-0-00034-8

6. The images from Haarig et al 2018 are more convincing for the case the authors are making. Perhaps another CALIPSO image should be used if the authors would like to show satellite measurements.

REPLY: We improved the images to better demonstrate our arguments.

7. Page 8, Line 12-13: The authors state: What is interesting here is that the retrieved sizes for near-spherical smoke particles are absent in the AERONET climatology product. However, the difference in using a mono-modal versus bi-modal distribution is something that should be explored or at least discussed more in the text. Are we seeing the result of an "effective" radius in a mon-modal distribution that presents a possible solution for the high depolarization and spectral dependence, when there could also be another solution obtained from a mixture in a bi-modal distribution?

REPLY: Thank you for this comment. We have provided a reply to a similar comment made by anonymous Reviewer 1: Regarding the kind of the distribution used, as discussed in Hansen and Travis (1974), the sensitivity of the optical properties of the particles to the type of the size distribution is limited. Regarding the second (coarse) mode, similar simulations presented by Bi et al., (2018; Fig 2), suggest that for near-spherical particles the measured spectral dependence of PLDR could not be reproduced by coarse mode particles. Thus, an optically significant coarse mode would have to be investigated with a different shape model. Maybe the reviewer is further interested in the answer provided for Comment 11 made by anonymous Reviewer 3.

In the revised version of the manuscript, we have also included the following paragraph (**page 4, line 20**): "The fixed width of the size distribution σ_g is again a simplification we used in order to reduce the retrieval complexity, considering that this parameter does not greatly affect the lidar-derived optical properties (e.g. Burton et al., 2016). Choosing a log-normal size distribution over any other plausible type of distribution is not expected to alter our results significantly (Hansen and Travis, 1974)."

References *(that are not included in the initial version of the manuscript)*:

Hansen, J.E., Travis, L.D. Light scattering in planetary atmospheres. Space Sci Rev 16, 527–610 (1974). https://doi.org/10.1007/BF00168069

8. Sections 4.2 and 4.3: Is this all that can be said for these solutions... we tried these shapes and they didn't work? It would seem that more could be gleaned from these failed attempts. For instance, these shapes show the correct trend in spectral dependence even though the absolute values/relative differences do not fit the measurements.

REPLY: We would like to thank the reviewer for this comment. Updated discussion on the results for Chebyshev particles has been included in the manuscript ***page 5, line 4***):

"For Chebyshev particles of second (T_2) and fourth degree (T_4) used herein, the search in the constructed look-up-tables provided the solutions listed in Table 4. For all the solutions, deformation parameter for Chebyshev particles of the second degree ranges from u = –0.25 to 0.15, while for particles of the fourth degree only one solution was found with u = -0.1. These u values suggest small deviations from sphericity, meaning that these morphologies also resemble near-spherical shapes. Only for two cases the size of the particles was found to be larger than for the near-spherical shaped particles. In particular r_g ranges from 0.15μm ($reff$ = 0.2μm) to 0.55μm ($reff$ = 0.8μm). For the complex refractive index, values in some cases exceed the corresponding values for near-spherical particles. The imaginary part m_i ranges from i0.005 to i0.055,and the real part m_r ranges from 1.35 to 1.8. The minimization of the cost function (Eq. 8) is achieved for Chebyshev particles of the second degree with u = -0.25 (resembling an oblate near-spherical particle), complex refractive index m = 1.65 + i(0.03) and mean geometric radius r_g = 0.2μm. For Chebyshev particles of the fourth degree, the sole solution presented values u = -0.1, m = 1.35 + i(0.01) and r_g = 0.55μm. All possible solutions as well as those that minimize the cost function are presented in Fig. 10 and 11."

We decided to remove fractal aggregates from the present study, since as pointed out by Anonymous Reviewer 3 the range of the parameters used in our study to model fractal aggregates was limited.

9. Page 9, Line 18: Can the authors offer an explanation for the low angstrom exponents other than coarse particles?

REPLY: We have provided an answer to a similar comment made by anonymous Reviewer 3. We summarize also here: According to Eck et al. (1999), the strong curvature between the extinction related Angstrom exponent (EAE) at 355/532nm (-0.3 ± 0.4) and the corresponding values at 532/1064nm (0.85 ± 0.3) can be attributed to the pronounced accumulation mode of the size distribution, which is in good agreement with the retrieved size distribution for near-spherical particles of $reff$ = 0.38μm. Another possible reason could be a spectrally-dependent absorption, although this is not shown in our results due to the assumed spectrally-independent value of the imaginary part of refractive index. To address this comment we added the following paragraph to the manuscript (**page 8, line 22**):

"We note here that all the retrievals indicate fine particles, with mean geometric radius that does not exceed the value of 0.35μm. The simulations presented by Bi et al., (2018; Fig. 2) suggest that for the near-spherical particles the measured spectral dependence of PLDR (steeply decreasing from the UV to the Near-IR) could not be reproduced by coarse particles. Thus, the possibility of an optically significant coarse mode would have to be investigated with a different shape model. In any case though, the retrieved fine mode is in good agreement with in-situ measurements of aged smoke particles (i.e. Dahlkoetter et al., 2014). The presence of a pronounced accumulation mode is also suggested by the extinction related Angstrom exponent (EAE) measured in Leipzig (-0.3±0.4 at 355/532nm and 0.85 0.3 at 532/1064nm). According to Eck et al. (1999), a strong spectral slope in EAE can be associated with a prominent accumulation mode of the size distribution for smoke particles”

References *(that are not included in the initial version of the manuscript)*:

Eck, T. F., Holben, B. N., Reid, J. S., Dubovik, O., Smirnov, A., O’Neill, N. T., Slutsker, I., and Kinne, S.: Wavelength dependence of the optical depth of biomass burning, urban, and desert dust aerosols, Journal of Geophysical Research: Atmospheres, 104, 31333-31349, 10.1029/1999JD900923, 1999.

Response to Anonymous Reviewer 3

General comments:

The more frequent occurrence of pyro-Cb smoke plumes lofted into the stratosphere is a rich target for analysis into a kind of aerosol about which we know relatively little. I'm particularly interested to see apparently successful modeling of three-wavelength values of both linear particle depolarization ratio and lidar ratio from lidar measurements of one such plume. This is a new result and potentially quite useful, since previous particle modeling studies did not have access to such a complete lidar observation and also because they, in general, resorted to much more complicated models than what the current authors have found to be useful. So, for this reason, primarily, I would like to see this paper published. On the other hand, many aspects of the manuscript seem rather weak and unconvincing, so I believe major revisions are appropriate.

REPLY: We thank very much Reviewer #3 for his/her careful reading, comments and suggestions, which we address in the following. With his/her suggestions, we believe that the new version of the manuscript is significantly improved, and our findings are promoted in a better way. The author's answers along with the changes in the manuscript are listed below.

Remark: The figure numbers and the page numbers in the referee comments and in our replies correspond to the original manuscript.

First, the discussion and elimination of other models is not convincing. It may not be strictly necessary to show that other models perform worse if the near-spherical model is able to reproduce all the available measurements (because a simple model that fits all the observations has benefits over a more complicated *model just by virtue of being simpler), but since an attempt is made to do so, it should be done thoroughly and correctly.*

REPLY: We thank the reviewer for this comment. We added a more extensive discussion in the introduction on how our study differentiates for previous studies. Please see specific comments 3, 10 and 14 for the detailed changes according to this comment.

Second, an unsubstantiated claim is made that this could improve AERONET retrievals. The idea of the new model improving or complementing AERONET is potentially quite appealing, and if done right this could be a major focus of the paper, so again it should be addressed thoroughly, not haphazardly.

REPLY: We thank the reviewer for this very constructive comment. We improved the manuscript following the Reviewer's suggestions. Please refer to response for specific comment 13.

Finally, the speculation about the role of sulfuric acid for explaining the depolarization measurements seems a bit far-fetched and very difficult to validate while other potential explanations have not been adequately discussed. In my opinion, this is the weakest part of the manuscript and the best solution may be to simply not offer explanations for the shape at all, but rather to present this work as an advancement in the modeling of the optical properties alone. Otherwise, if the authors want to keep this, then a better, more thorough discussion of alternate theories and ways to distinguish between theories is needed.

REPLY: We thank the reviewer for this comment. At the current stage the discussion on the possible physical explanation for the smoke PLDR values is removed from the manuscript. More efforts will be made to investigate this issue and re-assess the possible coexistence of smoke particles and particles of sulfuring nature and whether this could affect the former in such a way to form near-spherical particles.

Specific comments:

1. page 3, line 10: *I think rather than "an explanation that could justify" the values, you're more fundamentally searching for "a model that can reproduce" the observations. This is a more precise statement of what this calculation is able to do and valuable enough at this stage.*

REPLY: Thank you for this comment, please find our answer below.

2. page 3, line 10. *"non-typical spectral dependence". What do you mean non-typical? Compared to what? It's my understanding that there are only a very small number of observations of three wavelengths of smoke particle linear depolarization ratio and not much discussion of two-wavelength observations. So, how do we know what spectral dependence is typical?*

REPLY: We thank the reviewer, we rephrased the following paragraph in order better position our research and to highlight the two comments above (**page 3, line 9**):

In contrast to prior studies, for our investigation for the stratospheric smoke originating from the Canadian wildfires, we do not adopt morphologically complex shapes of bare or coated smoke aggregates, which are associated with excessive computations. Instead, we propose a much simpler model of compact near-spherical particles. Our starting point and main assumption is that the particle near-spherical-shape can be highly depolarizing, as shown in the work of Mishchenko and Hovenier (1995) and Bi et al. (2018). Our analysis shows that for the Canadian stratospheric smoke observed above Europe in August 2017, the PLDR and LR measurements along with their spectral dependence, can be successfully reproduced with the proposed model of compact near-spherical particles. The size and refractive index of the particles are estimated as well, and seem to agree well with past observations for aged smoke. We further examine the capability of this model to be used on an operational level and in particular as an extension to the AERONET operational aerosol retrieval (Dubovik et al., 2006), since it provides a much simpler and faster solution with respect to more complicated shapes for stratospheric smoke particles (e.g. Mishchenko et al.,2016; Ishimoto et al., 2019)."

3. Besides just listing three papers at page 3, line 14, the introduction should discuss how this study is similar and different to the modeling studies in those and other papers, including those that use other modelled particle shapes other than near-spherical. Besides the 3 references listed, consider Kahnert (2017), Liu and Mishchenko (2018), Kanngießer and Kahnert (2018), Ceolato et al. (2018), and Luo et al. (2019) (some of these are mentioned later in the manuscript but not the introduction). Also Mishchenko et al. (2016) used multiple particle shapes, not just the near-spherical.

REPLY: Thank you for your comments, an updated discussion has been included in the introduction to point how our study is different from the previous work. We specifically added the following paragraph (**page 2, line 25**):

"In the past, many studies have used simpler or more complicated particle shape models in order to reproduce the lidar measurements of smoke and provide a physical insight on light interaction with these particles. In Kahrent (2017), the PLDR of black carbon aggregates covered by a cell of sulphates was simulated by two different models; a closed cell (i.e. each monomer in the aggregate is coated separately) and a coated aggregate model (i.e. the whole aggregate is coated). Their analysis showed that for thicker coating the coated cell model of volume equivalent radius of 0.3 to 0.4μm, can provide PLDR values of the order of 15% at 532nm. Mishchenko et al. (2016) and Liu and Mishchenko (2018) used rather complex morphologies for smoke particles, in order to reproduce the PLDR values measured by Burton et al. (2015). Amongst others, these morphologies included a) a fractal aggregate partially embedded in a spherical sulphate cell, b) two-externally-mixed spherical sulphate cells, each hosting an aggregate (models 6 and 11 in Fig. 1 in Liu and Mishchenko, 2018) and c) a high-density aspherical soot core, encapsulated in a circumscription spheroid cell (with axial ratio of 0.9 to 1.2; model 4 in Fig. 2 in Mishchenko et al., 2016). All these morphologies reproduced successfully the smoke optical properties measured by Burton et al. (2015). Moreover, Luo et al. (2019) used twenty different configurations of coated fractal aggregates and showed that for relatively small fractal dimension (i.e. relatively fresh aggregates), and for small black carbon fractions (i.e. densely coated aggregates; configuration C in Fig. 2 in Luo et al. (2019)), the PLDR values can reach up to 40, 15 and 6% at 355, 532 and 1064nm, respectively. Ishimoto et al. (2019) used fractal aggregates and artificial surface tension induced on the particles to mimic the effect of coating by water soluble materials forming around the particles. This particular study present results for both the PLDR and the lidar ratio (LR), which is indicative of the composition of the particles. In Liu and Mishchenko (2019), tar ball aggregates were used to model exceptionally strong PLDR as those measured by Burton et al. (2015). The aforementioned studies highlighted the fact that that in order to reproduce significant PLDR values (higher than 20% at 532nm), the fractals need to be coated (i.e. shapes of "Type-B, size 11, Vr = 20" shown in Fig. 4 of Ishimoto et al. 2019). We should point out though that most of them refer to monodispersed particles, and averaging over size could possibly supress some of the observed features.".

References *(that are not included in the initial version of the manuscript)*:

Kahnert, M.: Optical properties of black carbon aerosols encapsulated in a shell of sulfate: comparison of the closed cell model with a coated aggregate model, Optics Express, 25, 24579-24593, 10.1364/OE.25.024579, 2017.

Kanngießer, F., and Kahnert, M.: Calculation of optical properties of light-absorbing carbon with weakly absorbing coating: A model with tunable transition from film-coating to spherical-shell coating, Journal of Quantitative Spectroscopy and Radiative Transfer, 216, 17-36, https://doi.org/10.1016/j.jqsrt.2018.05.014, 2018.

Liu, L., and Mishchenko, M.: Scattering and Radiative Properties of Morphologically Complex Carbonaceous Aerosols: A Systematic Modeling Study, Remote Sensing, 10, 1634, 2018.

Luo, J., Zhang, Q., Luo, J., Liu, J., Huo, Y., and Zhang, Y.: Optical Modeling of Black Carbon with Different Coating Materials: The Effect of Coating Configurations, Journal of Geophysical Research: Atmospheres, 124, 13230-13253, doi:10.1029/2019JD031701, 2019.

4. How are the ranges arrived at that are shown in Table 1, and also specifically the fixed values for the distribution widths?

REPLY: The fixed width of the size distribution is a simplification we used in order to reduce the retrieval complexity, considering that this parameter does not greatly affect the lidar-derived optical properties (e.g. Burton et al., 2016). We specifically chose the fixed σ_g = 0.4 to represent a moderately wide size distribution.

The fixed width of the shape distribution σ_s is also necessary for the reduction of the retrieval complexity. A small value of this width is used to avoid the wash-out of the characteristic optical properties of near-spherical particles which are shown for a relatively narrow aspect ratio range (e.g. Bi et al., 2018).

For the other microphysical properties used as inputs for the T-matrix calculations, the ranges were selected based on the ranges found in the literature for smoke particles. More specifically, in Muller et al. (2005) for aged Canadian and Siberian smoke, values of effective radius $reff$ from 0.16 (± 0.04) to 0.41 (± 0.14)μm, and real part of the refractive index m_r values of 1.37 (± 0.04) to 1.65 (± 0.03) were retrieved from 3b + 2a lidar data inversion. In a following study by Muller et al. (2007) the $reff$ of one-day-old smoke plumes was found to be 0.13 (± 0.04)μm, while for 18-day-old smoke plumes, the $reff$ was much larger, equal to 0.37 (± 0.06)μm. Nicolae et al. (2013), combined lidar measurements and mass spectroscopy for 3/4-day-old SW Romanian smoke, and derived an $reff$ of 0.19 (± 0.11)μm, while for 3-old Ukraine smoke the corresponding value was 0.40 (± 0.12)μm. For the same case studies, the complex refractive index values spanned from m = 1.41 (± 0.07) + i0.005 (± 0.003) to m = 1.66 (± 0.09) + i0.05 (± 0.01). In Giannakaki et al. (2015) for South Africa smoke, the $reff$ values derived from lidar data inversion at 355nm spanned from 0.11 to 0.28μm, and the complex refractive index values were derived to be m = 1.43 (± 0.07) + i0.016 (± 0.01). In Dubovik et al. (2002), the climatological mean value of the complex refractive index derived from AERONET measurements for tropospheric smoke in the United States and Canada is m = 1.5 (± 0.05) + i0.0094 (± 0.003).

To cover the range of the reported values in the studies listed above, in the initial version of the manuscript we used ranges shown in Table.1. For the revised version, we further extended the refractive index values as follows: m_r= 1.35 – 1.85 and m_i = 0.005 – 0.55.

We included the information above in the revised manuscript (page 3, lines 24 - 26 and page 18, Table 1).

References *(that are not included in the initial version of the manuscript)*:

Burton, S. P., Chemyakin, E., Liu, X., Knobelspiesse, K., Stamnes, S., Sawamura, P., Moore, R. H., Hostetler, C. A., and Ferrare, R. A.: Information content and sensitivity of the $3\beta + 2\alpha$ lidar measurement system for aerosol microphysical retrievals, Atmos. Meas. Tech., 9, 5555–5574, https://doi.org/10.5194/amt-9-5555-2016, 2016

5. Can you eliminate water or ice cloud as an explanation for the measurements in CALIOP?

REPLY: CALIOP measurements at the northeastern Canada on 15 August 2017 (https://www-calipso.larc.nasa.gov/products/lidar/browse_images/show_v4_detail.php?s=production&v=V4-

10&browse_date=2017-08-15&orbit_time=17-55-33&page=3&granule_name=CAL_LID_L1-Standard-V4-10.2017-08-15T17-55-33ZD.hdf), show the stratospheric smoke layer at 11-14.5 km, where radiosonde measurements show temperatures below -40°C (Fig. 1 below). The radiosonde temperature profiles are from three stations close to the position of the smoke plume (Fig. 4b in manuscript): Churchill (Lat: 58.73, Lon: -94.08), Inukjuak (Lat: 58.45, Lon: -78.11) and Baker Lake (Lat: 64.31, Lon: -96.00). These low temperatures should exclude the presence of water clouds from CALIOP data, since even without the presence of aerosol particles, at these temperatures water can freeze homogeneously (Wallace and Hobbs, 2006; Fig. 6.29). Moreover, the ground-based lidar measurements on 23 August 2017 at Leipzig, show the stratospheric smoke layer at 14-16 km, where radiosonde measurements from the closest station (Lindenberg) provide temperatures below -50°C. Again the low temperatures indicate the absence of water clouds.

Regarding ice formation, the CALIOP PLDR values are below 20% both for the aforementioned overpass and for the closest overpass from Leipzig on 23 August 2017 (https://www-calipso.larc.nasa.gov/products/lidar/browse_images/show_v4_detail.php?s=production&v=V4-10&browse_date=2017-08-23&orbit_time=01-29-01&page=1&granule_name=CAL_LID_L1-Standard-V4-10.2017-08-23T01-29-01ZN.hdf (~90 km away and approximately 1 hour after the end of the ground based lidar measurements reported from Haarig et al., 2018), while the attenuated color ratio (i.e., the ratio of particle backscatter coefficient at 532nm to particle backscatter coefficient at 1064nm) is below 1. Further analysis of CALIOP data provides a mean (median) value of the backscatter related Angstrom exponent (BAE) at 532/1064nm, of 0.9 (0.9) with a standard deviation on 1.07. For PLDR, typical values for cirrus clouds are usually no less than 40% (Chen at al., 2002; Noel et al., 2002; Voudouri et al., 2020) and the color ratio is expected to be close to 1 due to the large size of ice crystals compared to the lidar wavelengths. For the BAE, values close to zero are expected, although the CALIPSO data are highly noisy at these altitudes as indicated by the standard deviation.

Moreover, for the overflight close to Leipzig on 23 August 2017, the lidar ratio (LR) measured from the ground based system is (66 ± 12) sr at 532nm. This is similar to the LR observed in the past for aged smoke particles (i.e. Fiebig et al., 2002; Veselovskii et al., 2015; Burton et al., 2012) but quite high for cirrus clouds (Gouveia et al., 2017).

Based on the above, although we cannot exclude the possibility of small ice crystals formed inside the stratospheric plume, we believe that the aforementioned characteristics indicate that this is not an ice cloud but rather a large smoke plume. Similar questions were raised also from Anonymous Reviewer 1, and Anonymous Reviewer 2. Hence we added the following paragraph to the manuscript to address the reviewers comment (**page 6, line 24**):

"Owning to the altitude of the smoke plume, one could attribute such PLDR values to the beginning of ice formation. Indeed, radiosonde temperature profiles from three stations located underneath the smoke plume (green stars on Fig.3b), reveal that the temperature above 11 km drops below -40C, at which point homogeneous ice formation can occur (Wallace and Hobbs, 2006). However, the PLDR values of cirrus clouds are usually no less than 40% (Chen at al., 2002; Noel et al., 2002; Voudouri et al., 2020). Further analysis of CALIOP data provides a mean (median) value of the backscatter related Angstrom exponent (BAE) at 532/1064nm of 0.9 (0.9) with a standard deviation on 1.07. For the BAE values close to zero are expected for cirrus clouds, although, as indicated by the large standard deviation, CALIPSO data are highly noisy at these altitudes. A recent study by Yu et al. (2019) also showed that the largest fraction of stratospheric smoke particles consisted of organic carbon (98% compared to 2% for black carbon). Particles of such high organic carbon content serve poorly as ice nuclei (Kanji et al., 2017; Phillips et al., 2013). Although the possibility of small ice crystals formed inside the smoke layers cannot be excluded, (largely due to the absence of in situ measurements) the aforementioned characteristics indicate that this plume consists of smoke particles rather than ice crystals.”

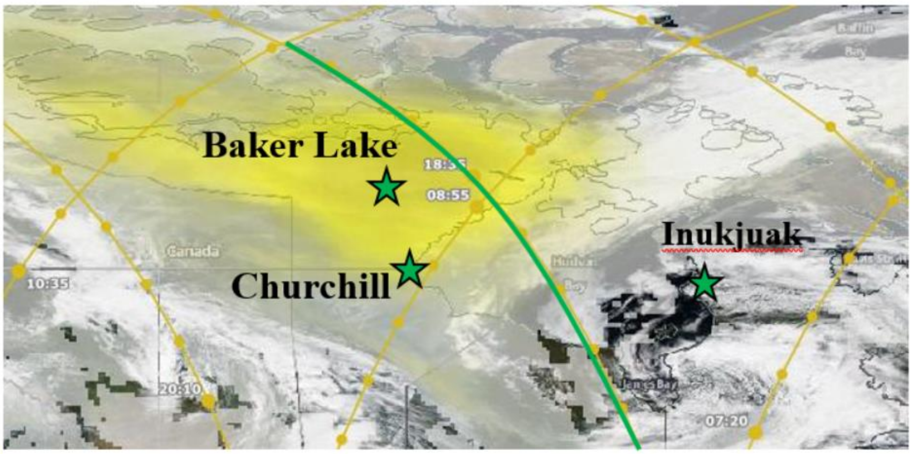

5 **Figure 1.** Corrected surface reflectance from MODIS on 15 August 2017, over-plotted with the PyroCb aerosol index product from Suomi NPP/OMPS (in yellow). Green stars indicate the position of the radiosonde stations used, while green line marks the CALIPSO overflight during 18:22 – 18:35 UTC. Maps are generated from the NASA Worldview Snapshots.

Figure 2. Same as Fig. 1 but for 23 August 2017. The CALIPSO overflight is approximately 90 km from Leipzig station, at 01:23 – 01:48 UTC, 1 hour after the end of the ground based lidar measurements.

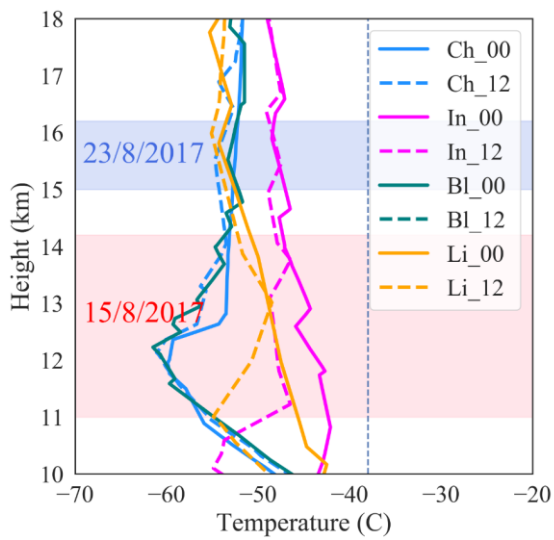

Figure 3. Radiosonde temperature (T) profiles from Churchill (Ch), Inukjuak (In), Baker Lake (Bl) and Lindenberg stations. Solid lines represent denote the measurements at 00:00 UTC, while dashed lines the measurements at 12:00 UTC. For the first three stations (Ch, In, Bl) measurements from 15 August 2017 are used, while for Li station from 23 August 2017. The pink box indicates the height of the smoke plume above northeastern Canada (11 -14 km) and the blue box the height of the plume after 8 days above Leipzig station (15 - 16 km).

References *(that are not included in the initial version of the manuscript)*:

Burton, S. P., Ferrare, R. A., Hostetler, C. A., Hair, J. W., Rogers, R. R., Obland, M. D., Butler, C. F., Cook, A. L., Harper, D. B., and Froyd, K. D.: Aerosol classification using airborne High Spectral

Resolution Lidar measurements – methodology and examples, Atmos. Meas. Tech., 5, 73–98, https://doi.org/10.5194/amt-5-73- 2012, 2012.

Chen WN, Chiang CW, Nee JB. Lidar ratio and depolarization ratio for cirrus clouds. *Appl Opt*. 2002;41(30):6470-6476. doi:10.1364/ao.41.006470

Fiebig, M., Petzold, A., Wandinger, U., Wendisch, M., Kiemle, C., Stifter, A., Ebert, M., Rother, T., and Leiterer, U.: Optical closure for an aerosol column: Method, accuracy, and inferable properties applied to a biomass-burning aerosol and its radiative forcing, J. Geophys. Res., 107, 8130, https://doi.org/10.1029/2000JD000192, 2002.

Gouveia, D. A., Barja, B., Barbosa, H. M. J., Seifert, P., Baars, H., Pauliquevis, T., and Artaxo, P.: Optical and geometrical properties of cirrus clouds in Amazonia derived from 1 year of ground-based lidar measurements, Atmos. Chem. Phys., 17, 3619–3636, https://doi.org/10.5194/acp-17-3619-2017, 2017.

Noel, V., Chepfer, H., Ledanois, G., Delaval, A., and Flamant, P.: Classification of Particle Effective Shape Ratios in Cirrus Clouds Based on the Lidar Depolarization Ratio, Appl. Optics, 41, 4245–4257, https://doi.org/10.1364/AO.41.004245, 2002.

Veselovskii, I., Whiteman, D. N., Korenskiy, M., Suvorina, A., Kolgotin, A., Lyapustin, A., Wang, Y., Chin, M., Bian, H., Kucsera, T. L., Pérez-Ramírez, D., and Holben, B.: Characterization of forest fire smoke event near Washington, DC in summer 2013 with multi-wavelength lidar, Atmos. Chem. Phys., 15, 1647– 1660, https://doi.org/10.5194/acp-15-1647-2015, 2015.

Voudouri, K. A., Giannakaki, E., Komppula, M., and Balis, D.: Variability in cirrus cloud properties using a Polly^{XT} Raman lidar over high and tropical latitudes, Atmos. Chem. Phys., 20, 4427–4444, https://doi.org/10.5194/acp-20-4427-2020, 2020.

Wallace, J.M., Hobbs, P.V. Atmospheric Science: An Introductory Survey: Second Edition (2006), DOI: 10.1016/C2009-0-00034-8

***6. Figure 7** had a panel of water vapor mixing ratio but no explanation of this measurement or description of what impact this figure has on the analysis of this case.*

REPLY: Thank you for noticing this. Figure 7 (b) was actually used to indicate the prevailing stratospheric conditions for the months following the smoke injection. Since the physical process explanation is removed from the revised version of the manuscript (please refer to comments 20 to 24 below), Fig. 7 (b) is removed also.

7. For Figure 8 and Table 4 and others, please define the meaning of the error bars. Is this a true calculated uncertainty including both random and systematic error, or is this the standard deviation of available measurements, or something else? If it's standard deviation, how well do you think this captures the actual uncertainty of the lidar measurements at each wavelength? I ask because you mentioned that the 1064 nm extinction measurement is more challenging to make and we also know from literature that particle depolarization ratio in particular can be subject to significant systematic error in some circumstances (e.g. Burton et al. 2015, Freudenthaler 2016, Belegante et al. 2018).

REPLY: The values in Tab. 4 and Fig. 8 are the systematic uncertainty of the PLDR in the given layer boundaries. It is good that the reviewer points out the standard deviation of points within the layer as an additional source of uncertainty. The standard deviation for the PLDR in the stratospheric smoke layer is 0.010 at 355 nm, 0.006 at 532 nm and 0.016 at 1064 nm and is now included in the revised manuscript (see Table 4 and Fig. 8 in the revised manuscript). PLDR at 1064 nm was measured during a different in a separate time window (23:45 – 00:30 UTC, compared to 20:45 – 23:15 for the rest of the measurements), because it is not possible to measure the extinction coefficient and the depolarization ratio at that wavelength at the same time for the current configuration of BERTHA lidar system. The increased standard deviation at 1064 nm is caused by the shorter averaging period, 40 minutes instead of 2h30min, and the geometrically thinner aerosol layer, around 0.5 km instead of 1 km.

We included the standard deviation of PLDR measurements to the revised manuscript and we added the following (**page 7, line 22**): “The layer-integrated PLDR value at 355 nm is 22.4 ± 2.5 %, decreasing to 18.4 ± 1.2 % at 532 nm and 4 ± 2.3 % at 1064 nm. The, uncertainties in PLDR values include both the systematic error and the standard deviation of the measurements.”

8. page 7, line 20-21. *Lidar ratio increase from UV-visible suggests that it also increases from visible to near-IR. This should be deleted. There’s nothing in Muller et al. (2007) that addresses the lidar ratio values in the near-IR one way or the other.*

REPLY: Thank you for this comment. We rephrased the following paragraph (**page 7, lines: 19 - 21**): “The increasing tendency of the LR from the UV to the visible part of the spectrum has been also reported before for aged Canadian smoke (Müller et al., 2007). Measurements reported in Haarig et al. (2018) suggest that there is an increase also at the Near-IR, although currently there are no other available measurements of the LR of smoke particles at this wavelength.”

9. page 7, line 22 "far from typical". I urge you to reword and avoid "typical". Muller et al. 2007 was a quite valuable paper, but the cases in it are somewhat limited, and it is now more than a decade old. Something that does not conform to Muller et al. 2007 is not necessarily "non-typical". We are still seeing new and different observations, by now including many of depolarizing smoke. I would say that this manuscript and other recent papers make a more convincing case that there is no "typical" for smoke *or else that we do not have sufficient observations yet to know what is "typical", rather than that the depolarization ratios in this case are non-typical.*

REPLY: We agree with the reviewer; this terminology is now changed throughout the manuscript. To address the comment specifically, we rephrased the following sentence (**page 8, line 22**): "On the other hand, the PLDR values of stratospheric smoke are much larger than those usually reported for tropospheric smoke (e.g. Muller et al., 2007)."

and (**page 8, line 24**): "So far, the only study presenting comparable results for tropospheric smoke is Burton et al. (2015)."

10. The notation in Equation 8 is confusing and doesn't really make sense. Please define what are i and n? Is this a summation over the three wavelengths? In that case, you have two subscripts (i and lambda) that mean the same thing? Or maybe i is binary and means lidar ratio and depolarization ratio, but in that case, you do not show how the different wavelength measurements are combined. Equation 8 furthermore should arguably have the measurement uncertainty rather than the measurement itself in the denominator. This would be a more meaningful cost function considering you intend to compare the result to the measurement uncertainty in Eq. 9. Doing this could have a significant impact on your results, specifically the result for the Chebyshev model that is shown in Figure 12. The only simulated point that doesn't fit the measurements is the 532 nm depolarization which has a very small reported uncertainty and therefore not much tolerance. But if the cost function reflected the error bars as well, you might find there is a solution that fits that point at the expense of slightly larger discrepancy in another quantity where the uncertainty tolerance is much larger (e.g. lidar ratios). I'm also curious how many solutions fit the criteria in Eq. 9 (or revised criteria) besides the minimum. Looking at this would *give some insight into the uncertainty of your modeled results and the degree to which the set of measurements is sensitive to the complete set of free parameters in your model.*

REPLY: In the original version of the manuscript Eq. 8 and 9 are written as following:

$$\sum_{i=1}^{n}\left(\frac{M_\lambda^i - S_\lambda^i}{M_\lambda^i}\right) = min \qquad \textbf{(Eq. 8)}$$

$$S_\lambda^i \leq e\left(M_\lambda^i\right) \qquad \textbf{(Eq. 9)}$$

For both equations subscript “i” is indeed binary, and denotes to depolarization (δ) and lidar ratio (LR) values at the three lidar wavelengths λ (6 values in total), so that n = 6. “M” denotes to measurements and “S” denotes to simulations. If we expand Eq. 8 we get:

$$\frac{\left(\delta_{355}^{M} - \delta_{355}^{S}\right)^2 + \left(\delta_{532}^{M} - \delta_{532}^{S}\right)^2 + \left(\delta_{1064}^{M} - \delta_{1064}^{S}\right)^2 + \left(LR_{355}^{M} - S_{355}^{S}\right)^2 + \left(LR_{532}^{M} - S_{532}^{S}\right)^2 + \left(LR_{1064}^{M} - S_{1064}^{S}\right)^2}{\left(\delta_{355}^{M} + \delta_{532}^{M} + \delta_{1064}^{M} + LR_{355}^{M} + LR_{532}^{M} + LR_{1064}^{M}\right)} = \mathbf{min}$$

While for Eq. 9 we get:

$\delta_{355}^{S} \leq e(\delta_{355}^{M})$, $\delta_{532}^{S} \leq e(\delta_{532}^{M})$, $\delta_{1064}^{S} \leq e(\delta_{1064}^{M})$, $LR_{355}^{S} \leq e(LR_{355}^{M})$, $LR_{532}^{S} \leq e(LR_{532}^{M})$, $LR_{1064}^{S} \leq e(LR_{1064}^{M})$

We also realized that we erroneously reversed the order of these two equations in the manuscript. Equation 9 actually precedes Eq. 8.

We revised our methodology according to the reviewer's suggestions: First, we search through the pre-calculated T-matrix look-up-tables for all the results that satisfy Eq. 9 (i.e. for each measured δ and LR, at each wavelength λ, the simulated value must be within the corresponding measurement error e). These are then the "possible solutions". Then, the best solution is selected based on the minimization criteria of Eq. 8.

Based on the reviewer comments we see now how the notation in Eq. 8 and 9 can be confusing. We updated it in the revised version, and we also included the measurement error "e" in the denominator of Eq. 9:

$$\left|\delta_{\lambda}^{M} - \delta_{\lambda}^{S}\right| \leq e(\delta_{\lambda}^{M}) \text{ and } \left|LR_{\lambda}^{M} - LR_{\lambda}^{S}\right| \leq e(LR_{\lambda}^{M}) \qquad \textbf{(Eq. 8)}$$

$$\sum_{\lambda = 355,\, 532,\, 1064} \left(\left(\frac{\delta_{\lambda}^{M} - \delta_{\lambda}^{S}}{e\,(\delta_{\lambda}^{M})} \right)^2 + \left(\frac{LR_{\lambda}^{M} - LR_{\lambda}^{S}}{e\,(LR_{\lambda}^{M})} \right)^2 \right) = \mathbf{min} \qquad \textbf{(Eq. 9)}$$

Again "M" denotes to measurement, "S" to simulation and λ to wavelength.

Following the reviewer's suggestion, we present our results in the updated manuscript, including all possible solutions (Tables 3,4 and Figures 7-10).

For the near-spherical particles we found ten possible solutions, with the mean geometric radius r_g to range from 0.25 to 0.45μm ($reff$ = 0.4 to 0.7μm), the refractive index to range at m_r = 1.35-1.55 and m_i = 0.005-0.03, while for the shape distribution the mean axial ratio ε_s ranges at 1.1-1.4. We should note that although significantly larger values of m_i were included in the updated simulations (originally was m_i (max) = 0.05, while now m_i (max) = 0.5), no possible solutions were found for m_i higher than 0.03.

The solution selected, that minimizes, the new cost function in Eq. 9 in updated manuscript, is r_g = 0.25μm ($reff$ = 0.38μm), m_r = 1.55, m_i = 0.03 and ε_s = 1.3, which is the same with the solution in the original version of the manuscript. By adding the error of the measurements to the denominator of Eq. (9), solutions were provided also using Chebyshev particles of second (T2) and fourth (T4) degree. For T2 the deformation parameter ranges from u = –0.25 to 0.15, while for T4 particles only one solution was found with u = -0.1. These u values suggest small deviations from sphericity, meaning that these morphologies also resemble near-spherical shapes. For Chebyshev particles, slightly larger particles were retrieved (maximum r_g found is 0.55μm ($reff$ = 0.8μm) while for the refractive index, both the imaginary and the real part were found to exceed the values found for near-spherical particles. Specifically, m_i ranges from i0.005 to i0.055 and m_r ranges from 1.35 to 1.8.

We included the following in the manuscriot to highlight this comment (***page 5, line 3***):

"Following this methodology, for the near-spherical particles ten possible solutions were found, listed in Table 3 along with the resulting cost functions calculated by Eq. (8). For these solutions, the mean axial ratio ε_s of the particles covers the range 1.1 to 1.4 while the mean geometric radius is always higher than 0.25μm ($reff$ = 0.4μm) and up to 0.45μm ($reff$ = 0.7μm). For the complex refractive index m, the imaginary part m_i does not exceed i0.03, while the real part m_r takes values of 1.35 to 1.55. The minimization of the cost function (Eq. 8) is achieved for near-spherical particles with ε_s = 1.4 (Fig.9), m = 1.55 + i0.025 and r_g = 0.25μm (Fig. 10), suggesting a strong accumulation mode for the size distribution of the particles, with sufficiently small m_i so as the characteristic enhancement in PLDR does not wash out due to the strong absorption (Bi et al., 2018). All possible solutions as well as the solution that minimizes the cost function are presented in Fig. 8 and 9."

And (***page 5, line 4***):

"For Chebyshev particles of second (T_2) and fourth degree (T_4) used herein, the search in the constructed look-up-tables provided the solutions listed in Table 4. For all the solutions, deformation parameter for Chebyshev particles of the second degree ranges from u = –0.25 to 0.15, while for particles of the fourth degree only one solution was found with u = -0.1. These u values suggest small deviations from sphericity, meaning that these morphologies also resemble near-spherical shapes. Only for two cases the size of the particles was found to be larger than for the near-spherical shaped particles. In particular r_g ranges from 0.15μm ($reff$ = 0.2μm) to 0.55μm ($reff$ = 0.8μm). For the complex refractive index, values in some cases exceed the corresponding values for near-spherical particles. The imaginary part m_i ranges from i0.005 to i0.055,and the real part m_r ranges from 1.35 to 1.8. The minimization of the cost function (Eq. 8) is achieved for Chebyshev particles of the second degree with u = -0.25 (resembling an oblate near-spherical particle), complex refractive index m = 1.65 + i(0.03) and mean geometric radius r_g = 0.2μm. For Chebyshev particles of the fourth degree, the sole solution presented values u = -0.1, m = 1.35 + i(0.01) and r_g = 0.55μm. All possible solutions as well as those that minimize the cost function are presented in Fig. 10 and 11."

Simulations were also performed for other reported spectrally dependent PLDR and LR values found in the literature for smoke exhibiting large PLDR values (Burton et al., 2015; Hu et al., 2017; Ohneiser et al., 2020). Results for these fittings are presented in the manuscript Supplement (Tables 4-9 and Figures 4-9). Results are in line with the results presented for the case study of Haarig et al. (2017).

11. In the figure 10 comparison with AERONET, the use of a generic biomass burning solution instead of a solution for the same smoke plume seems like a needless shortcut that undercuts your ability to draw *conclusions from it. I realize there were no precisely coincident AERONET measurements, but a previous paper studying the same event that you already reference by a coauthor (Haarig et al. 2019) shows an AERONET retrieval that is at least of the same smoke plume, and also apparently better agreement, so clearly it's possible to get better fidelity than the unrelated generic case given by Dubovik et al. (2002).*

Furthermore, comparing a fit to a mono-modal size distribution to the fit from a bimodal size distribution and then noting that the modes don't line up is not particularly useful, and it's not obviously tied to the presence or absence of near-spherical particles per se. If you must compare a mono-modal fit to a bimodal fit, then at least calculate the effective radius and variance (quantities that are more comparable from different distribution types) from each of them and compare that instead.

REPLY: We agree with the reviewer. Unfortunately, in AERONET Version 3 Inversion products, the quality-assured Level 2 data have excluded the size distribution presented in Haarig et al. (2018). The same holds for Level 2 data of Version 2 Inversion products (the previous AERONET version):

https://aeronet.gsfc.nasa.gov/cgi-bin/type_one_station_opera_v2_inv2?site=MetObs_Lindenberg&nachal=0&year=25&month=7&day=22&aero_water=0&level=2&if_day=0&if_err=0&place_code=10&year_or_month=0

https://aeronet.gsfc.nasa.gov/cgi-bin/data_display_inv_v3?site=MetObs_Lindenberg&nachal=0&year=2017&month=8&day=23&aero_water=0&level=2&if_day=0&if_err=0&place_code=10&DATA_TYPE=76&year_or_month=0

We can speculate that this particular retrieval was rejected from Level 2 by failing to fulfill some criteria for the quality control or for the success of the fit (i.e. the sky residual error is as high as 6.5%), thus we cannot include it in the paper. However, in order to reply to the reviewer's question, since we agree that the comparison with the climatological-mean size distribution for biomass burning aerosols does not provide a solid conclusion, we performed the comparison with the AERONET retrievals discussed in Haarig et al. (2018). We agree with the reviewer that the comparison using the effective radius $reff$ and effective variance $veff$ is more meaningful and we present the comparison with the AERONET data in Table 1 below. We can see that for AERONET retrievals $reff$ is slightly higher (by 10%) while $veff$ is much higher (by 33%).

The calculation of r_g and $veff$ from $reff$ and σ_g provided by AERONET, is done using Eq. 1 and 2 (Hansen and Travis, 1974):

$$v_{eff} = \exp\left(\ln(\sigma_g^2)\right) - 1 \qquad \textbf{(Eq. 1)}$$

$$r_{eff} = r_g(1 + v_{eff})^{5/2} \qquad \textbf{(Eq. 2)}$$

Table 1. Comparison of $reff$ and $veff$ for the size distributions retrieved by AERONET on 23 August, 2017 at Lindenberg site, and the size distribution retrieved from the measurements at Leipzig on the same date, using near-spherical particles.

		AERONET	
Date	**Time**	$reff$	$veff$
23.08.2017	05.42.40	0.42 µm	0.24
		Near spherical particles	
		0.38 µm	0.18

(*) Provided by AERONET
(**) Calculated using Eq. (1) and Eq. (2)

References *(that are not included in the initial version of the manuscript)*:

Hansen, J.E., Travis, L.D. Light scattering in planetary atmospheres. Space Sci Rev 16, 527–610 (1974). https://doi.org/10.1007/BF00168069

12. On a related note, could there be a coarse mode that your model is ignoring that might explain some of the features of your observations? Have you tried to eliminate the possibility of an optically significant coarse mode?

REPLY: The features observed by the ground-based lidar measurements (Haarig et al., 2018) are adequately reproduced by the assumed size distribution. Similar simulations presented by Bi et al., (2018; Fig 2), suggest that for near-spherical particles the measured spectral dependence of PLDR (i.e. steeply decreasing from UV to Near-IR) could not be reproduced by coarse mode particles. Thus, an optically significant coarse mode would have to be investigated with a different shape model.

The following has been added to highlight the reviewer's comment (**page 8, line 22**): "A common feature observed in our results is that the ground based lidar measurements are adequately reproduced by the assumed monomodal size distributions for which the mean particle geometric radius r_g did not exceed 0.55μm. This fits well with in-situ measurements of aged smoke particles (i.e. Dahlkoetter et al., 2014). The presence of a pronounced accumulation mode is also suggested by the extinction related Angstrom exponent (EAE) values measured in Leipzig. According to Eck et al. (1999), a strong spectral slope in EAE can be associated with a prominent accumulation mode of the size distribution for smoke particles. Similar simulations presented by Bi et al., (2018; Fig 2), suggest that for near-spherical particles the measured spectral dependence of PLDR (steeply decreasing from the UV to the Near-IR) could not be reproduced by coarse mode particles. Thus, the possibility of an optically significant coarse mode would have to be investigated with a different shape model. In any case though, the retrieved fine mode is in good agreement with in-situ measurements of aged smoke particles (i.e. Dahlkoetter et al., 2014). The presence of a pronounced accumulation mode is also suggested by the extinction related Angstrom exponent (EAE) measured in Leipzig (-0.3±0.4 at 355/532nm and 0.85 0.3 at 532/1064nm). According to Eck et al. (1999), a strong spectral slope in EAE can be associated with a prominent accumulation mode of the size distribution for smoke particles."

13. Page 7, line 10. This brief sentence about extending AERONET to include near spherical particles is an interesting idea, but unsupported. To address this properly, please consider at least these 3 points. First, as stated above, there would have to be a fair comparison between AERONET results and your results for similar cases. As part of this, there would have to be an assessment of not just the size distribution, but also a reconstruction of the lidar measurements using the AERONET solution.

- *Can you show that the AERONET retrieval fails to reproduce the lidar ratio and linear particle depolarization ratio adequately?*
- *Conversely, how does your near-spherical model do in reproducing AERONET radiances at all AERONET wavelengths?*

Whatever the answer to each of these questions, there's something to be learned. If the near-spherical model does a better job of reproducing lidar measurements and is also better at modeling AERONET measurements, then it could genuinely be an improvement for AERONET. If it doesn't improve the AERONET fits but improves the lidar fits, it might be less useful for AERONET alone (at least it would suggest that it might be hard for AERONET to operationally use the model if there is not sufficient *measurement information content to distinguish near-spherical from spherical particle shapes), but might still be potentially of significant value for combined AERONET-lidar retrievals (e.g. constrained backscatter lidar retrievals). Even if the near-spherical model does a worse job at modeling AERONET measurements but a better job at modeling lidar measurements, it at least points us to the need for further modeling studies to find a single model that can unify both types of measurements.*

We thank the reviewer for the constructive comment, which gives us the opportunity to provide a more thorough analysis in the updated manuscript, that better positions our research.

Considering the first question, unfortunately there are no available AERONET retrievals that we can use (please see reply for Comment 11).

We should note though that the recent study by Hu et al. (2019) for the same stratospheric smoke used the forward model of AERONET and failed to reproduce the measured depolarization ratios, indicating the limitations of this model for non-spherical smoke particles. Specifically, Hu et al. (2019) used the GARRLiC algorithm (Lopatin et al., 2013), which combines lidar with sunphotometer measurements in order to derive the optical and miscrophysical properties of particles in the atmosphere. GARRLiC utilizes the forward model of AERONET (Dubovik et al., 2006).

As mentioned above, the inversion retrievals for Lindenberg site on 23 August 2017 at 05:42 UTC were rejected both from Level 1.5 and Level 2 quality-assured data of AERONET Version 3 algorithm. Products from Version 2 (the AERONET version used for the products presented in Haarig et al. 2018) does not include lidar ratio and depolarization ratio values. Thus, there are no available, coincident AERONET lidar ratio and depolarization ratio products to compare.

Considering the second question, instead of reproducing the sun-photometer measurements (which entails taking into account the multiple scattering in the atmospheric column), we reproduce the phase function of the stratospheric smoke particles, as a first-level approximation (single scattering) of the full solution. Since there are no available retrievals of phase functions from AERONET for this case to compare (please see reply for Comment 11), we follow an invert procedure to reply to reviewer's comment. We specifically try to reproduce the calculated phase function of near-spherical particles, using the non-spherical model of AERONET. As shown below this is not possible, at least within a residual error of <5% (Holben et al., 2006), indicating the limitations of the AERONET non-spherical model in reproducing the scattered light from near-spherical particles in the atmosphere.

Specifically, in Fig. 4-7 we present the phase function at 440nm calculated for the near-spherical stratospheric smoke particles (purple line in the plots), and the comparison with the phase functions at 440nm calculated using the AERONET non-spherical model, using a large suite of size distributions and refractive indices (blue lines). In Fig. 4-7 we show the results only for r_g of 0.1, 0.25, 0.5 and 1μm, respectively, for all refractive indices. The complete set of results (more r_g and AERONET wavelengths of 670, 870 and 1020nm) are provided in the Supplement.

In Fig. 4-7, the phase function is presented in the left plots, whereas we also include the degree of linear polarization (-P12/P11) in the middle plots and the values of P22/P11 in the right plots, for the sake of completeness. On a relative note, the large differences seen for -P12/P11 and P22/P11 highlight the higher information content for near-spherical particles in polarized measurements (as the PLDR measurements).

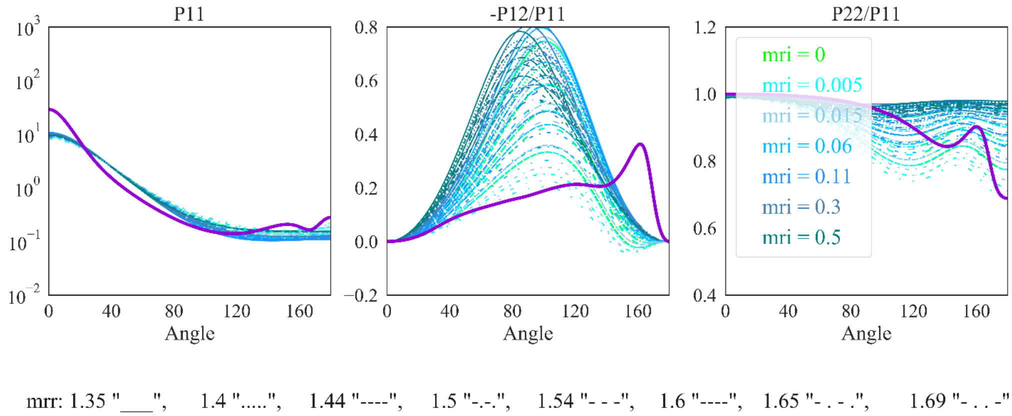

Figure 4. The elements of the scattering matrix at λ = 440nm. Left: P11 (phase function), middle: -P12/P11 (degree of linear polarization), right: P22/P11. Purple lines in the plots: calculations considering the near-spherical particle properties derived for the stratospheric smoke particles from the Canadian fires, with mean axial ratio ε_s = 1.3, monomodal, log-normal size distribution with r_g = 0.25, σ_g = 0.4, and complex refractive index m = 1.55 – i0.03. Blue lines in the plots: calculations considering the shape distribution of the AERONET non-spherical model, and monomodal, log-normal size distributions with r_g = 0.1μm and refractive indices of m_r = 1.35, 1.40, 1.44, 1.50, 1.54, 1.60, 1.65, 1.69 for the real part (different line styles in the plot) and m_i = 0, 0.005, 0.015, 0.06, 0.11, 0.3, 0.5 for the imaginary part (different line colors in the plot).

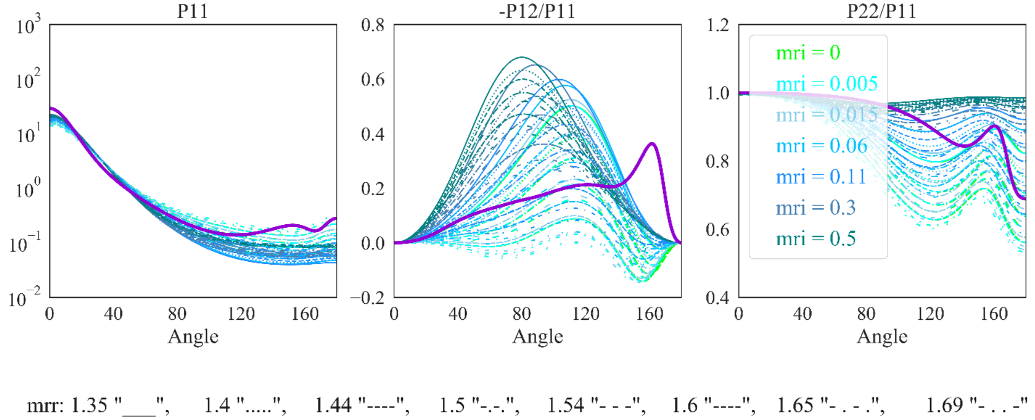

Figure 5. Same as Fig. 4. For the calculations with the AERONET non-spherical model (blue lines) we consider $r_g = 0.25 \mu m$.

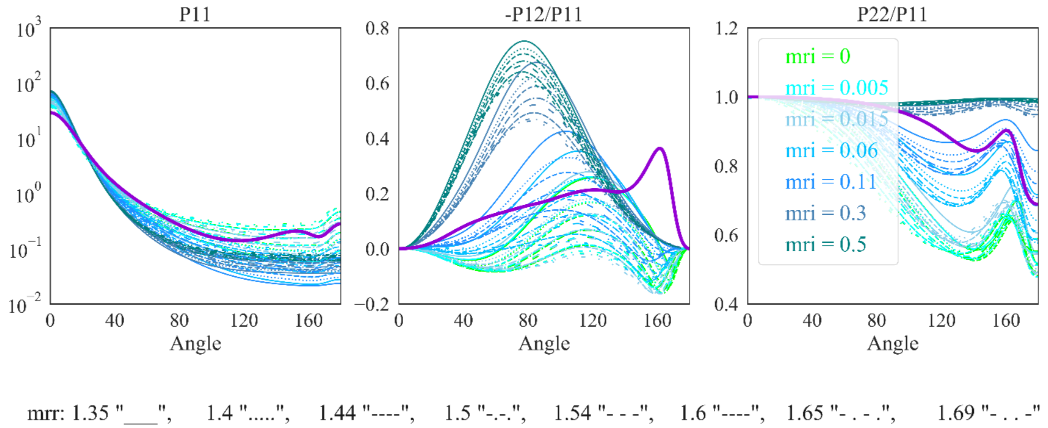

Figure 6. Same as Fig. 4. For the calculations with the AERONET non-spherical model (blue lines) we consider $r_g = 0.5\mu m$.

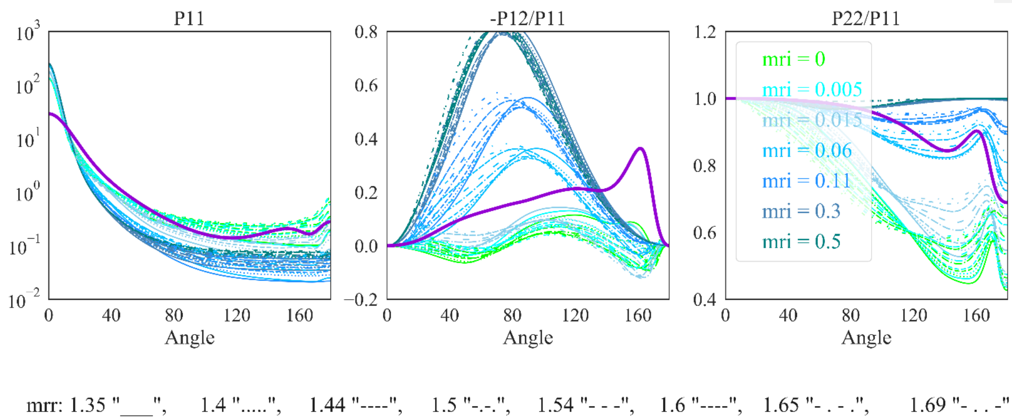

Figure 7. Same as Fig. 4. For the calculations with the AERONET non-spherical model (blue lines) we consider r_g = 1.0μm.

In order to quantify the residual of fitting we calculate the "residual error" (Err) as shown in Eq. 3 (https://aeronet.gsfc.nasa.gov/new_web/Documents/Inversion_products_for_V3.pdf).

$$Err = \sqrt{\frac{\sum_{i=1}^{n}(lnf^* - lnf)^2}{N}} * 100 = \%Error \qquad \textbf{(Eq. 3)}$$

where $f*$ denotes the P_{11} values calculated with the near-spherical model, f denotes the P_{11} values calculated with the AERONET non-spherical model, and N is the number of values, in terms of wavelengths and scattering angles. Specifically, we consider the four wavelengths of 440, 670, 870 and 1020nm and the scattering angles from 0 to 150 degrees.

Figure 8 shows the residual error “Err” for fitting the phase function of the near-spherical particles presented in the manuscript with the phase functions calculated with the AERONET non-spherical model, considering the big suite of sizes and refractive indices discussed above. The minimum residual error is 9.4%, whereas the limit of a successful AERONET retrieval is 5% (Holben et al., 2006). However, the latter threshold denotes to the multiple-scattered light, which may mask the big differences seen in the single-scattering properties in Fig. 8.

Similar 2D plots for the residual error considering only the wavelengths at 440, 670, 870 and 1020nm are provided in the Supplement.

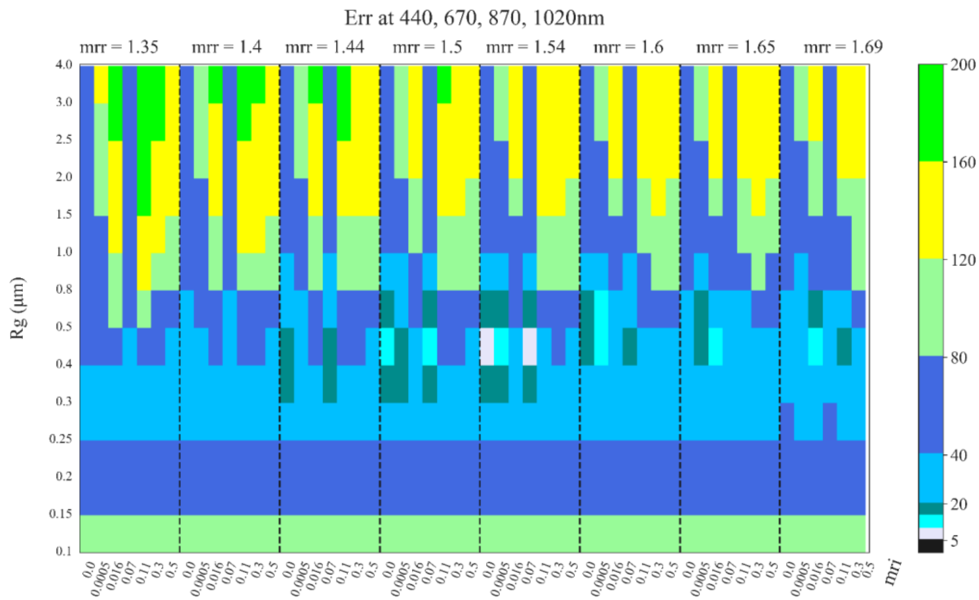

Figure 8. The residual error (Err) of fitting the phase functions at 440, 670, 870 and 1020nm of the near-spherical particles presented in the manuscript, with the phase functions calculated with the AERONET non-spherical model, for r_g and m shown in y- and x-axis, respectively.

Based on the above w a new subsection in Discussion section of the paper, entitled:

5.1 Comparison with AERONET products, elements of the scattering matrix

We understand that this analysis is not conclusive and in order to have a clear understanding of whether the near-spherical shape model could in fact improve the AERONET retrieval for stratospheric smoke, further analysis is imperative. We consider this only as a first step and we make sure to emphasize this in the manuscript.

References *(that are not included in the initial version of the manuscript)*:

Holben, B. N., T. F. Eck, I. Slutsker, A. Smirnov, A Sinyuk, J. Schafer, D. Giles, O. Dubovik, 2006: Aeronet's Version 2.0 quality assurance criteria, Proc. SPIE 6408, Remote Sensing of the Atmosphere and Clouds, 64080Q, doi:10.1117/12.706524.

Lopatin, A., Dubovik, O., Chaikovsky, A., Goloub, P., Lapyonok, T., Tanré, D., and Litvinov, P.: Enhancement of aerosol characterization using synergy of lidar and sun-photometer coincident observations: the GARRLiC algorithm, Atmos. Meas. Tech., 6, 2065–2088, https://doi.org/10.5194/amt-6-2065-2013, 2013.

14. Fractal aggregates: *Fractal aggregates require a lot of parameters to describe them, and some of them you held fixed instead of varying. If you cannot explore the full parameter space, how do you know that fractal aggregates can't fit the observations? At line 25, you then point out that previous authors (not just Ishimoto et al. 2019, but see also Kahnert 2018, Kanngeisser and Kahnert 2018, Luo et al. 2019 and Ceolato et al. 2018, as noted above) have already established that bare aggregates are not able to reproduce measurements as well as coated aggregates, so I don't see a lot of value in running a model type that has already been shown not to work without also running a related model type that has been used with some success in the past (granted with less complete measurements in the past; indeed, the new measurements are the real strength of this contribution and where you have the opportunity to go beyond prior work).*

REPLY: We included this analysis in order to emphasize the fact that fractal aggregates do not reproduce the measured optical properties of stratospheric smoke from the Canadian fires. Considering the limited parameter space by using only fixed, typical values for the fractal dimension D_f, we refer the reviewer to the comprehensive study of Paulien et. al. (2019), which shows that this parameter has only weak influence on the lidar-relevant optical properties. Moreover, in order to define the different monomer number N_m = 244, 579 and 1953 and monomer radius r_m = 40, 60 and 80 nm (volume equivalent radius of R_v= 500 nm) we followed the work of Ceolato et. al (2018). However, we see the reviewer's point on the limited range of parameters used to describe fractal aggregates and we agree this is not an excessive analysis, so we decided to remove this section from the revised version of the manuscript.

References *(that are not included in the initial version of the manuscript)*:

Paulien, L., Ceolato, R., Soucasse, L., Enguehard, F., Soufiani, A.: Lidar-relevant radiative properties of soot fractal aggregate ensembles. Journal of Quantitative Spectroscopy and Radiative Transfer, Elsevier, 2019, 241, pp.106706, DOI: 10.1016/j.jqsrt.2019.106706.

Ceolato, R., Gaudfrin, F., Pujol, O., Riviere, N., Berg, M. J., Sorensen, C. M.: Lidar cross-sections of soot fractal aggregates: Assessment of equivalent-sphere models, Journal of Quantitative Spectroscopy and Radiative Transfer, Volume 212, 2018, Pages 39-44, ISSN 0022-4073, https://doi.org/10.1016/j.jqsrt.2017.12.004.

15. page 9, line 16. See also Kablick et al. 2018 for another case discussing ice.

REPLY: Thank you, this part has been removed from the manuscript.

16. page 9, line 17. In 2015, Burton et al. could not have extensively discussed studies that were published 3 or 4 years later. Specifically, there's no discussion in Burton et al. 2015 about the ice hypothesis. It *would be better for this manuscript's authors to take the opportunity to address these newer theories more completely here.*

REPLY: Thank you, this part has been removed from the manuscript.

17. page 9, line 17-18. I'm not following the statement "soil lifting ...could explain the...observations presented in this study". Do you mean to eliminate this possibility or support this possibility?

REPLY: This part is now removed from the original version of the manuscript.

18. page 7, line 18. The Angstrom exponent is indeed confusing, primarily because we don't know what wavelengths you're referring to either in the measurements or in the comparison dataset that causes you to say this is "low". It's not uncommon for smoke measurements to have significant curvature in the spectral AOD (or extinction) (see Eck et al. 1999) and in fact Haarig et al. 2018 show a significant difference between the 355-532 nm and 532-1064 nm Angstrom exponents for their analysis of this smoke plume. Taking this into account, do you still believe the Angstrom exponent for this case indicates coarse mode particles? Please add a more complete discussion.

REPLY: We thank the reviewer for noticing this. Indeed, as the reviewer points out, there is a strong curvature between the AE at 355/532nm (-0.3 ± 0.4) and the corresponding values at 532/1064nm (0.85 ± 0.3). According to Eck et al. (1999) this behavior can be associated with a size distribution presenting a pronounced accumulation mode, as well as a spectral dependence in the absorption, with higher absorption at the smaller wavelengths. This is in agreement with the retrieved size distribution for near-spherical particles of r_{eff} = 0.38 μm. The spectral dependence of the absorption can indeed be another reason, although it is not shown in our results due to the assumed spectrally-independent value of the imaginary part of refractive index. To address this comment we rephrased this part of the manuscript (**page 8, line 22)**:

"A common feature observed in our results is that the ground based lidar measurements are adequately reproduced by the assumed monomodal size distributions for which the mean particle geometric radius did not exceed 0.35μm. This fits well with in-situ measurements of aged smoke particles (i.e. Dahlkoetter et al., 2014). The presence of a pronounced accumulation mode is also suggested by the extinction related Angstrom exponent (EAE) values measured in Leipzig. According to Eck et al. (1999), a strong spectral slope in EAE can be associated with a prominent accumulation mode of the size distribution for smoke particles. Similar simulations presented by Bi et al., (2018; Fig 2), suggest that for near-spherical particles the measured spectral dependence of PLDR (steeply decreasing from the UV to the Near-IR) could not be reproduced by coarse mode particles. Thus, the possibility of an optically significant coarse mode would have to be investigated with a different shape model. In any case though, the retrieved fine mode is in good agreement with in-situ measurements of aged smoke particles (i.e. Dahlkoetter et al., 2014). The presence of a pronounced accumulation mode is also suggested by the extinction related Angstrom exponent (EAE) measured in Leipzig (-0.3±0.4 at 355/532nm and 0.85 0.3 at 532/1064nm). According to Eck et al. (1999), a strong spectral slope in EAE can be associated with a prominent accumulation mode of the size distribution for smoke particles."

References *(that are not included in the initial version of the manuscript)*:

Eck, T. F., Holben, B. N., Reid, J. S., Dubovik, O., Smirnov, A., O'Neill, N. T., Slutsker, I., and Kinne, S.: Wavelength dependence of the optical depth of biomass burning, urban, and desert dust aerosols, Journal of Geophysical Research: Atmospheres, 104, 31333-31349, 10.1029/1999JD900923, 1999.

19. page 7, line 21 "surface roughness alterations"? I don't follow where this idea comes in the paper. Is this what the Chebyshev particle shape is meant to represent? There are other model representations of surface roughness (e.g. Liu et al. 2013, Kemppinen et al. 2015) so this label is probably too non-specific (vague) in this context and should be made more precise.

REPLY: This part is now removed from the original version of the manuscript.

20. For the comments 20 to 24: At the current stage the discussion on the possible physical explanation for the smoke PLDR values is removed from the manuscript. More efforts will be made to investigate this issue and re-assess the possible coexistence of smoke particles and particles of sulfuring nature and whether this could affect the former in such a way to form near-spherical particles.

21. While informal titles can catch people's attention, I wonder if this one is really a good idea? "The new black" means "fashionable" or "popular", which is probably not quite what you're hoping for from your new smoke particle model. In general, I appreciate funny titles but if it is a pun, I'm not getting it, since I don't see what scientific meaning "black" has in this title. Also, the phrase "the new black" is itself something of a fad which may fade quickly, leaving readers 5 or 10 years from now completely confused about what the title means. But of course it is up to the author; this isn't a comment that needs a response, just a perspective on how one reader sees it, in case you find this helpful.

REPLY: We thank the reviewer for this comment.

22. page 2, line 26. The sentence starting "implication for enrichment of smoke plumes with dust particles" should probably be deleted. Later on, you mention several possible explanations from previous literature, *but here you only mention one without discussion that you later dismiss. Better to delete it here and hold the discussion until you are ready for it in the later section.*

REPLY: Thank you, we removed this phrase from the introduction.

23. page 7, line 21 "not currently supported by other observation evidence found in the literature". Probably should be reworded. It seems like you're saying there is other evidence found in the literature that doesn't support your finding, but my understanding is that there is no contradictory observational evidence because lidar ratio at 1064 nm for this kind of observation has never been reported before! Please make this clearer. Having unique measurements is a real strength! No need to muddy the picture with imagined controversy.

REPLY: The following has been rephrased (**page 7, line 21**): "…although there are currently no other available measurements of the LR of smoke particles at this wavelength. "

24. page 7, line 11, probably delete the brief mention of pollen, which has not been addressed at all in this paper. We have no way of knowing whether the near-spherical model has any success in modeling pollen.

REPLY: Thank you, it has been deleted.

25. page 9, line 12, "results in near-spherical shapes" should be reworded. Logically, the finding that the near-spherical particle model reproduces a set of measurements better than a few other models could still be merely a very useful approximation. It does not necessarily mean the particles are literally shaped like Figure 2.

REPLY: This part has been removed from the manuscript.

26. page 9, line 12, "previous studies" should be "some previous studies" (i.e. but not all, see for example Murayama et al. 2004, Burton et al. 2015 who specifically dispute it for certain other cases).

REPLY: This part has been removed from the manuscript.

27. page 9, line 14, Sugiomoto et al. what year? (typo)

REPLY: Thank you, this part has been removed from the manuscript.

28. page 9, line 23, "advocate dissuasive towards" should be changed to (e.g.) "argues against"

REPLY: Thank you, this part has been removed from the manuscript.

2*9. page 9, line 26, "while up to now the LR values are not reproduced either". Again, I feel like this should be reworded, because it's making a confusing (or perhaps just incomplete) point when a much stronger one is indicated. Most previous modeling papers did not have the opportunity to reproduce three-wavelength lidar ratios because these observations have only just recently been published. The strength of the current manuscript is these new and unique measurements.*

REPLY: Actually in the study we are referring to, it is explicitly stated that tar ball aggregates were not found to reproduce the PLDR values at 532nm, as presented by Haarig et al. (2018) and Hu et al. (2019). However, we deleted this statement.

30. page 9 line 30. I think 15 micrometer monomers must be a typo.

REPLY: Thank you, this part has been removed from the manuscript.

31. page 10 line 4. "Thought" should be "Although"'

REPLY: Thank you, this part has been removed from the manuscript.

32. Table 4 caption. Please specify the instrument that made these measurements.

REPLY: We added the instrument, it is the BERTHA (Backscatter Extinction lidar-Ratio Temperature Humidity profiling Apparatus) multi-wavelength polarization Raman lidar system.

33. Figure 6. The red dashed lines appear to be in the wrong place.

REPLY: An updated the figure has been provided.

34. It would be good to include a figure explaining what Chebyshev particles look like.

REPLY: Thank you, we added a figure.

35. Figure 7. What do the white pixels near the top of the layer signify, in both the linear depolarization ratio and the water vapor mixing ratio? What do the black down-arrows on the latitude and longitude axes represent? Please indicate in 7c the portions of the track that are represented in 7a and 7b.

REPLY: The figure has been updated.

36. Figure 14. Please mark the location of the smoke plume and consider plotting this on an altitude (rather than pressure) scale and with altitude range more comparable to the ranges shown in Figures 6 and 7. Please also consider putting an indicator of distance scale on Figures 6, 7, and 14.

REPLY: The figure has been removed from the manuscript.

Is the near–spherical shape the "new black" for smoke?

Anna Gialitaki[1,2], Alexandra Tsekeri[1], Vassilis Amiridis[1], Romain Ceolato[3], Lucas Paulien[3], Anna Kampouri[1,2], Antonis Gkikas[1], Stavros Solomos[4,1], Eleni Marinou[5,1], Moritz Haarig[6], Holger Baars[6], Albert Ansmann[6], Tatyana Lapyonok[7], Anton Lopatin[8], Oleg Dubovik[7], Silke Groß[5], Martin Wirth[5] and Dimitris Balis[2]

[1] National Observatory of Athens / IAASARS, Athens, Greece
[2] Laboratory of Atmospheric Physics, Physics Department, Aristotle University of Thessaloniki, Greece
[3] ONERA, The French Aerospace Lab, Toulouse, France
[4] Research Centre for Atmospheric Physics and Climatology, Academy of Athens, Athens, Greece
[5] Institute of Atmospheric Physics, German Aerospace Center (DLR), Oberpfaffenhofen, Germany
[6] Leibniz Institute for Tropospheric Research (TROPOS), Leipzig, Germany
[7] Laboratoire d'Optique Atmosphérique, CNRS/Université Lille, Villeneuve d'Ascq, France
[8] GRASP-SAS, Villeneuve d'Ascq, France

Correspondence to: Anna Gialitaki (togialitaki@noa.gr)

Abstract. We examine the capability of near-spherical-shaped particles to reproduce the ~~non-typical~~ Particle Linear Depolarization Ratio (PLDR) values measured over Europe for stratospheric smoke originating from Canadian wildfires. The smoke layers were detected both in the troposphere and the stratosphere, though in the latter case the particles presented PLDR values of almost 18% at 532 nm as well as a strong spectral dependence from the UV to the Near-IR. The assumption that the smoke particles have a near-spherical shape allows for the reproduction of the observed PLDR and Lidar Ratio (LR), whereas this was not possible when using more complicated shapes. The results presented here are supported by recent findings in the literature, showing that up to now the near-spherical shape (or closely similar shapes) is the only morphology found capable of reproducing the observed intensive optical properties of stratospheric smoke, as well as their spectral dependence.

1 Introduction

Particles originating from biomass burning activities are known to have a significant effect on radiation and climate (Kaufman et al., 2002). The factors affecting the optical properties of smoke are mainly the black carbon fraction and the impact of the ageing processes (Amiridis et al. 2009). Various findings from field measurements suggest that the smoke particles' surface may serve as highly effective cloud nuclei (Ackerman et al, 2000; Koch et al., 2010; Hoose & Möhler, 2012; Marinou et al., 2019; Nichman et al., 2019), modifying cloud properties and lifetime and thus indirectly affecting the radiative budget. Their various impacts depend also on their lifetime, since they tend to alternate their properties i.e. become less absorbing or more hydrophilic due to atmospheric processes (Amiridis et al., 2009; Adachi and Buseck, 2011).

Smoke particles in the atmosphere can be identified with lidar measurements which provide valuable information on the optical ~~To estimate their optical and microphysical characteristics in ambient conditions, with large spatial and temporal resolution, lidar measurements are frequently used. Lidars provide valuable measurements~~ properties ~~for monitoring the properties~~ of ~~smoke~~aerosol particles, such as the depolarization of the backscattered ~~light~~ light in terms of the particle linear depolarization ratio (PLDR). Spherical particles do not depolarize the incident radiation, hence the PLDR can be used to derive information on morphologically complex particles such as smoke. Fresh smoke tends to form fluffy, mostly hydrophobic aggregates composed of many single small monomers. As the particles age in the atmosphere, this aggregate structure collapses, the particles become more hydrophilic and are frequently found covered by cells composed of water soluble components such as sulphates or organic materials (Worringen et al., 2008; Wu et al., 2016).

~~that is used here to derive new information for the smoke particle shape. On a first level, the PLDR provides information about the particle non-sphericity, since spherical particles do not depolarize the backscattered light. Moreover~~.~~,~~ Owning to the aforementioned processes, the PLDR of smoke particles may ~~numerus studies have shown that the PLDR of smoke~~ present~~s~~ a large variability related to the age of the particles (Baars et al. 2019a), the presence of other aerosol types found inside the smoke layers (Tesche et al., 2009; Groß et al., 2011) or even the particle water uptake due to different humidity conditions (Cheng et al., 2014). These processes alter smoke particle shape, size and composition, resulting in PLDR values that may vary from 2 to 10% at 532 nm for aged and fresh smoke. These values can be even lower/higher in cases of mixtures with low/high depolarizing components, respectively (i.e. marine/dust particles). Müller et al. (2007) carried out an extensive study on the optical properties and the effect of atmospheric ageing of long-range-transported smoke from Siberia and Canada and found that PLDR at 532 nm did not exceed 1–3 % for 10-day-old plumes. This is comparable to findings by Nicolae et al. (2013), showing that smoke plumes up to 4-day-old present PLDR values of almost 4% at 532 nm. Moreover, measurements conducted in South Africa (Giannakaki et al., 2016) showed that for pure smoke the PLDR values at 355 nm are less than 6%. On the other hand, smoke PLDR has been found to reach values up to 12–14 % at 532 nm if significant concentrations of highly depolarizing components (i.e. soil or dust particles) exist inside lofted smoke layers (Tesche et al. 2009; Veselovskii et al. 2016).

Lately, there have been observational evidence of smoke originating from large-scale fires with PLDR values that exceed the typical range. For example, in Sugimoto et al. (2010) values of 12–15 % at 532 nm are presented for both tropospheric and stratospheric smoke plumes reaching from Mongolia to Nagasaki and Tsukuba in 2007. Nisantzi et al. (2014) reported values of 9–18 % at 532 nm for smoke originating from Turkish fires and observed above Cyprus after 1 to 4 days of transport. A spectral dependence of smoke PLDR with decreasing values from UV to Near-IR was presented for the first time by Burton et al. (2015). The measurements were performed above Denver, Colorado with an airborne HSRL instrument during the DISCOVER-AQ (Deriving Information on Surface Conditions from Column and Vertically Resolved Observations Relevant to Air Quality) field mission. This particular smoke plume was found at 8 km height, originating from Pacific Northwest wildfires and exhibited PLDR values of 20%, 9.3% and 1.8 % at 355, 532 and 1064 nm, respectively. ~~Implications for enrichment of smoke plumes with dust particles during the emission have been reported, a process that could justify the high depolarization values recorded for tropospheric smoke~~.

In the past, many studies have used simpler or more complicated particle shape models in order to reproduce the lidar measurements of smoke. In Kahnert (2017), the PLDR of black carbon aggregates covered by a cell of sulphates was simulated by two different models; a closed cell (i.e. each monomer in the aggregate is coated separately) and a coated aggregate model (i.e. the whole aggregate is coated). Their analysis showed that for thicker coating the coated cell model of volume equivalent radius of 0.3 to 0.4μm, can provide PLDR values of the order of 15% at 532nm. Mishchenko et al., (2016) and Liu and Mishchenko (2018) used rather complex morphologies for smoke particles, in order to reproduce the PLDR values measured by Burton et al. (2015). Amongst others, these morphologies included a) a fractal aggregate partially embedded in a spherical sulphate cell, b) two-externally-mixed spherical sulphate cells, each hosting an aggregate (models 6 and 11 in Fig. 1 in Liu and Mishchenko, 2018 and c) a high-density aspherical soot core, encapsulated in a circumscription spheroid cell (with axial ratio of 0.9 to 1.2; model 4 in Fig. 2 in Mishchenko et al., 2016). All these morphologies reproduced successfully the smoke optical properties measured by Burton et al. (2015). Moreover, Luo et al. (2018) used twenty different configurations of coated fractal aggregates and showed that for relatively small fractal dimension (i.e. relatively fresh aggregates), and for small black carbon fractions (i.e. densely coated aggregates; configuration C in Fig. 2 in Luo et al., 2018), the PLDR values can reach up to 40, 15 and 6% at 355, 532 and 1064nm, respectively. Ishimoto et al. (2019) used fractal aggregates and artificial surface tension induced on the particles to mimic the effect of coating by water soluble materials forming around the particles. This study present results for both the PLDR and the LR, which is indicative of the composition of the particles. In Liu and Mishchenko (2019), tar ball aggregates were used to model exceptionally strong PLDR as those measured by Burton et al. (2015). The aforementioned studies highlighted the fact that in order to reproduce significant PLDR values (higher than 20% at 532nm), the fractals need to be coated (i.e. shapes of “Type-B, size 11, Vr = 20” shown in Fig. 4 of Ishimoto et al., 2019). We should point out though that most of the aforementioned studies refer to monodispersed particles, and averaging over size could possibly supress some of the observed features.

In the spotlight of the large scale Canadian fires of 2017, the discussion regarding the high PLDR values and their spectral dependence for smoke has been opened also for stratospheric smoke. These wildfires inserted large amounts of smoke to the lower stratosphere by explosive Pyro-cumulonimbus activity (Khaykin et al. 2018). In fact, the smoke load in the stratosphere was found to be comparable to that of a moderate volcanic eruption (Peterson et al. 2018). The smoke plumes encircled the Northern hemisphere in nearly 20 days, reaching Europe in less than 10 days. Above Europe, their properties were intensively studied by the European Aerosol Research Lidar Network (EARLINET; Pappalardo et al., 2014). Multi-wavelength lidar measurements in Central (Ansmann et al., 2018; Haarig et al., 2018; Hu et al., 2019) and South Europe (Gialitaki et al., 2019; Sicard et al., 2019) revealed high PLDR values at 355 and 532 nm and a strong spectral dependence from the UV to the Near-

IR. However, despite of the extensive analysis of this event, the microphysical characterization of the stratospheric smoke particles is not yet adequate and further analysis is imperative to draw conclusions. Most of the microphysical properties reported for the stratosphere are retrieved from lidar measurements using inversion algorithms and assumed scattering models that are applied in EARLINET (e.g. Veselovskii et al., 2002; Dubovik et al., 2006). For example, the derived microphysical properties presented in Haarig et al. (2018) and Hu et al. (2019) are based on the lidar backscatter and extinction coefficient profiles that were used as inputs to inversion schemes. However, the observed ~~unusual~~ PLDR values could not be reproduced by these studies due to the assumed shapes.

In contrast to prior studies, for our investigation for the stratospheric smoke originating from the Canadian wildfires, we do not adopt morphologically complex shapes of bare or coated smoke aggregates, which are associated with excessive computations. Instead, we propose a much simpler model of compact near-spherical particles. Our starting point and main assumption is that the particle near-spherical-shape can be highly depolarizing, as shown in the work of Mishchenko and Hovenier (1995) and Bi et al. (2018). Our analysis shows that for the Canadian stratospheric smoke observed above Europe in August 2017, the PLDR and LR measurements along with their spectral dependence, can be successfully reproduced with the proposed model of compact near-spherical particles. The size and refractive index of the particles are estimated as well, and seem to agree well with past observations for aged smoke. We further examine the capability of this model to be used on an operational level and in particular as an extension to the AERONET operational aerosol retrieval (Dubovik et al., 2006), since it provides a much simpler and faster solution with respect to more complicated shapes for stratospheric smoke particles (e.g. Mishchenko et al., 2016; Ishimoto et al., 2019).

Our paper is organized as follows: in Sect. 2 we discuss the methodology followed for the retrieval of the microphysical properties of stratospheric smoke, by constructing look-up-tables of PLDR and LR at 355, 532 and 1064nm, assuming (a) near-spherical shapes, and (b) more complicated shapes for the particles. In Sect. 3 we provide a brief description of the Canadian wildfires during August 2017, describing the mechanism that introduced the smoke particles into the lower stratosphere and the route of the smoke plume from Canada to Europe. The lidar measurements performed over Leipzig, Germany are presented in this Section. In Sect.4 we provide the results of our microphysical retrieval. The discussion of these results and the future perspectives of our work are found in Sect. 5. Conclusions are summarized in Sect. 6.

2 ~~Methodology~~Construction of look-up-tables

For the retrieval of the smoke microphysical properties from the measured PLDR and LR at 355, 532 and 1064 nm, we constructed appropriate look-up-tables using near-spherical shapes and more complicated shapes (i.e. Chebyshev particles), along with a range of ~~particle shapes,~~ size distributions and refractive indices based on values reported in the literature for smoke particles (Dubovik et al., 2002; Müller, 2005; Müller et al., 2007; Nicolae et al., 2013; Giannakaki et al., 2016).

For the construction of the look-up-tables we used the T-matrix code (Mackowski and Mishchenko, 1996; Mishchenko & Travis, 1998; Mackowski & Mishchenko, 2011). The T-matrix outputs are used to calculate PLDR and LR as shown in Eq. (1) and (2):

$$\text{PLDR}\ (\lambda) = \frac{P_{11}(180°) - P_{22}(180°)}{P_{11}(180°) + P_{22}(180°)} \tag{1}$$

$$\text{LR}\ (\lambda) = \frac{4\pi\ C_{ext}(\lambda)}{C_{sca}(\lambda)\ P_{11}(180°)} \tag{2}$$

where P_{ij} are the elements of the scattering matrix, C_{ext} and C_{sca} are the extinction and scattering cross sections, and λ is the wavelength (Fig. 1).

2.1 Near - spherical shapes

We modelled the near-spherical shapes using spheroid particles with different axial ratios ε. The axial ratio of a spheroid is defined as the ratio of the ellipse rotational axis (a) to the axis perpendicular to the rotational axis (b) as $\varepsilon = {}^{a}\!/_{b}$. If $\varepsilon > 1$ then the spheroid is characterized as prolate, whereas if $\varepsilon < 1$, the spheroid is characterized as oblate (Mishchenko et al., 2002; Dubovik et al., 2006). To describe the spheroidal shape in the spherical coordinate system we use Eq. (3) where r is the radius of the volume equivalent sphere and θ, φ are the zenith and azimuth angles respectively.

$$\text{r}\ (\theta,\varphi) = \text{a}\ \left[\sin^2\theta + \frac{a^2}{b^2}\ \cos^2\theta\right]^{-1/2} \tag{3}$$

For the present study we used ε values from 0.6 to 1.55. Figure 2 presents some examples of the near-spherical shapes used, embedded in a perfectly spherical shell to demonstrate their deviation from the perfect sphere.

We assumed that the shape distribution of the near-spherical particles is a mono-modal, normal distribution $n_s(\varepsilon)$ as shown in Eq. (4), with σ_s the sigma of the distribution fixed to 0.05, and ε_s the mean axial ratio (Table 1). We also assume that the shape distribution does not change with particle size. The fixed width of the shape distribution σ_s is necessary for the reduction of the retrieval complexity. Its' small value is used to avoid the wash-out of the characteristic optical properties which are shown for a relatively narrow axial ratio range for near-spherical particles (e.g. Bi et al., 2018).

$$n_s\,(\varepsilon) = \frac{1}{\sqrt{2\pi}\,\sigma_s}\exp\left(-\frac{(\varepsilon\,-\,\varepsilon_s)}{2\sigma_s^{\,2}}\right) \tag{4}$$

The size distributions considered for the near-spherical particles are mono-modal and log-normal with mean geometric radius r_g, and geometric standard deviation σ_g , as shown in Eq. (5). The grid used for r_g is 0.1 – 0.7μm, while σ_g is fixed at 0.4. The fixed width of the size distribution σ_g is again a simplification we used in order to reduce the retrieval complexity, considering that this parameter does not greatly affect the lidar-derived optical properties (e.g. Burton et al., 2016). Choosing a log-normal size distribution over any other plausible type of distribution is not expected to alter our results significantly (Hansen and Travis, 1974).

$$n\,(r) = \frac{1}{\sqrt{2\pi}\,r\,\sigma_g}\exp\left[-\frac{1}{2}\left(\frac{\ln\,(r/r_g)}{\sigma_g}\right)^2\right] \tag{5}$$

Moreover, a wavelength-independent complex refractive index m was assumed, with real part (m_r) varying from 1.~~4~~ 35 to 1.~~75~~ 85 and imaginary part (m_i) varying from 0.005 to 0.~~05~~ 5 (Dubovik et al., 2002; Müller et al., 2005; Nicolae et al., 2013; Giannakaki et al., 2016). An overview of the values used for the generation of the look-up-tables for the near-spherical particles is presented in Table 1.

2.2 Chebyshev particles

In order to investigate whether particles of more complicated shapes than the near-spherical shape can reproduce both the PLDR and LR measurements of stratospheric smoke, we also constructed look-up-tables for smoke particles resembling "Chebyshev particles" using the T-matrix code. Chebyshev particles (Fig. 3) are produced by the deformation of a sphere by means of a Chebyshev polynomial. In the spherical coordinates system, their shape is described as shown in Eq. (6), where r_0 is the radius of the perfect sphere, u is the deformation parameter and $T_n(cos\theta)$ is the Chebyshev polynomial of degree n (Mishchenko and Travis, 1998).

$$r\,(\theta,\varphi) = r_0\,(1 + u\,T_n\,(cos\theta)), \qquad |u|<1 \tag{6}$$

Only Chebyshev polynomials of second and fourth degree were used, with deformation parameter values of u = ± 0.05, ± 0.10, ± 0.15, ± 0.20, ± 0.25 and u = ± 0.05 ~~to~~, ± 0.10, ± 0.15 respectively. We considered the same refractive indices as the ones used for the generation of the look-up-tables of the near-spherical particles, while for the size distribution we used also mono-modal, log-normal distributions. Table ~~2~~ 1 summarizes the properties ~~chosen~~ used for the construction of the look-up-tables for Chebyshev particles.

3 Description of the dispersion and vertical distribution of smoke

The extreme pyro-convection (Fromm et al. 2010) that was recorded in the area of British Columbia (western Canada) during summer 2017, resulted in particularly strong updrafts that penetrated and released large amounts of smoke particles into the lower stratosphere (Peterson et al., 2018). Here we use an ensemble of satellite observations from MODIS (Moderate Resolution Imaging Spectroradiometer) on board Terra and Aqua, OMPS (Ozone Mapping and Profiler Suite) on board Suomi NPP and CALIOP (Cloud-Aerosol Lidar with Orthogonal Polarization) on board CALIPSO, to identify the dispersion and vertical distribution of the plume above Canada~~,~~. ~~as well as the profile of PLDR at 532 nm from CALIOP~~. The combination of these observations is shown in Fig. 4, where true-color images from MODIS are overlaid with the fire active regions and thermal anomalies (red dots) from Suomi NPP, and CALIPSO (~~yellow~~ green lines) overpasses on 8 and 15 August 2017~~, when the smoke plume has already reached Europe.~~ .

Figures 5 and 6 show the b~~B~~ackscatter c~~C~~oefficient and PLDR curtain plots at 532 nm from CALIPSO measurements. Based on these observations smoke plumes were found above the regions of fire activity since the beginning of August (Fig. 4a), when the plumes remained in the troposphere, below 5-6 km (39º – 45º N, 123º – 125º W) (Fig. 5a, red dashed lines), exhibiting low PLDR values of the order of 3 – 4 % (Fig. 5b). Then on 12 August ~~12~~2017, the unprecedented buoyancy force caused by the strong fire activity started lifting the plumes up towards the tropopause, while already on 15 August 2017~~15~~ smoke covered a large part of North Canada (Fig. 4b). CALIPSO observations on 15 August ~~12~~ reveal that the plume lies into the stratosphere at 11 - 14 km height (63º – 69º N, 89º – 94º W) (Fig. 6a, red dashed lines) and PLDR values exceed 15% at 532 nm (Fig. 6b). Owning to the altitude of the smoke plume, one could attribute such PLDR values to the beginning of ice formation. Indeed, radiosonde temperature profiles from three stations located underneath the smoke plume (green stars in Fig.4b), reveal that the temperature above 11 km drops below -40°C, at which point homogeneous ice formation can occur (Wallace and Hobbs, 2006). However, the PLDR values of cirrus clouds are usually no less than 40% (Chen et al., 2002; Noel et al., 2002; Voudouri et al., 2020). Further analysis of CALIOP data provides a mean (median) value of the backscatter related Angstrom exponent (BAE) at 532/1064nm of 0.9 (0.9) with a standard deviation on 1.07. For the BAE values close to zero are expected for cirrus clouds, although, as indicated by the large standard deviation, CALIPSO data are highly noisy at these altitudes. A recent study by Yu et al. (2019) also showed that the largest fraction of stratospheric smoke particles consisted of organic carbon (98% compared to 2% for black carbon). Particles of such high organic carbon content serve poorly as ice nuclei (Kanji et al., 2017; Phillips et al., 2013). Although the possibility of small ice crystals formed inside the smoke layers cannot be excluded, (largely due to the absence of in situ measurements) the aforementioned characteristics indicate that this plume consists of smoke particles rather than ice crystals.

Inside the lower stratosphere, unaffected by the intensive tropospheric interactions, smoke particles started drifting, following a North-Easterly direction and first appeared over Europe approximately after mid-August (Khaykin et al., 2018; Ansmann et al., 2018; Hu et al., 2019).

Interestingly, even after two months of the initial stratospheric smoke injection the plume seems to have sustained its high depolarization capability. During this period the smoke plume has already encircled the Northern hemisphere and it was detected by ~~A~~airborne lidar measurements performed above the Atlantic near the west coast of Ireland (Fig. 7a). Lidar observations showed PLDR values in the range of 10 – 14 % at 532nm between 10 and 12 km (Fig. ~~7a~~7b) ~~near the west coast of Ireland (Fig. 7c).~~ These observations were conducted in the framework of Wave-driven ISentropic Exchange (WISE) mission organised by the German Aerospace Centre (DLR) and support the high depolarization values detected for months over Europe by EARLINET, as shown in Fig. 7 in (Baars et al., 2019).

3.1 Lidar measurements in Leipzig

The highest smoke load over EARLINET ~~stations has~~was been reported at Leipzig, Germany (A. Ansmann et al. 2018; Baars et al. 2019a). Measurements at the Leibniz Institute of Tropospheric Research (TROPOS) were conducted with the BERTHA (Backscatter Extinction lidar-Ratio Temperature Humidity profiling Apparatus) multi-wavelength polarization Raman lidar system. The system measures the total and cross-polarized component of the elastic backscattered light at 355, 532 and 1064 nm, which are used to derive the PLDR at these wavelengths. It is also able to perform independent measurements of the aerosol extinction coefficient at 387, 607 nm and (after optics re-arrangement) at 1058 nm, and thus has ~~a~~ the capability to provide the LR profiles at 355, 532 and 1064 nm (M. Haarig et al. 2017). On 22 August 2017, the profiles of the stratospheric smoke backscatter and extinction coefficients at 355, 532 and 1064 nm and the smoke PLDR at 355 and 532 nm were derived from two-and-a-half-hour averaging of the lidar signals between 20:45 and 23:17 UTC. The PLDR value at 1064 nm was calculated using a forty-minute averaging between 23:50 and 00:30 UTC (M. Haarig et al. 2018). The gap between the end of the first measurement and the beginning of the second, corresponds to the necessary time for the rearrangement of BERTHA optics. To ensure the high quality of depolarization measurements, the Δ±45 depolarization calibration method proposed by Freudenthaler et al., (2009) was followed, while the effect of different parameters on the depolarization measurements of the BERTHA lidar system has been carefully assessed and is presented in detail in (Haarig et al., 2017).

Layer-integrated values of PLDR and LR for the stratospheric smoke layer are shown in Fig. 8 and Table ~~1~~ 2 along with their associated uncertainties. The derived LRs are typical for aged Canadian smoke at 355 nm (40 ± 16 sr) and 532nm (66 ± 12 sr) (Müller et al., 2007). Low signal-to-noise ratio at the plume height prevented detailed retrievals of particle extinction coefficient at 1058 nm. Thus, for the LR values at 1064 nm only few measurement points could be derived (Haarig et al., 2018). This yields a LR value of 92 ± 27 sr at 1064 nm. The increasing tendency of the LR from the UV to the visible part of the spectrum has been also reported before for aged Canadian smoke (Müller et al., 2007). ~~, advocating to a possible increase~~ Measurements reported in Haarig et al. (2018) suggest that there is an increase also at the Near-IR, although there are currently no other available measurements of the LR of smoke particles at this wavelength. ~~this is not currently supported by other observational evidence found in the literature.~~. On the other hand, the PLDR values of stratospheric smoke are much larger than those usually reported in the past for tropospheric smoke. ~~far from typical for aged smoke~~. The layer-integrated PLDR value at 355 nm is 22.4 ± 2.5 %, decreasing to 18.4 ± 1.2 % at 532 nm and 4 ± ~~0.8~~2.3 % at 1064 nm. The uncertainties in PLDR values include both the systematic errors and the standard deviation of the measurements.

These results are in agreement with the PLDR values measured above Lille and Palaiseu from 24 – 31 August ~~24 to 28~~, 2017 (Hu et al., 2019). To the best of our knowledge, up to now the majority of observations for such smoke PLDR values, refer to smoke particles found in the stratosphere (i.e. Ohneiser et al., 2020). The sole exception is the case study reported by Burton et al. (2015) (see also Table 2).

4 Smoke microphysical retrieval

4.1 Near – spherical particles

First, we present the smoke microphysical retrieval considering the near-spherical shape for the smoke particles, as described in section 2.2. All the possible solutions are selected from the pre-calculated T-matrix look-up-tables, based on Eq. (7). For each measured PLDR and LR, at each wavelength λ, the simulated value must be within the corresponding measurement error e.

~~The search in the T-matrix look-up tables is performed on the basis of achieving the minimum sum of squares of relative differences between measurements and simulations as shown in, Eq. (8) (see also Fig. 1).~~

$$\left|\delta_\lambda^M - \delta_\lambda^S\right| \leq e(\delta_\lambda^M) \text{ and } \left|LR_\lambda^M - LR_\lambda^S\right| \leq e(LR_\lambda^M) \qquad (\cancel{8}7)$$

$$\cancel{\sum_{i=1}^{n}\left(\frac{M_\lambda^i - S_\lambda^i}{M_\lambda^i}\right)^2 = min}$$

Where M_λ^i denotes to measured PLDR and LR at wavelength λ = 355, 532 and 1064 nm and S_λ^i denotes to the corresponding simulations. ~~Out of the results, the~~ The solution is ~~accepted~~selected amongst the possible solutions based on the minimization criteria of Eq. (8) (see also Fig. 1). ~~on the requirement that each simulated value has to be within the measurement error (Eq. 9).~~

$$\sum_{\lambda=355,\,532,\,1064}\left(\left(\frac{\delta_\lambda^{M}-\delta_\lambda^{S}}{e\,(\delta_\lambda^{M})}\right)^2+\left(\frac{LR_\lambda^{M}-LR_\lambda^{S}}{e\,(LR_\lambda^{M})}\right)^2\right)=\mathbf{min} \qquad (\cancel{9}8)$$

$$\cancel{S_\lambda^i \le e(M_\lambda^i)}$$

Following this methodology, for the near-spherical particles ten possible solutions were found, listed in Table 3 along with the resulting cost functions calculated with Eq. (8). For these solutions, the mean axial ratio ε_s of the particles covers the range 1.1 to 1.4 while the range of the mean geometric radius is from 0.25μm ($reff$ = 0.4μm) up to 0.45μm ($reff$ = 0.7μm). For the complex refractive index m, the imaginary part m_i does not exceed the value of i0.03, while the real part m_r takes values from 1.35 to 1.55. The minimization of the cost function (Eq. 8) is achieved for near-spherical particles with ε_s = 1.4, m = 1.55 + i0.025 and r_g = 0.25μm, suggesting a strong accumulation mode for the size distribution of the particles, with sufficiently small m_i so as the characteristic enhancement in PLDR does not wash out due to the strong absorption (Bi et al., 2018). All possible solutions as well as the solution that minimizes the cost function are presented in Fig. 9 and 10.

4.2 Chebyshev particles

For Chebyshev particles of second (T_2) and fourth degree (T_4) used herein, the search in the constructed look-up-tables provided the solutions listed in Table 4. For all the solutions, deformation parameter for Chebyshev particles of the second degree ranges from u = –0.25 to 0.15, while for particles of the fourth degree only one solution was found with u = -0.1. These u values suggest small deviations from sphericity, meaning that these morphologies also resemble near-spherical shapes (see also Fig. 3). Only for two cases the size of the particles was found to be larger than the size of the near-spherical shaped particles. In particular the range of r_g was from 0.15μm ($reff$ = 0.2μm) to 0.55μm ($reff$ = 0.8μm). The complex refractive index, in some cases exceed the corresponding values for near-spherical particles. The range of the imaginary part m_i is from 0.005 to 0.055,and the range of the real part m_r is from 1.35 to 1.8. The minimization of the cost function (Eq. 8) is achieved for Chebyshev particles of the second degree with u = -0.25 (resembling an oblate near-spherical particle), complex refractive index m = 1.65 + i0.03 and mean geometric radius r_g = 0.2μm (Fig. 11). For Chebyshev particles of the fourth degree, the sole solution presented values of u = -0.1, m = 1.35 + i(0.01) and r_g = 0.55μm (Fig. 12).

~~For Chebyshev particles of second (T_2) and fourth degree (T_4) used herein, the search in the constructed look-up-tables did not produce a successful fitting of the measurements (Fig. 12). Specifically, the PLDR values at 532 nm deviate from the measured values. Table 6 presents indicatively the results that provided the minimum relative difference with respect to the measured mean values.~~

4.3 More case studies

Although the available literature on the PLDR and LR values of stratospheric smoke is for now limited, we see that we can reproduce all reported PLDR and LR listed in Table 2, using the near-spherical shape model (Fig. 4-9 in the Supplement). All cases listed in Table 2 are associated with Pyro-cumulonimbus activity. As already mentioned the case studies of Burton et al. (2015), Hu et al. (2019) and Haarig et al. (2018) refer to Canadian smoke, while the most recent case study presented by Ohneiser et al. (2020) refer to Australian wildfires of 2019-2020. Tables 4-9 in the Supplement present the properties of near-spherical particles and Chebyshev particles that reproduce the PLDR and LR observations reported in the aforementioned studies. Results are in line with the results presented for Haarig et al. (2017).

We note here that all the retrievals indicate fine particles, with mean geometric radius that does not exceed the value of 0.55μm. The simulations presented by Bi et al., (2018; Fig. 2) suggest that for the near-spherical particles the measured spectral dependence of PLDR (steeply decreasing from the UV to the Near-IR) could not be reproduced by coarse particles. Thus, the possibility of an optically significant coarse mode would have to be investigated with a different shape model. In any case though, the retrieved fine mode is in good agreement with in-situ measurements of aged smoke particles (i.e. Dahlkötter et al., 2014). The presence of a pronounced accumulation mode is also suggested by the extinction related Angstrom exponent (EAE) measured in Leipzig (-0.3±0.4 at 355/532nm and 0.85 0.3 at 532/1064nm). According to Eck et al. (1999), a strong spectral slope in EAE can be associated with a prominent accumulation mode of the size distribution for smoke particles.

5 Discussion

5.1 Potential of near-spherical model for AERONET products

Up to now, the use of near-spherical particles is found to well-reproduce the lidar measurements of smoke optical properties, as well as their wavelength dependence. In this section, we further extend our study to examine the potential of using the near-spherical shape model with sun-photometer measurements, on an operational level. Our main idea is whether the AERONET non-spherical scattering model could be extended to include also near-spherical particles for stratospheric smoke. In the current AERONET retrieval scheme, non-spherical particles are modelled as spheroids with axial ratios of 0.33-0.7 and 1.44-2.99, thus omitting the near-spherical particles. These ranges of axial ratios were selected towards an optimized retrieval for dust particles (Dubovik et al., 2006).

As an indication of the limitation of the current AERONET non-spherical model on reproducing the stratospheric smoke cases, we refer to AERONET Version 2 morning observations (05:42 UTC) from Lindenberg site on 23 August 2017 (180 km from Leipzig) and Version 3 noon observations (11:03) from Punta Arenas on 8 January 2020. For these two cases, the sun-photometer measurements should be affected by the presence of stratospheric smoke as shown in Haarig et al. (2018) and Ohneiser et al. (2020). The corresponding AERONET retrievals present residual errors higher than 5%, which marks the threshold of a successful AERONET retrieval (Holben et al., 2006). For the first case over Lindenberg site, the retrievals were rejected from the quality assured Level 2 AERONET products, while they are absent from the latest AERONET Version 3.

The following analysis shows possible benefits for the AERONET retrievals of stratospheric smoke, from including the near-spherical model in the retrieval scheme. Towards this end, we show that the AERONET non-spherical model is limited in reproducing the phase function of particles with near-spherical shapes. We should note here that this is only a first-level approximation of the full solution, since we do not account for the multiple scattering along the column of the sun-photometer measurements, but rather assume only single scattering.

In the following we tried to reproduce the phase function (P_{11}) of the near-spherical stratospheric smoke particles presented herein, using the phase functions calculated with the AERONET non-spherical model. For the latter we used the pre-calculated AERONET Kernels (Dubovik et al., 2006), for a large suite of refractive indices and size distributions (Table 6). The comparison is performed for the sun-photometer wavelengths at 440, 670, 870 and 1020 nm. Figure 13 (left plot) shows the phase function at 440 nm calculated for the near-spherical stratospheric smoke particles (purple line in the plots), and the comparison with the phase functions at 440 nm calculated using the AERONET non-spherical model (blue lines) with r_g = 0.25 μm and all refractive indices in Table 6. The complete set of calculations (for all r_g and refractive indices in Table 6, and AERONET wavelengths of 670, 870 and 1020 nm) is provided in the Supplement. Figure 13 shows also the degree of linear polarization ($-P_{12}/P_{11}$) (middle plot) and the values of P_{22}/P_{11} (right plot). These plots are provided to show the potential of polarized measurements in better discerning the features of near-spherical particles (as is the case with the PLDR measurements).

In order to quantify the residual of fitting we use Eq. (9) (https://aeronet.gsfc.nasa.gov/new_web/Documents/Inversion_products_for_V3.pdf).

$$Err = \sqrt{\frac{\sum_{i=1}^{n}(lnf^{*} - lnf)^{2}}{N}} * 100 = \%Error \qquad \text{Eq.(9)}$$

Where lnf^{*} denotes to P_{11} values calculated with the near-spherical model, lnf denotes the P_{11} values calculated with the AERONET non-spherical model, and N is the number of values, in terms of wavelengths and scattering angles. Err is calculated considering the four AERONET wavelengths at 440, 670, 870 and 1020 nm and the scattering angles from 0° to 150°, which indicate the measurement geometry of the AERONET sun-photometers.

The residuals (Err) for fitting the phase function of the near-spherical particles with the AERONET non-spherical model, are presented in Fig. 11. The minimum Err is 9.4%, whereas, the limit of a successful AERONET retrieval is 5% (Holben et al., 2006), indicating the limitations of the AERONET non-spherical model in reproducing the phase function of near-spherical smoke particles. Similar results for the Err considering only the wavelengths at 440, 670, 870 and 1020 nm are provided in the Supplement.

Again, we should emphasize the fact that the residual threshold of 5% denotes to the multiple-scattered light, which may mask the differences seen in the single-scattering properties in Fig. 12 and 13. In order to have a clear understanding of whether the near-spherical shape model could in fact improve the AERONET retrieval for stratospheric smoke, further analysis is imperative. For example, although a large range of the parameters affecting the retrieval and combination of these parameters were used, there are always other possible combinations that were not accounted for. To draw any strong conclusions one would have to perform a numerical inversion of the stratospheric smoke measurements, and investigate the corresponding residuals. This is part of our future work, continuing the characterization of stratospheric smoke particles with the combination of sun-photometer and lidar measurements.

6 Conclusions

The unique optical properties of transported stratospheric smoke, originating from the Pyro-cumulonimbus activity of the large Canadian fires 2017, were reproduced using T-matrix simulations and assuming near-spherical shapes for smoke. This is consistent with results of past studies showing that near-spherical particles produce PLDR values that can reach up to 100% depending also on their size and composition (Bi et al., 2018) and that smoke particles in particular, when heavily coated or even ~~coated with~~ encapsulated with weakly absorbing materials, ~~and resemble near-spherical shapes,~~ can produce large depolarization with a noticeable spectral dependence (Mishchenko et al. 2016; Ishimoto et al., 2019).

As a next step we examined whether the AERONET retrieval could possibly be benefited by taking into account the near-spherical shape for stratospheric smoke. Sun-photometer measurements from Lindenberg and Punta Arenas revealed that for the current algorithm configuration, AERONET retrievals for stratospheric smoke cases are associated with high residual errors (higher than 5%) and are eventually rejected. The extension of the AERONET scattering model to include the near-spherical shapes could possibly improve the retrieval for these cases that seem to become frequent. Our analysis does not mean to generalize on the performance of the AERONET retrieval on tropospheric biomass burning cases. It is focused on the stratospheric smoke cases, related to PyroCb activity.

Concluding, studying the stratospheric smoke from the Canadian wildfire activity provided us with the great opportunity to show the potential of remote sensing measurements in investigating and deducing new optical and microphysical properties for the stratospheric smoke particles. Our analysis highlighted also the need for coordinated ground-based lidar network measurements such as the ones provided by EARLINET, as an exploratory tool in investigating unknown processes in the stratosphere.

Data availability. The satellite products used in this study are the CALIPSO 5 km aerosol profile product (Vaughan et al., 2019) publicly available at the AERIS/ICARE database (ICARE data and services center, 2019); the Microwave Limb Sounder (MLS) H_2O data, publicly available at the GES DISC (Goddard Earth Sciences Data and Information Services Center, 2019) ftp server (https://disc.gsfc.nasa.gov/datasets?page=1&keywords=ML2H2O_004) and the MODIS Corrected Reflectance (True Color) images (Gumley et al., 2010) publicly available on the NASA Worldview center (NASA Worldview snapshots application center, 2019). The HALO-DLR aircraft lidar observations (level 2 data of depolarization and water vapour mixing ratio profiles) used in this study are available via the HALO database (https://halo-db.pa.op.dlr.de/). All datasets created during the calculation of the scattering properties of near-spherical and Chebyshev particles can be accessed through the ReACT-NOA database upon request to the corresponding author.

Author contributions. VA, AT and AG conceived the presented idea; VA and AT supported AG on the analysis, manuscript preparation, and figures design; AT guided and supervised AG on the scattering model calculations and results interpretation; RC and LP performed the analysis on fractal aggregates scattering properties and provided AG with the results (not shown in the final manuscript); AG, AK and SS analyzed the MLS water vapour data and performed Flexpart model runs to support the dispersion of the smoke and volcanic plumes (not shown in the final manuscript); EM prepared the CALIPSO data and figures; MH, HB and AA collected and analyzed Leipzig lidar measurements; TL, AL and OD supported AG to confirm T-matrix results for near-spherical particles; SG and MW performed the airborne lidar measurements and the corresponding analysis; DB advised AG on the interpretation of the results of this study. All authors provided critical feedback and helped shape the research, analysis and manuscript.

Competing interests. The authors declare that they have no conflict of interest.

Special issue statement. This article is part of the special issue "EARLINET aerosol profiling: contributions to atmospheric and climate research". It is not associated with a conference.

Acknowledgements. We are grateful to EARLINET (https://www.earlinet.org/, last access: 10 January 2020), ACTRIS (https://www.actris.eu, last access: 10 January 2020), for the data collection, calibration, processing and dissemination. We are grateful to the AERIS/ICARE Data and Services Center for providing access to the CALIPSO data used and their computational center (http: //www.icare.univ-lille1.fr/, last access: 10 January 2020). We thank the NASA/LaRC/ASDC for making available the CALIPSO products. We are grateful to the entire GRASP-OPEN (https://www.grasp-open.com/) team for the algorithm development. We acknowledge the use of imagery from the Worldview Snapshots application (https://wvs.earthdata.nasa.gov/, last access: 10 January 2020), part of the Earth Observing System Data and Information

System (EOSDIS). We acknowledge the PANGEA datacenter for supporting all computations for the development of datasets for the calculation of the scattering properties of near-spherical and Chebyshev particles.

Financial support. The research leading to these results was supported through the European Research Council (ERC) under the European Community's Horizon 2020 research and innovation framework program – ERC grant agreement 725698 (D-TECT). Anna Gialitaki acknowledges support of this work by the project “PANhellenic infrastructure for Atmospheric Composition and climatE chAnge” (MIS 5021516), which is implemented under the action “Reinforcement of the Research and Innovation Infrastructure”, funded by the operational program “Competitiveness, Entrepreneurship and Innovation” (NSRF 2014–2020) and co-financed by Greece and the European Union (European Regional Development Fund). NOA team acknowledges the support of Stavros Niarchos Foundation (SNF).

References

Adachi, K., and P.R. Buseck. 2011. “Atmospheric Tar Balls from Biomass Burning in Mexico.” *Journal of Geophysical Research Atmospheres* 116 (5). https://doi.org/10.1029/2010JD015102.

Amiridis, V., D.S. Balis, E. Giannakaki, A. Stohl, S. Kazadzis, M.E. Koukouli, and P. Zanis. 2009. “Optical Characteristics of Biomass Burning Aerosols over Southeastern Europe Determined from UV-Raman Lidar Measurements.” *Atmospheric Chemistry and Physics* 9 (7): 2431–40. https://doi.org/10.5194/acp-9-2431-2009.

Ansmann, A., H. Baars, A. Chudnovsky, I. Mattis, I. Veselovskii, M. Haarig, P. Seifert, R. Engelmann, and U. Wandinger. 2018. “Extreme Levels of Canadian Wildfire Smoke in the Stratosphere over Central Europe on 21-22 August 2017.” *Atmospheric Chemistry and Physics* 18 (16): 11831–45. https://doi.org/10.5194/acp-18-11831-2018.

Ansmann, Albert, Holger Baars, Alexandra Chudnovsky, Ina Mattis, Igor Veselovskii, Moritz Haarig, Patric Seifert, Ronny Engelmann, and Ulla Wandinger. 2018. “Extreme Levels of Canadian Wildfire Smoke in the Stratosphere over Central Europe on 21–22 August 2017.” *Atmospheric Chemistry and Physics* 18 (16): 11831–45. https://doi.org/10.5194/acp-18-11831-2018.

Baars, Holger, Albert Ansmann, Kevin Ohneiser, Moritz Haarig, Ronny Engelmann, Dietrich Althausen, Ingrid Hanssen, et al. 2019a. “The Unprecedented 2017&Amp;#8211;2018 Stratospheric Smoke Event: Decay Phase and Aerosol Properties Observed with the EARLINET.” *Atmospheric Chemistry and Physics* 19 (23): 15183–98. https://doi.org/10.5194/acp-19-15183-2019.

———. 2019b. “The Unprecedented 2017&Amp;#8211;2018 Stratospheric Smoke Event: Decay Phase and Aerosol Properties Observed with the EARLINET.” *Atmospheric Chemistry and Physics* 19 (23): 15183–98. https://doi.org/10.5194/acp-19-15183-2019.

Bi, L., W. Lin, D. Liu, and K. Zhang. 2018. “Assessing the Depolarization Capabilities of Nonspherical Particles in a Super-Ellipsoidal Shape Space.” *Optics Express* 26 (2): 1726–42. https://doi.org/10.1364/OE.26.001726.

Burton, S.P., J.W. Hair, M. Kahnert, R.A. Ferrare, C.A. Hostetler, A.L. Cook, D.B. Harper, et al. 2015. “Observations of the Spectral Dependence of Linear Particle Depolarization Ratio of Aerosols Using NASA Langley Airborne High Spectral Resolution Lidar.” *Atmospheric Chemistry and Physics* 15 (23): 13453–73. https://doi.org/10.5194/acp-15-13453-2015.

Burton, Sharon P., Eduard Chemyakin, Xu Liu, Kirk Knobelspiesse, Snorre Stamnes, Patricia Sawamura, Richard H. Moore, Chris A. Hostetler, and Richard A. Ferrare. 2016. “Information Content and Sensitivity of the 3 β + 2 α Lidar Measurement System for Aerosol Microphysical Retrievals.” *Atmospheric Measurement Techniques* 9 (11): 5555–74. https://doi.org/10.5194/amt-9-5555-2016.

Chen, Wei-Nai, Chih-Wei Chiang, and Jan-Bai Nee. 2002. “Lidar Ratio and Depolarization Ratio for Cirrus Clouds.” *Applied Optics* 41 (30): 6470–76. https://doi.org/10.1364/AO.41.006470.

Dahlkötter, F., M. Gysel, D. Sauer, A. Minikin, R. Baumann, P. Seifert, A. Ansmann, M. Fromm, C. Voigt, and B. Weinzierl.

2014. “The Pagami Creek Smoke Plume after Long-Range Transport to the Upper Troposphere over Europe &Ndash; Aerosol Properties and Black Carbon Mixing State.” *Atmospheric Chemistry and Physics* 14 (12): 6111–37. https://doi.org/10.5194/acp-14-6111-2014.

Dubovik, O., A. Sinyuk, T. Lapyonok, B.N. Holben, M. Mishchenko, P. Yang, T.F. Eck, et al. 2006. “Application of Spheroid Models to Account for Aerosol Particle Nonsphericity in Remote Sensing of Desert Dust.” *Journal of Geophysical Research Atmospheres* 111 (11). https://doi.org/10.1029/2005JD006619.

Dubovik, Oleg, Brent Holben, Thomas F Eck, Alexander Smirnov, Yoram J Kaufman, Michael D King, Didier Tanré, and Ilya Slutsker. 2002. “Variability of Absorption and Optical Properties of Key Aerosol Types Observed in Worldwide Locations.” *Journal of the Atmospheric Sciences* 59 (3): 590–608. https://doi.org/10.1175/1520-0469(2002)059<0590:VOAAOP>2.0.CO;2.

Eck, T. F., B. N. Holben, J. S. Reid, O. Dubovik, A. Smirnov, N. T. O’Neill, I. Slutsker, and S. Kinne. 1999. “Wavelength Dependence of the Optical Depth of Biomass Burning, Urban, and Desert Dust Aerosols.” *Journal of Geophysical Research Atmospheres* 104 (D24). https://doi.org/10.1029/1999JD900923.

Freudenthaler, Volker, Michael Esselborn, Matthias Wiegner, Birgit Heese, Matthias Tesche, Albert Ansmann, Detlef MüLLER, et al. 2009. “Depolarization Ratio Profiling at Several Wavelengths in Pure Saharan Dust during SAMUM 2006.” *Tellus B: Chemical and Physical Meteorology* 61 (1): 165–79. https://doi.org/10.1111/j.1600-0889.2008.00396.x.

Fromm, Michael, Daniel T. Lindsey, René Servranckx, Glenn Yue, Thomas Trickl, Robert Sica, Paul Doucet, and Sophie Godin-Beekmann. 2010. “The Untold Story of Pyrocumulonimbus.” *Bulletin of the American Meteorological Society* 91 (9): 1193–1210. https://doi.org/10.1175/2010BAMS3004.1.

Giannakaki, E., P.G. Van Zyl, D. Müller, D. Balis, and M. Komppula. 2016. “Optical and Microphysical Characterization of Aerosol Layers over South Africa by Means of Multi-Wavelength Depolarization and Raman Lidar Measurements.” *Atmospheric Chemistry and Physics* 16 (13): 8109–23. https://doi.org/10.5194/acp-16-8109-2016.

Groß, S., M. Esselborn, B. Weinzierl, M. Wirth, A. Fix, and A. Petzold. 2013. “Aerosol Classification by Airborne High Spectral Resolution Lidar Observations.” *Atmospheric Chemistry and Physics* 13 (5): 2487–2505. https://doi.org/10.5194/acp-13-2487-2013.

Groß, Silke, Matthias Tesche, Volker Freudenthaler, Carlos Toledano, Matthias Wiegner, Albert Ansmann, Dietrich Althausen, and Meinhard Seefeldner. 2011. “Characterization of Saharan Dust, Marine Aerosols and Mixtures of Biomass-Burning Aerosols and Dust by Means of Multi-Wavelength Depolarization and Raman Lidar Measurements during SAMUM 2.” *Tellus B: Chemical and Physical Meteorology* 63 (4): 706–24. https://doi.org/10.1111/j.1600-0889.2011.00556.x.

Haarig, M., A. Ansmann, D. Althausen, A. Klepel, S. Groß, V. Freudenthaler, C. Toledano, et al. 2017. “Triple-Wavelength

Depolarization-Ratio Profiling of Saharan Dust over Barbados during SALTRACE in 2013 and 2014.” *Atmospheric Chemistry and Physics* 17 (17): 10767–94. https://doi.org/10.5194/acp-17-10767-2017.

Haarig, M., A. Ansmann, H. Baars, C. Jimenez, I. Veselovskii, R. Engelmann, and D. Althausen. 2018. “Depolarization and Lidar Ratios at 355, 532, and 1064 Nm and Microphysical Properties of Aged Tropospheric and Stratospheric Canadian Wildfire Smoke.” *Atmospheric Chemistry and Physics* 18 (16): 11847–61. https://doi.org/10.5194/acp-18-11847-2018.

Haarig, Moritz, Albert Ansmann, Dietrich Althausen, André Klepel, Silke Groß, Volker Freudenthaler, Carlos Toledano, et al. 2017. “Triple-Wavelength Depolarization-Ratio Profiling of Saharan Dust over Barbados during SALTRACE in 2013 and 2014.” *Atmospheric Chemistry and Physics* 17 (17): 10767–94. https://doi.org/10.5194/acp-17-10767-2017.

Hansen, James E, and Larry D Travis. 1974. “Light Scattering in Planetary Atmospheres.” *Space Science Reviews* 16 (4): 527–610. https://doi.org/10.1007/BF00168069.

Holben, B. N., T. F. Eck, I. Slutsker, A. Smirnov, A. Sinyuk, J. Schafer, D. Giles, and O. Dubovik. 2006. “Aeronet’s Version 2.0 Quality Assurance Criteria.” In , edited by Si-Chee Tsay, Teruyuki Nakajima, Ramesh P. Singh, and R. Sridharan, 64080Q. https://doi.org/10.1117/12.706524.

Hoose, C., and O. Möhler. 2012. “Heterogeneous Ice Nucleation on Atmospheric Aerosols: A Review of Results from Laboratory Experiments.” *Atmospheric Chemistry and Physics* 12 (20): 9817–54. https://doi.org/10.5194/acp-12-9817-2012.

Hu, Q., P. Goloub, I. Veselovskii, J.-A. Bravo-Aranda, I. Elisabeta Popovici, T. Podvin, M. Haeffelin, et al. 2019. “Long-Range-Transported Canadian Smoke Plumes in the Lower Stratosphere over Northern France.” *Atmospheric Chemistry and Physics* 19 (2): 1173–93. https://doi.org/10.5194/acp-19-1173-2019.

Hu, Qiaoyun, Philippe Goloub, Igor Veselovskii, Juan-Antonio Bravo-Aranda, Ioana Elisabeta Popovici, Thierry Podvin, Martial Haeffelin, et al. 2019. “Long-Range-Transported Canadian Smoke Plumes in the Lower Stratosphere over Northern France.” *Atmospheric Chemistry and Physics* 19 (2): 1173–93. https://doi.org/10.5194/acp-19-1173-2019.

Ishimoto, Hiroshi, Rei Kudo, and Kouji Adachi. 2019. “A Shape Model of Internally Mixed Soot Particles Derived from Artificial Surface Tension.” *Atmospheric Measurement Techniques* 12 (1): 107–18. https://doi.org/10.5194/amt-12-107-2019.

Kahnert, Michael. 2017. “Optical Properties of Black Carbon Aerosols Encapsulated in a Shell of Sulfate: Comparison of the Closed Cell Model with a Coated Aggregate Model.” *Optics Express* 25 (20): 24579. https://doi.org/10.1364/OE.25.024579.

Kanji, Zamin A, Luis A Ladino, Heike Wex, Yvonne Boose, Monika Burkert-Kohn, Daniel J Cziczo, and Martina Krämer. 2017. “Overview of Ice Nucleating Particles.” *Meteorological Monographs* 58 (May): 1.1-1.33. https://doi.org/10.1175/AMSMONOGRAPHS-D-16-0006.1.

Kaufman, Y.J., D. Tanré, and O. Boucher. 2002. “A Satellite View of Aerosols in the Climate System.” *Nature* 419 (6903): 215–23. https://doi.org/10.1038/nature01091.

Khaykin, S.M., S. Godin-Beekmann, A. Hauchecorne, J. Pelon, F. Ravetta, and P. Keckhut. 2018. “Stratospheric Smoke With Unprecedentedly High Backscatter Observed by Lidars Above Southern France.” *Geophysical Research Letters* 45 (3): 1639–46. https://doi.org/10.1002/2017GL076763.

Liu, L., and M.I. Mishchenko. 2018. “Scattering and Radiative Properties of Morphologically Complex Carbonaceous Aerosols: A Systematic Modeling Study.” *Remote Sensing* 10 (10). https://doi.org/10.3390/rs10101634.

———. 2019. “Modeling Study of Scattering and Absorption Properties of Tar-Ball Aggregates.” *Applied Optics* 58 (31): 8648–57. https://doi.org/10.1364/AO.58.008648.

Luo, Jie, Yongming Zhang, and Qixing Zhang. 2018. “A Model Study of Aggregates Composed of Spherical Soot Monomers with an Acentric Carbon Shell.” *Journal of Quantitative Spectroscopy and Radiative Transfer* 205 (January): 184–95. https://doi.org/10.1016/j.jqsrt.2017.10.024.

Marinou, E., M. Tesche, A. Nenes, A. Ansmann, J. Schrod, D. Mamali, A. Tsekeri, et al. 2019. “Retrieval of Ice-Nucleating Particle Concentrations from Lidar Observations and Comparison with UAV in Situ Measurements.” *Atmospheric Chemistry and Physics* 19 (17): 11315–42. https://doi.org/10.5194/acp-19-11315-2019.

Mishchenko, M.I., J.M. Dlugach, and L. Liu. 2016. “Linear Depolarization of Lidar Returns by Aged Smoke Particles.” *Applied Optics* 55 (35): 9968–73. https://doi.org/10.1364/AO.55.009968.

Mishchenko, M.I., and J.W. Hovenier. 1995. “Depolarization of Light Backscattered by Randomly Oriented Nonspherical Particles.” *Optics Letters* 20 (12): 1356–58. https://doi.org/10.1364/OL.20.001356.

Mishchenko, M.I., and L.D. Travis. 1998. “Capabilities and Limitations of a Current FORTRAN Implementation of the T-Matrix Method for Randomly Oriented, Rotationally Symmetric Scatterers.” *Journal of Quantitative Spectroscopy and Radiative Transfer* 60 (3): 309–24. https://doi.org/10.1016/S0022-4073(98)00008-9.

Mishchenko, Michael I, Larry D Travis, and Andrew A Lacis. 2002. *Scattering, Absorption and Emission of Light by Small Particles*. Cambridge: Cambridge University Press.

Müller, D., A. Ansmann, I. Mattis, M. Tesche, U. Wandinger, D. Althausen, and G. Pisani. 2007. “Aerosol-Type-Dependent Lidar Ratios Observed with Raman Lidar.” *Journal of Geophysical Research* 112 (D16): D16202. https://doi.org/10.1029/2006JD008292.

Müller, D., I. Mattis, A. Ansmann, U. Wandinger, C. Ritter, and D. Kaiser. 2007. “Multiwavelength Raman Lidar Observations of Particle Growth during Long-Range Transport of Forest-Fire Smoke in the Free Troposphere.” *Geophysical Research Letters* 34 (5). https://doi.org/10.1029/2006GL027936.

Müller, Detlef. 2005. “Raman Lidar Observations of Aged Siberian and Canadian Forest Fire Smoke in the Free Troposphere over Germany in 2003: Microphysical Particle Characterization.” *Journal of Geophysical Research* 110 (D17): D17201.

https://doi.org/10.1029/2004JD005756.

Nichman, Leonid, Martin Wolf, Paul Davidovits, Timothy B. Onasch, Yue Zhang, Doug R. Worsnop, Janarjan Bhandari, Claudio Mazzoleni, and Daniel J. Cziczo. 2019. "Laboratory Study of the Heterogeneous Ice Nucleation on Black-Carbon-Containing Aerosol." *Atmospheric Chemistry and Physics* 19 (19): 12175–94. https://doi.org/10.5194/acp-19-12175-2019.

Nicolae, D., A. Nemuc, D. Müller, C. Talianu, J. Vasilescu, L. Belegante, and A. Kolgotin. 2013. "Characterization of Fresh and Aged Biomass Burning Events Using Multiwavelength Raman Lidar and Mass Spectrometry." *Journal of Geophysical Research Atmospheres* 118 (7): 2956–65. https://doi.org/10.1002/jgrd.50324.

Nisantzi, A., R.E. Mamouri, A. Ansmann, and D. Hadjimitsis. 2014. "Injection of Mineral Dust into the Free Troposphere during Fire Events Observed with Polarization Lidar at Limassol, Cyprus." *Atmospheric Chemistry and Physics* 14 (22): 12155–65. https://doi.org/10.5194/acp-14-12155-2014.

Noel, Vincent, Helene Chepfer, Guy Ledanois, Arnaud Delaval, and Pierre H. Flamant. 2002. "Classification of Particle Effective Shape Ratios in Cirrus Clouds Based on the Lidar Depolarization Ratio." *Applied Optics* 41 (21): 4245. https://doi.org/10.1364/AO.41.004245.

Pappalardo, G., A. Amodeo, A. Apituley, A. Comeron, V. Freudenthaler, H. Linné, A. Ansmann, et al. 2014. "EARLINET: Towards an Advanced Sustainable European Aerosol Lidar Network." *Atmospheric Measurement Techniques* 7 (8): 2389–2409. https://doi.org/10.5194/amt-7-2389-2014.

Peterson, David A, James R Campbell, Edward J Hyer, Michael D Fromm, George P Kablick, Joshua H Cossuth, and Matthew T DeLand. 2018. "Wildfire-Driven Thunderstorms Cause a Volcano-like Stratospheric Injection of Smoke." *Npj Climate and Atmospheric Science* 1 (1): 30. https://doi.org/10.1038/s41612-018-0039-3.

Phillips, Vaughan T J, Paul J Demott, Constantin Andronache, Kerri A Pratt, Kimberly A Prather, R Subramanian, and Cynthia Twohy. 2013. "Improvements to an Empirical Parameterization of Heterogeneous Ice Nucleation and Its Comparison with Observations." *Journal of the Atmospheric Sciences* 70 (2): 378–409. https://doi.org/10.1175/JAS-D-12-080.1.

Sicard, M., M.J. Granados-Muñoz, L. Alados-Arboledas, R. Barragán, A.E. Bedoya-Velásquez, J.A. Benavent-Oltra, D. Bortoli, et al. 2019. "Ground/Space, Passive/Active Remote Sensing Observations Coupled with Particle Dispersion Modelling to Understand the Inter-Continental Transport of Wildfire Smoke Plumes." *Remote Sensing of Environment* 232. https://doi.org/10.1016/j.rse.2019.111294.

Sugimoto, N., B. Tatarov, A. Shimizu, I. Matsui, and T. Nishizawa. 2010. "Optical Characteristics of Forest-Fire Smoke Observed with Two-Wavelength Mie-Scattering Lidars and a High-Spectral-Resolution Lidar over Japan." *Scientific Online Letters on the Atmosphere* 6: 93–96. https://doi.org/10.2151/sola.2010-024.

Tesche, M., A. Ansmann, D. Müller, D. Althausen, R. Engelmann, V. Freudenthaler, and S. Groß. 2009. "Vertically Resolved Separation of Dust and Smoke over Cape Verde Using Multiwavelength Raman and Polarization Lidars during Saharan

Mineral Dust Experiment 2008.” *Journal of Geophysical Research* 114 (D13): D13202. https://doi.org/10.1029/2009JD011862.

Veselovskii, I., P. Goloub, T. Podvin, V. Bovchaliuk, Y. Derimian, P. Augustin, M. Fourmentin, et al. 2016. “Retrieval of Optical and Physical Properties of African Dust from Multiwavelength Raman Lidar Measurements during the SHADOW Campaign in Senegal.” *Atmospheric Chemistry and Physics* 16 (11): 7013–28. https://doi.org/10.5194/acp-16-7013-2016.

Voudouri, Kalliopi Artemis, Elina Giannakaki, Mika Komppula, and Dimitris Balis. 2020. “Variability in Cirrus Cloud Properties Using a Polly≪Sup≫XT≪/Sup≫ Raman Lidar over High and Tropical Latitudes.” *Atmospheric Chemistry and Physics* 20 (7): 4427–44. https://doi.org/10.5194/acp-20-4427-2020.

Wallace, J.M., and P.V. Hobbs. 2006. *Atmospheric Science: An Introductory Survey: Second Edition*. *Atmospheric Science: An Introductory Survey: Second Edition*. https://doi.org/10.1016/C2009-0-00034-8.

Worringen, Annette, Martin Ebert, Thomas Trautmann, Stephan Weinbruch, and Günter Helas. 2008. “Optical Properties of Internally Mixed Ammonium Sulfate and Soot Particles--a Study of Individual Aerosol Particles and Ambient Aerosol Populations.” *Applied Optics* 47 (21): 3835. https://doi.org/10.1364/AO.47.003835.

Wu, Yu, Tianhai Cheng, Lijuan Zheng, and Hao Chen. 2016. “Optical Properties of the Semi-External Mixture Composed of Sulfate Particle and Different Quantities of Soot Aggregates.” *Journal of Quantitative Spectroscopy and Radiative Transfer* 179 (August): 139–48. https://doi.org/10.1016/j.jqsrt.2016.03.012.

Yu, Pengfei, Owen B. Toon, Charles G. Bardeen, Yunqian Zhu, Karen H. Rosenlof, Robert W. Portmann, Troy D. Thornberry, et al. 2019. “Black Carbon Lofts Wildfire Smoke High into the Stratosphere to Form a Persistent Plume.” *Science* 365 (6453). https://doi.org/10.1126/science.aax1748.

Table 1. The parameters used for the generation of the look-up tables of the near – spherical and Chebyshev particles.

Parameter	Range
r_g(μm) [step]; r_{eff}(μm) [step]	0.1 – 0.7 [0.05]; 0.15 – 1.05 [0.07]
σ_g (fixed)	0.4
m_r [step]	1.4 – 1.75 [0.05]
m_i [step]	0.005 – 0.045 [0.005] and 0.05 – 0.5 [0.05]
ε_s [step]	0.6 – 1.55 [0.05]
σ_s (fixed)	0.05
u [step], T_2	±0.25 , ±0.20 , 0.15, ±0.05 [0.05]
u [step], T_4	±0.25 , ±0.20 , 0.15, ±0.05 [0.05]

Formatted: Centered

Table 2. LR and PLDR layer-integrated mean values at 355, 532 and 1064 nm for the stratospheric smoke layer, on 22 August 2017, at Leipzig, Germany (Haarig et al., 2018). Also shown are all the observations reported so far for stratospheric or tropospheric smoke particles exhibiting high PLDR values.

	$PLDR_{355}$ (%)	$PLDR_{532}$ (%)	$PLDR_{1064}$ (%)	LR_{355} (sr)	LR_{532} (sr)	LR_{1064} (sr)
Haarig et al. (2018)	22.4 ± 2.5	18.4 ± 1.2	4 ± 2.3	40 ± 16	66 ± 12	92 ± 27
Burton et al. (2015)	20.3 ± 3.6	9.3 ± 1.5	1.8 ± 0.2			
	23 ± 3	20 ± 3	5 ± 1	35 ± 6	54 ± 9	
Hu et al. (2019)	24 4	18 3	4 1	45 9	56 12	
	28 ± 8	18 ± 3	5 ± 1	34 ± 12	58 ± 20	
	23 ± 4.6	14 ± 1.4		83 ± 24.9	102 ± 20.4	
Ohneiser et al. (2020)	20 ± 4	14 ± 1.4		53 ± 15.9	76 ± 15.2	
	26 ± 5.2	15 ± 1.5		97 ± 29.1	104 ± 20.8	

Formatted Table

Table 3. Properties of near-spherical particles, that reproduce the PLDR and LR at 355, 532 and 1064 nm, as reported in Haarig et al., (2017). Also shown is the corresponding cost function of each solution. The solution that minimizes the cost function (Eq. 8) is highlighted in blue.

Measurements – Leipzig (22 August 2017)

$PLDR_{355}$	$PLDR_{532}$	$PLDR_{1064}$	LR_{355}	LR_{532}	LR_{1064}
22.4±1.5	41±16	18.4±0.6	66±12	4.3±0.7	92±27

Simulations-Near-spherical particles

r_g	ε_s	m_i	m_r	$PLDR_{355}$	$PLDR_{532}$	$PLDR_{1064}$	LR_{355}	LR_{532}	LR_{1064}	$Cost\ function$
0.45	1.1	0.005	1.35	23.19	17.73	2.08	33.03	67.37	118.96	2.54
0.5	1.1	0.005	1.35	23.85	19.53	2.80	29.08	56.02	121.76	4.02
0.35	1.2	0.02	1.45	23.21	17.22	3.89	43.14	62.77	106.10	1.48
0.35	1.2	0.025	1.45	23.10	17.29	3.85	54.30	75.10	117.69	3.25
0.3	1.3	0.025	1.5	22.2073	18.08	4.90	43.17	62.97	104.92	0.48
0.3	1.3	0.03	1.5	22.35	18.31	4.87	52.55	73.40	114.38	1.74
0.25	1.4	0.02	1.55	21.15	17.87	4.86	33.99	55.01	90.12	1.49
0.25	**1.4**	**0.025**	**1.55**	**21.38**	**18.09**	**4.78**	**40.60**	**62.91**	**96.87**	**0.37**
0.25	1.4	0.03	1.55	21.61	18.31	4.70	48.15	71.64	103.84	0.81

Table 4. Properties of Chebyshev particles of second and fourth degree, that reproduce the PLDR and LR at 355, 532 and 1064 nm, as reported in Haarig et al., (2017). Also shown is the corresponding cost function of each solution. The solution that minimizes the cost function (Eq. 8) is highlighted in blue.

Simulations-Chebyshev particles of 2nd degree

r_g	u	m_i	m_r	$PLDR_{355}$	$PLDR_{532}$	$PLDR_{1064}$	LR_{355}	LR_{532}	LR_{1064}	$Cost\ function$
0.5	-0.05	0.015	1.4	22.59	18.05	3.30	43.95	62.86	114.13	1.08
0.35	-0.1	0.02	1.45	23.94	19.03	4.31	41.38	61.94	105.71	1.04
0.35	-0.1	0.025	1.45	24.18	19.10	4.27	52.32	74.01	117.19	2.76
0.25	-0.2	0.03	1.6	21.47	18.59	6.42	38.73	54.84	94.68	1.90
0.25	-0.2	0.035	1.6	21.44	18.86	6.35	45.44	62.15	101.45	1.43
0.25	-0.2	0.04	1.6	21.44	19.11	6.26	52.96	70.14	108.40	2.37
0.25	0.1	0.045	1.6	22.96	17.65	4.99	45.19	58.42	106.28	1.32
0.25	0.1	0.05	1.6	23.08	17.81	4.93	52.22	65.98	113.89	1.63
0.2	-0.25	0.025	1.65	21.80	19.11	5.13	35.10	55.73	80.98	1.53
0.2	**-0.25**	**0.03**	**1.65**	**21.97**	**19.30**	**5.00**	**40.35**	**61.97**	**85.27**	**0.86**
0.2	-0.25	0.035	1.65	22.13	19.48	4.88	46.27	68.68	89.57	1.09
0.15	0.15	0.05	1.8	24.68	18.82	3.66	38.08	55.30	68.87	2.58
0.15	0.15	0.055	1.8	24.87	18.94	3.59	41.63	59.64	71.03	2.16

Simulations-Chebyshev particles of 4th degree

r_g	u	m_i	m_r	$PLDR_{355}$	$PLDR_{532}$	$PLDR_{1064}$	LR_{355}	LR_{532}	LR_{1064}	$Cost\ function$
0.55	**-0.1**	**0.01**	**1.35**	**23.02**	**17.73**	**5.07**	**44.13**	**67.51**	**122.24**	**1.82**

Table 5. Parameters used for the calculations of the optical properties of smoke particles, using the non-spherical model of AERONET, in Fig. 12 and 13.

.

$r_g\,(\mu m)$	0.1, 0.15, 0.2, 0.25, 0.3, 0.4, 0.5, 0.8, 1.0, 1.5, 2.0, 2.5, 3.0, 4.0

Formatted: Not Highlight

Formatted: Not Highlight

Formatted Table

m_r	1.35, 1.4, 1.44, 1.5, 1.54, 1.6, 1.65, 1.69
m_i	10^{-8}, 0.0005, 0.015, 0.07, 0.11, 0.3, 0.5

Table 2. The parameters used for the generation of the look-up tables of the Chebyshev particles.

Parameter	Range
r_g (μm)[step]	0.1 – 0.7 [0.05]
σ_g (fixed)	0.4
m_r [step]	1.4 – 1.75 [0.05]
m_i [step]	0.005 – 0.045 [0.005]
u [step], T	−0.15 – 0.15 [0.05], 4

Table 3. The parameters used for the generation of the look-up tables of the chain-like fractal aggregates.

Parameter	Range
R_v (μm)	0.5
R_m (μm)[step]	40 – 80 [20]
N_m	244, 579, 1953
D_f (fixed)	1.8
k_f (fixed)	1.3
m_r	1.4, 1.45, 1.5
m_i	0.005, 0.01, 0.03

Table 4. LR and PLDR layer-integrated mean values at 355, 532 and 1064 nm for the stratospheric smoke layer, on August 22, at Leipzig, Germany.

Table 5. The best fit of PLDR and LR at 355, 532 and 1064 nm, as calculated with the T-matrix code for near-spherical particles. The corresponding microphysical properties are shown in the first row. The relative differences with respect to the measured layer-integrated mean values are within the measurement errors shown in Table 4.

Solution: k = 1.55 + i0.025, ϵ = 1.4, r_g = 0.25μm			
	355 nm	532 nm	1064 nm
PLDR (%)	21.8	18.3	4.5

LR (sr)	41.7	64.2	98.5
PLDR rel. dif. (%)	2.8	0.6	12.5
LR rel. dif. (%)	4.3	2.7	7.1

Table 6. PLDR and LR at 355, 532 and 1064 nm, calculated with the T-matrix code considering Chebyshev particles for the microphysical properties shown in first row, and their relative difference with respect to the measured layer-integrated mean values. The relative differences that are highlighted in red, exceed the measurement errors of the layer-integrated mean values (Table 4).

T4, k = 1.5 + i0.02, u = 0.15, r_g = 0.3 μm			
	355 nm	532 nm	1064 nm
PLDR (%)	23.1	16.5	3.5
LR (sr)	39.0	60.8	101.8
PLDR rel. dif. (%)	2.9	10.3	10.6
LR rel. dif. (%)	2.4	7.9	10.6

Table 7. Example values of PLDR and LR at 355, 532 and 1064 nm, calculated with the MTSM code for the microphysical properties shown in first row and first column, considering chain-like fractal aggregates shown in Fig. 2c. Their relative difference with respect to the measured layer-integrated mean values is also shown, while values in red are found to exceed the measurement errors of the layer-integrated mean values (Table 4).

R_m = 80, D_f = 1.8, k_f = 1.3						
	PLDR			LR		
	355 nm	532 nm	1064 nm	355 nm	532 nm	1064 nm
Refractive index 1.4 + i0.03	7.4	3.6	0.8	86.2	77.9	82.6
Rel. dif. (%)	67.0	80.4	80.0	116.0	18.0	10.2
Refractive index 1.45 + i0.03	9.2	4.5	0.9	80.9	72.3	76.0
Rel. dif. (%)	58.9	75.5	77.5	102.3	9.5	17.4
Refractive index 1.5 +i0.03	11.3	5.4	1.2	77.3	67.5	71.1
Rel. dif. (%)	49.6	70.7	70	77.3	2.3	22.7

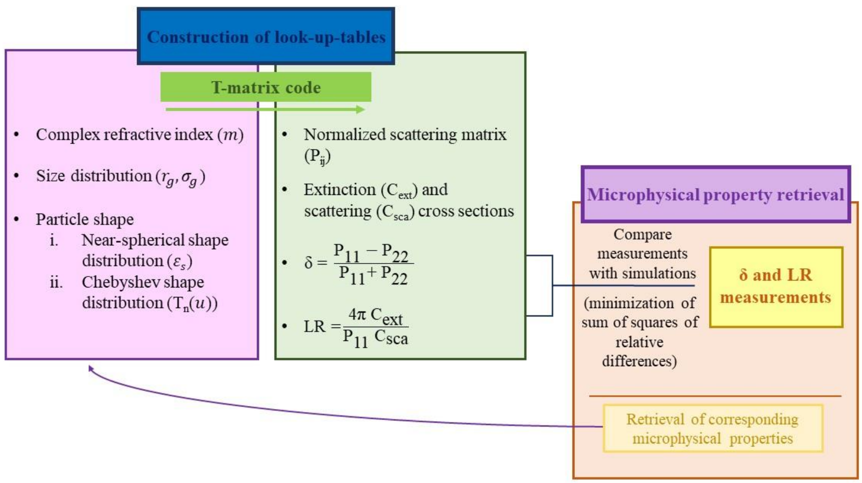

Figure 1. Overview of the methodology followed for the retrieval of the microphysical properties of the stratospheric smoke particles, using the PLDR and LR measurements at 355, 532 and 1064 nm: First, we construct appropriate ~~establishing~~ look-up-tables of PLDR and LR values for near-spherical and Chebyshev particles ~~and the retrievals from~~using -T-matrix ~~outputs~~calculations, and then we search in the look-up-tables for the solution that provides the best fit of the PLDR and LR measurements.

~~**Figure 1.** Overview of the methodology followed for establishing look-up-tables and the retrievals from T-matrix outputs~~.

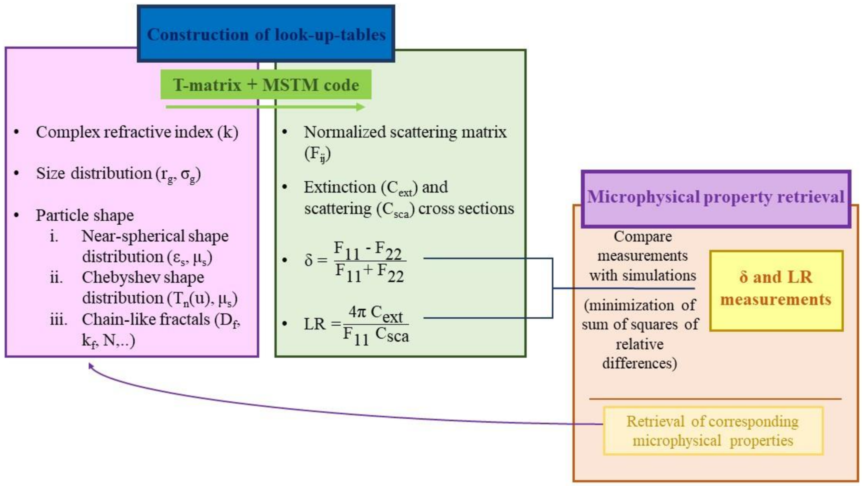

Construction of look-up-tables
T-matrix + MSTM code
Complex refractive index (k)
Size distribution (r_g, σ_g)
Particle shape
i. Near-spherical shape distribution (ε_s, μ_s)
ii. Chebyshev shape distribution ($T_n(u)$, μ_s)
iii. Chain-like fractals (D_f, k_f, N,..)
Normalized scattering matrix (F_{ij})
Extinction (C_{ext}) and scattering (C_{sca}) cross sections
$\delta = \frac{F_{11} - F_{22}}{F_{11} + F_{22}}$
$LR = \frac{4\pi\, C_{ext}}{F_{11}\, C_{sca}}$
Microphysical property retrieval
Compare measurements with simulations
(minimization of sum of squares of relative differences)
δ and LR measurements
Retrieval of corresponding microphysical properties

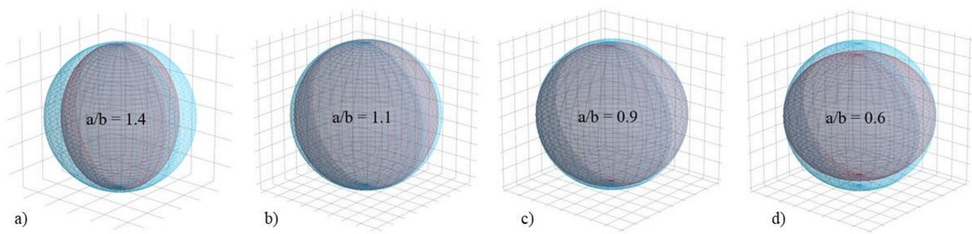

Figure 2: Examples of spheroids used (in ~~dark blue~~grey colour), embedded in a perfectly spherical shell (in light blue colour), to visualize their deviation from the perfect sphere. From left to right: ~~oblate~~prolate spheroids with (a) ε = ~~0.6~~1.4 and (b) ε = ~~0.9~~1.1 and ~~prolate~~oblate spheroids with (c) ε = ~~1.1~~0.9 and (d) ε = ~~1.4~~0.6.

~~**Figure 2:** Examples of spheroids used (in dark blue colour), embedded in a perfectly spherical shell (in light blue colour), to visualize their deviation from the perfect sphere. From left to right: oblate spheroids with **(a)** ε = 0.6 and **(b)** ε = 0.9 and prolate spheroids with **(c)** ε = 1.1 and **(d)** ε = 1.4.~~

Formatted: Font: Not Bold

Formatted: Font: Not Bold

Formatted: Font: Not Bold

Formatted: Font: Not Bold

Formatted: Font: Not Bold

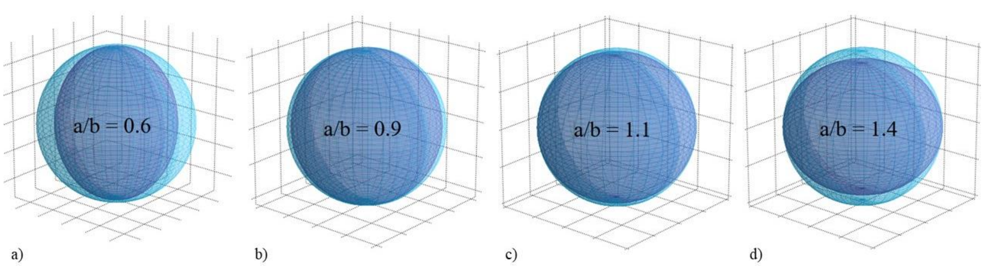

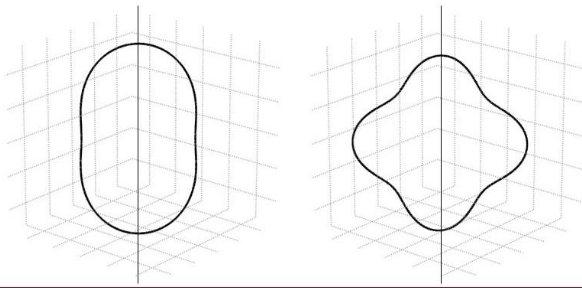

Figure 3: Examples of Cehbyshev particles used. Chebyshev particle of the second degree (T_2) with deformation parameter u = -0.25 (left) and Chebyshev particle of the fourth degree (T_4) with deformation parameter u = 0.15 (right).

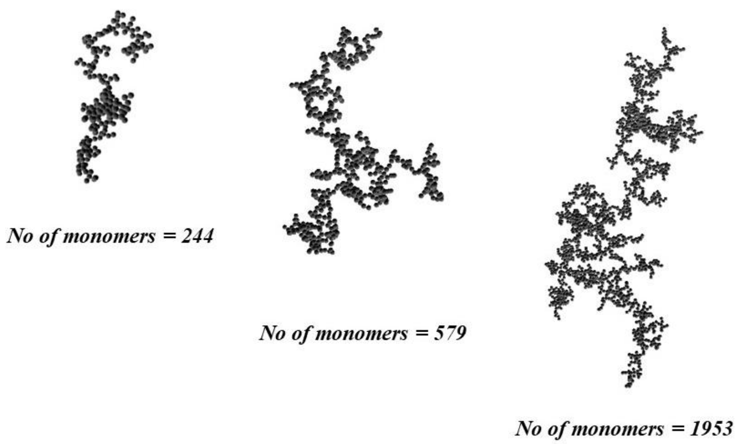

~~**Figure 3:** Fractal model morphologies composed of different number of monomers, used in MSTM code. For all fractals we use the same fixed value of fractal dimension~~ ~~D_f~~ ~~and fractal pre-factor~~ ~~k_f.~~

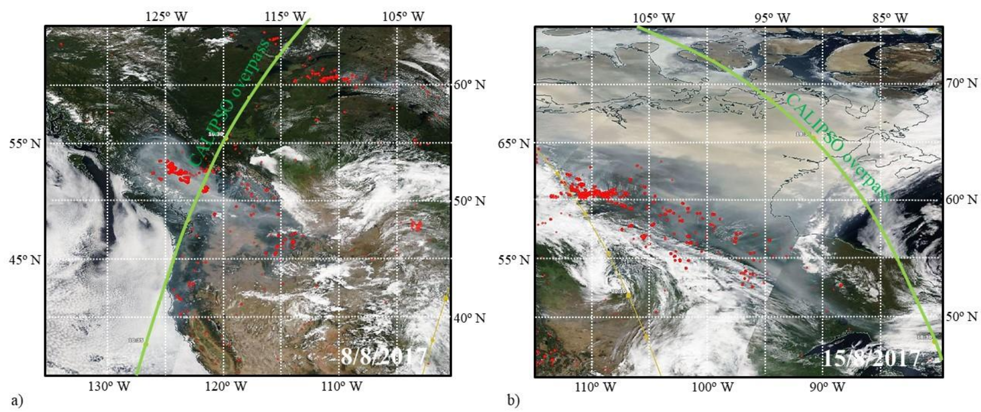

Figure ~~4~~4: Corrected surface reflectance from MODIS, over-plotted with active fire regions and thermal anomalies (red dots) and CALIPSO ascending and descending overpasses (yellow lines). Red circles denote the position of the smoke plume on (a) 8 August ~~8~~ 2017 and (b) 15 August ~~15~~ 2017. Maps are generated from NASA Worldview Snapshots.

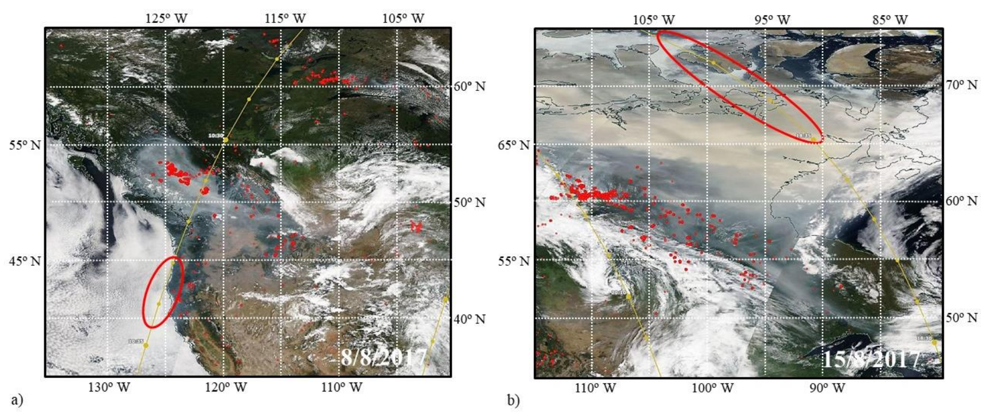

Figure ~~5~~5: CALIPSO ~~B~~backscatter ~~C~~coefficient (km^{-1}sr^{-1}) and ~~Particle Linear Depolarization Ratio~~PLDR (%) that correspond to the night-time overpass on ~~8/8/~~8 August 2017, 10:27 – 10:41 UTC shown in Fig. ~~4~~4a. (a) The smoke plume is located between 39 and 45 ° latitude, below 6 km in altitude. Red dashed lines denote the spatial averaging applied for the retrieval of optical properties shown on the right plot. (b) PLDR values at 532 nm, do not exceed values of 3 – 4 %.

Formatted: Superscript

Formatted: Superscript

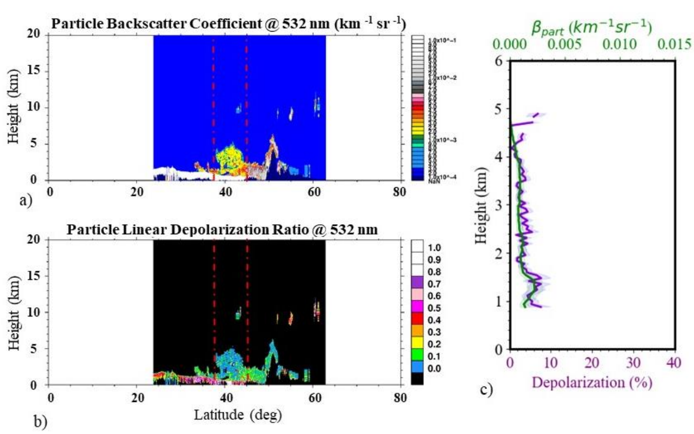

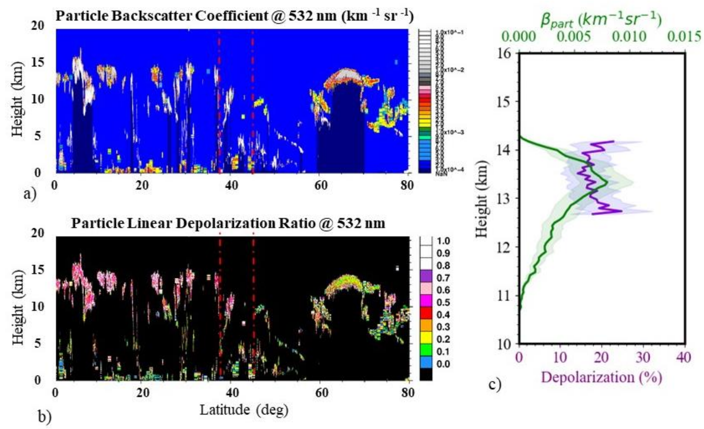

~~**Figure 6:** Same as Fig. 5 but for the night-time overpass of CALIPSO on 15/8/2017, 18:22 – 18:35 UTC shown in Fig.4b. (a) The smoke plume is now above the local tropopause at approximately 14 km, between 60 and 75 ° latitude. Red dashed lines denote the spatial averaging applied for the retrieval of optical properties shown on the right plot. (b) PLDR values at 532 nm (right plot, purple line) exceed 17%. (Note that the altitude range for this plot is from 10 to 16 km, whereas in Fig. 5b from 0 to 6 km).~~

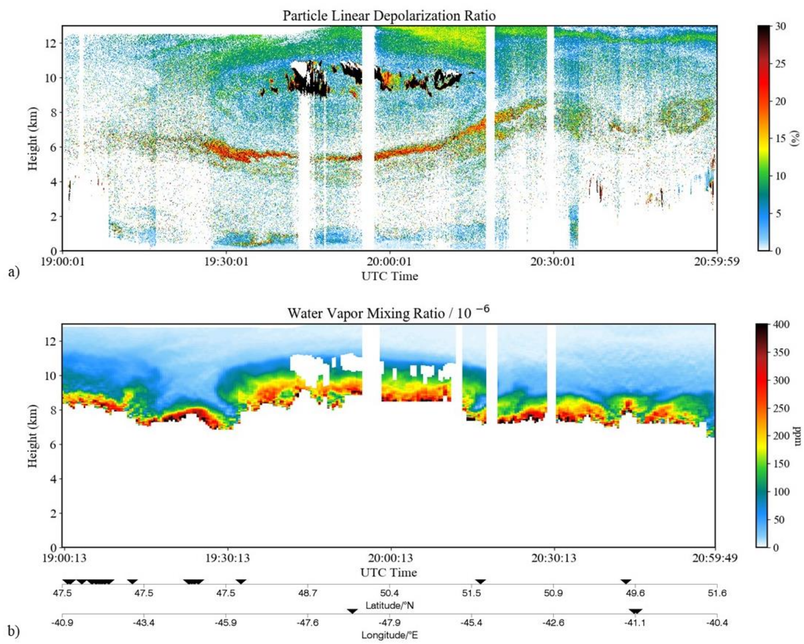

Particle Linear Depolarization Ratio
Height (km)
UTC Time
19:00:01
19:30:01
20:00:01
20:30:01
20:59:59
(%)
a)
Water Vapor Mixing Ratio / 10 $^{-6}$
Height (km)
UTC Time
19:00:13
19:30:13
20:00:13
20:30:13
20:59:49
ppm
Latitude/°N
47.5
47.5
47.5
48.7
50.4
51.5
50.9
49.6
51.6
Longitude/°E
-40.9
-43.4
-45.9
-47.6
-47.9
-45.4
-42.6
-41.1
-40.4
b)

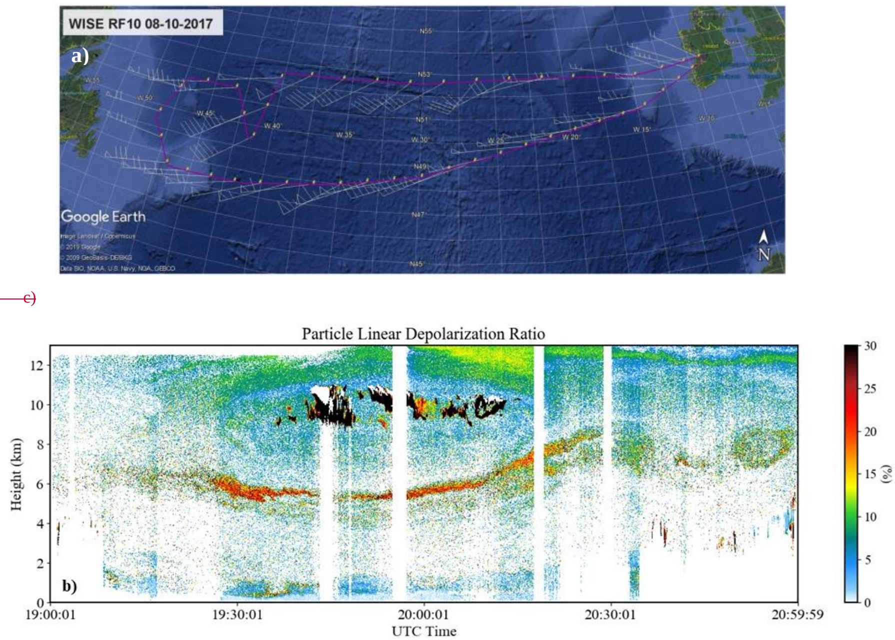

Formatted: Right

Figure ~~6~~7: Time–height airborne lidar observations of the PLDR at 532 nm (~~a~~b) and the Water Vapor Volume Mixing Ratio (b). Measurements were performed over the Atlantic Ocean, between 19:00 and 21:00 UTC on 7 October 2017 by the DLR HALO aircraft in the framework of WISE mission. The track of the aircraft is shown in (~~c~~a) over-plotted on Google Earth map.

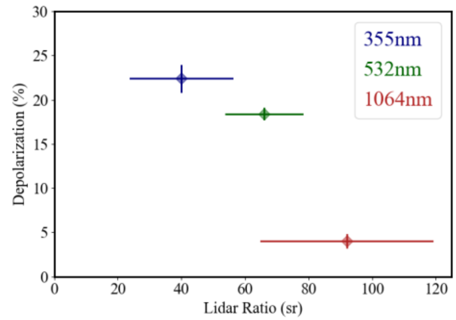

Figure ~~7~~8: Intensive optical properties of the smoke particles found in the stratosphere, as measured on August 22, at Leipzig, Germany. The LR mean values are plotted against the PLDR mean values, along with the corresponding errors. A typically increasing behaviour of LR for aged Canadian smoke is observed at 355 and 532 nm, while for the PLDR the effect is the opposite: the surprisingly large, layer-integrated mean values drop from the UV to the Near-IR.

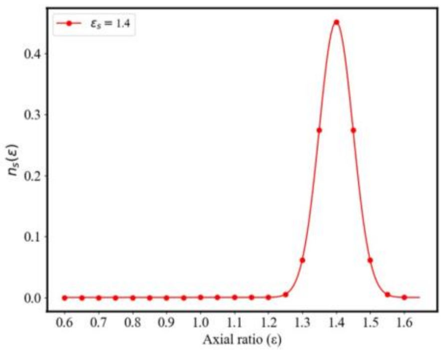

~~**Figure 9.** The retrieved axial-ratio distribution of the smoke particles assuming near-spherical shapes.~~

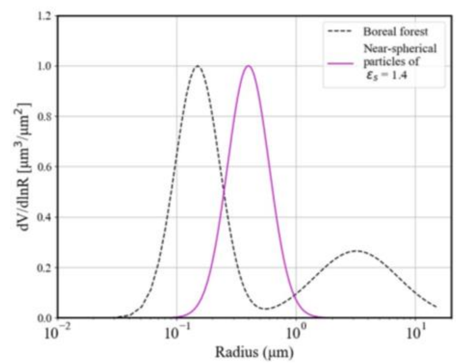

~~**Figure 10.** Typical AERONET size distribution for biomass burning (black dash line) (Dubovik et al., 2002), and the retrieved size distribution for near-spherical smoke particles (pink line). Both are normalized to their maximum value.~~

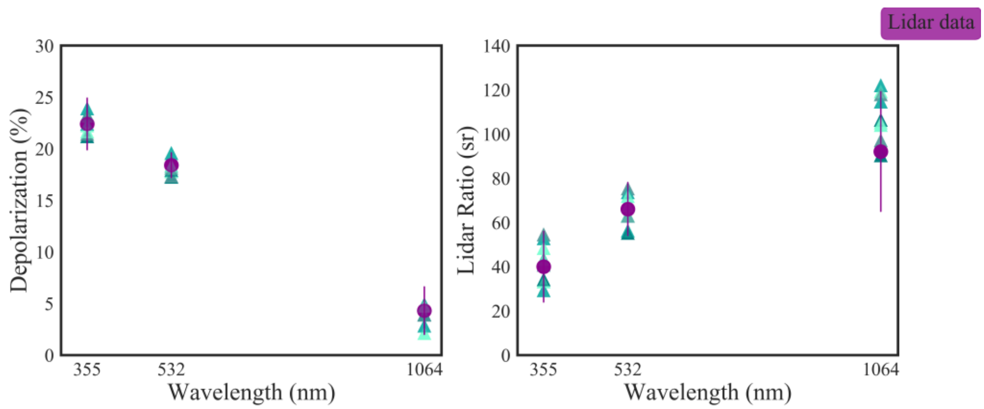

Figure 9: The reproduction of the measured PLDR and LR values, considering near-spherical particles. Purple circles correspond to measurements performed on 22 August 2017, at Leipzig, Germany, while blue markers denote to simulations performed with the T-matrix code, assuming near-spherical particles, for various values of the mean axial ratio $\boldsymbol{\varepsilon_s}$, ranging from 1.1 to 1.4, mean geometric radius r_g ranging from 0.25 to 0.45 μm, and a wavelength-independent complex refractive index *m*, for real part $\boldsymbol{m_r}$ ranging from 1.35 to 1.55 and imaginary part $\boldsymbol{m_i}$ ranging from 0.005 to 0.03.

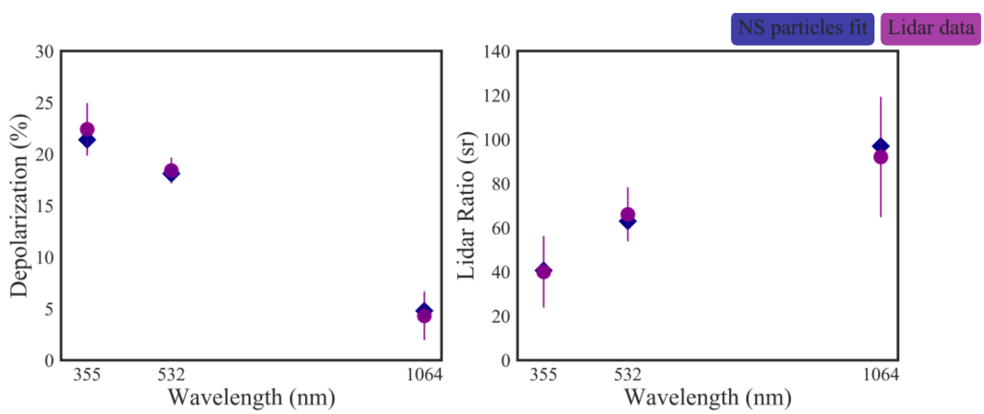

Figure 10: Same as Fig. 8 but only for the solution found to minimize the cost function of Eq. (8). Again, purple circles correspond to measurements on 22 August 2017, at Leipzig, Germany, while blue diamonds to simulations assuming near-spherical particles of mean axial ratio $\boldsymbol{\varepsilon_s}$ = 1.4, mean geometric radius r_g= 0.25 μm and a wavelength-independent complex refractive index *m* = 1.55 + i0.025.

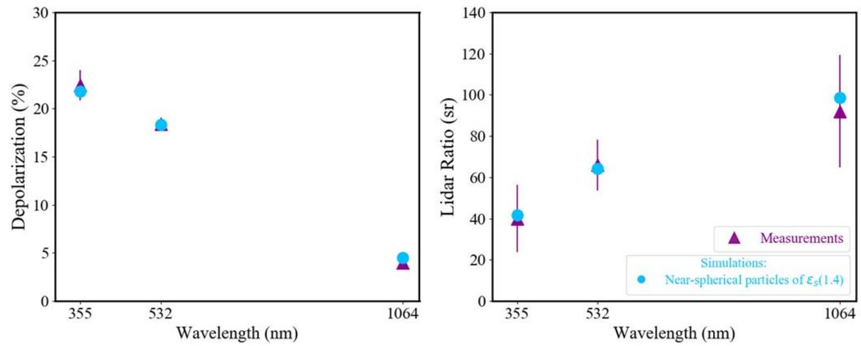

~~Figure 11: The fitting of measured PLDR (a) and LR (b) at 355, 532 and 1064 nm, with T-matrix simulations considering near-spherical particles. Purple triangles correspond to measurements on August 22, at Leipzig, Germany, while blue circles to simulations assuming near-spherical particles of mean axial ratio ε_g = 1.4, mean geometric radius r_g = 0.25μm and a wavelength independent complex refractive index "k =" 1.55 + i0.025.~~

Formatted: Normal

Formatted: Font: Times New Roman

Formatted: Font: Times New Roman

Formatted: Font: Times New Roman, Italic

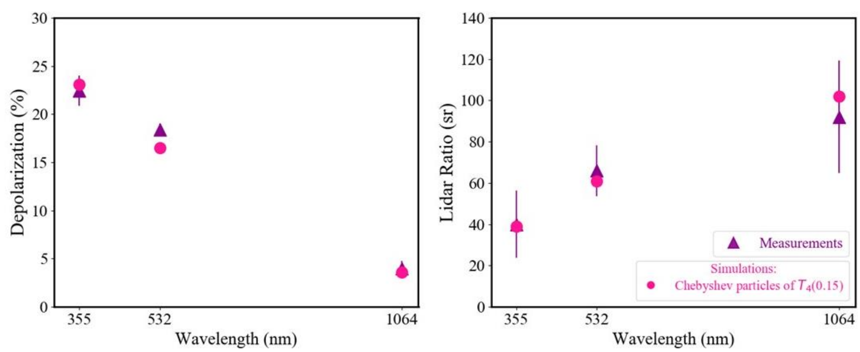

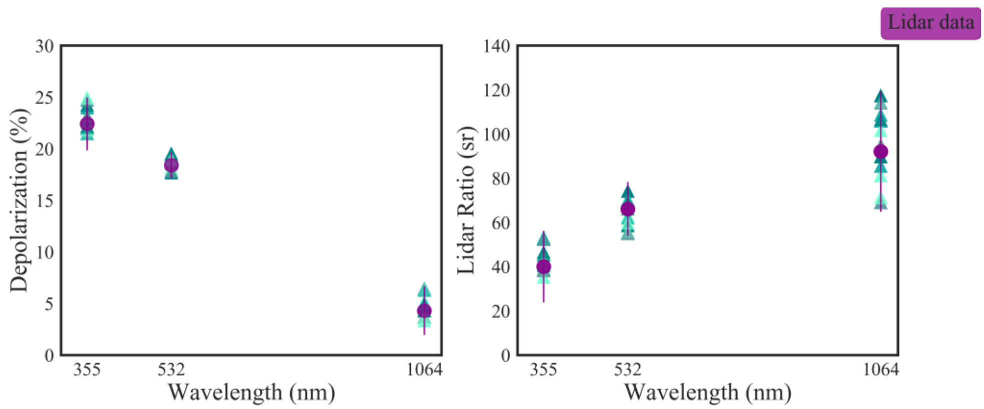

Figure 11: The reproduction of the measured PLDR and LR values, considering Chebyshev particles of the second degree (T_2). Purple circles correspond to measurements performed on 22 August 2017, at Leipzig, Germany, while blue markers denote to simulations performed with the T-matrix code, assuming Chebyshev particles of the second degree (T_2) for various values of the deformation parameter u ranging from -0.25 to 0.15, mean geometric radius r_g ranging from 0.2 to 0.5 μm, and a wavelength-independent complex refractive index *m*, for real part $\boldsymbol{m_r}$ ranging from 1.4 to 1.8 and imaginary part $\boldsymbol{m_i}$ ranging from 0.015 to 0.055.

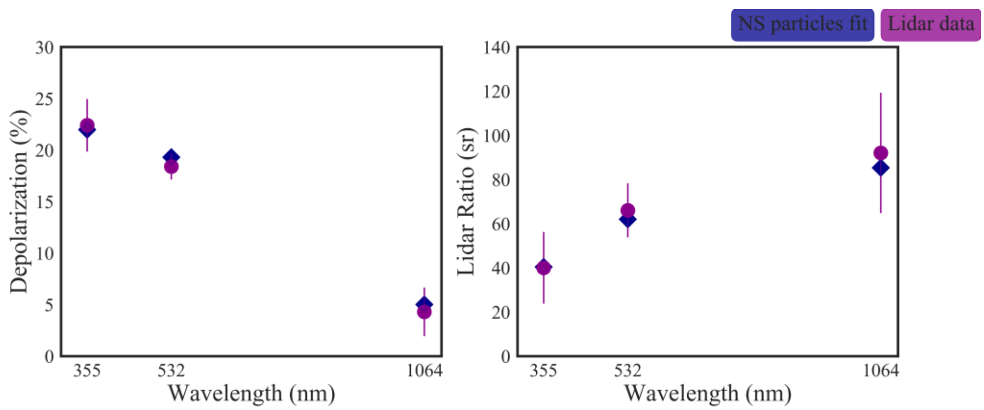

Figure 12: Same as Fig. 10 but only for the solution found to minimize the cost function of Eq. (8). Again, purple circles correspond to measurements on 22 August 2017, at Leipzig, Germany, while blue diamonds to simulations assuming Chebyshev particles of the second degree resembling oblate near-spherical particles, with deformation parameter $\boldsymbol{u}$ = -0.25, mean geometric radius r_g= 0.2 μm and a wavelength-independent complex refractive index *m* = 1.65 + i0.03.

Formatted: Normal

~~**Figure 12:** The fitting of the measured PLDR (a) and LR (b) at 355, 532 and 1064 nm, with T-matrix simulations considering Chebyshev particles. Purple triangles correspond to measurements on August 22, above Leipzig, Germany, while pink circles to simulations assuming Chebyshev particles of fourth degree.~~

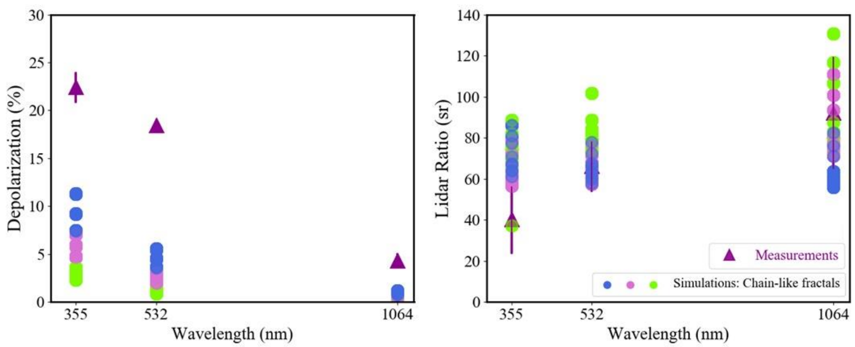

~~**Figure 13**: Fitting of the measured PLDR (a) and LR (b) at 355, 532 and 1064 nm, with MSTM simulations considering chain-like fractal aggregates. Purple triangles correspond to measurements on August 22, at Leipzig, Germany, while green (monomer radius R_m = 40μm) , pink (monomer radius R_m = 60μm) and blue (monomer radius R_m = 80μm) circles correspond to simulation results for the chain-like fractal aggregates shown in Fig. 3 with of D_f = 1.8 and k_f = 1.3.~~

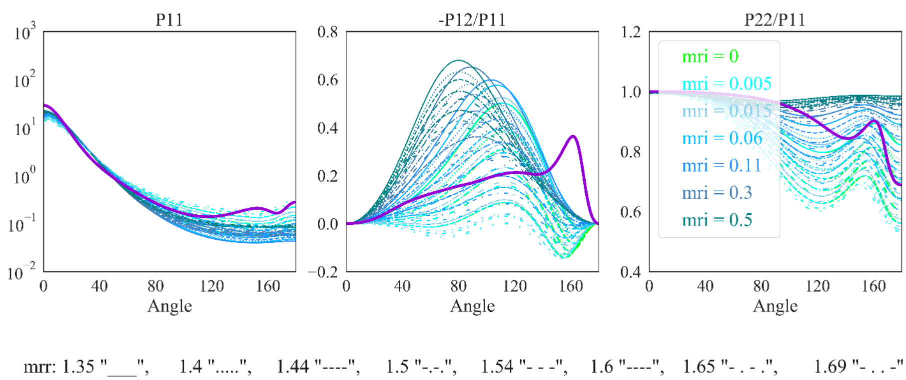

Figure 13. Comparison of the optical properties at λ = 440 nm for near-spherical particles (purple line) and the particles considered in the AERONET non-spherical model (blue lines). Left: P11 (phase function), middle: -P12/P11 (degree of linear polarization), right: P22/P11. Purple lines in the plots: calculations considering the near-spherical particle properties derived for the stratospheric smoke particles from the Canadian fires, with mean axial ratio ε_s = 1.3, mono-modal, log-normal size distribution with rg = 0.25, σg = 0.4, and complex refractive index m = 1.55 – i0.03. Blue lines in the plots: calculations using the AERONET non-spherical model, mono-modal, log-normal size distributions with rg = 0.25 µm and refractive indices of mr = 1.35, 1.40, 1.44, 1.50, 1.54, 1.60, 1.65, 1.69 for the real part (different line styles in the plot) and mi = 0, 0.005, 0.015, 0.06, 0.11, 0.3, 0.5 for the imaginary part (different line colors in the plot).

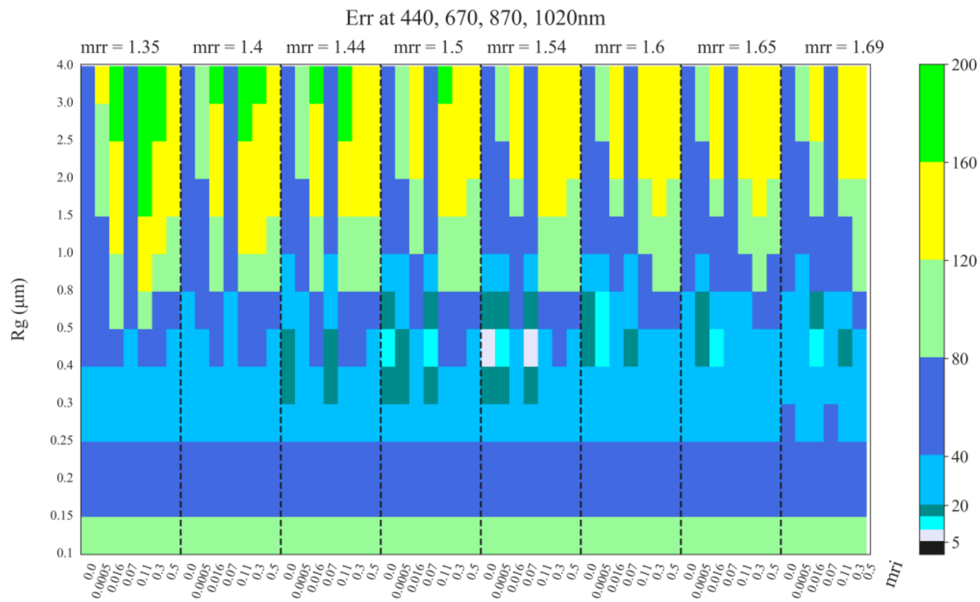

Figure 14. The residual error (Err) of fitting the phase functions at 440, 670, 870 and 1020 nm of the near-spherical particles presented in the manuscript, with the phase functions calculated with the AERONET non-spherical model for radius r_g and complex refractive index m shown in y- and x-axis, respectively.